3D Finite Difference Time Domain Method

for Anisotropic Materials : Theory and Application

By
Lixing Dou

A Thesis
in
The Department
of
Electrical and Computer Engineering

Presented in Partial Fulfillment of the Requirements
for the Degree of Master of Applied Science at
Concordia University
Montreal, Quebec, Canada

23 June 2005

Your file Votre référence
ISBN: 0-494-10234-9
Our file Notre référence
ISBN: 0-494-10234-9

Abstract

3D Finite Difference Time Domain Method

for Anisotropic Materials : Theory and Application

Lixing Dou

A 3-D FDTD method for full anisotropic medium was formulated and examined. Contrary to other methods, this approach is separated into two parts: dielectric properties parts and wave marching parts. Dielectric anisotropic properties are realized through the relationships of electric properties----electric flux versus electric field and magnetic properties---magnetic flux versus magnetic field. EM wave marching is realized through the relationships of magnetic field versus electric flux and electric field versus magnetic flux.

For the reason that medium properties are expressed separately, this method can avoid major modifications of core updating equations if the studied medium properties change. This can reduces the time necessary for making new FDTD programs for mediums with other properties. This is the reason that this method can also be extended to dispersive, anisotropic & dispersive mediums. A simplified perfect matched layer (PML) was modified and used as the absorbing boundary condition to match anisotropic medium. This method can yield good matching for anisotropic and dispersive mediums. And it can be seamlessly integrated into the main FDTD algorithms.

Three different 3D applications are studied: The first application is the medium with full anisotropic expression: a microstrip patch antenna with anisotropic substrates. The second application is ferrites having dispersive permeability property: weakly magnetic ferrite absorbers with punctured holes. The third application is magnetized ferrites with dispersive and anisotropic permeability: a waveguide loaded with heterogeneous anisotropic magnetic materials.

Good results are obtained from these applications, which show the effectiveness of this approach. From the simulation results, we can see that anisotropic can have great effects on the system properties, which can be another design freedom.

Acknowledgements

The author wishes to thank his graduate supervisor Professor A. R. Sebak for providing guidance, excellent suggestions, and valuable critical reviews of the drafts of this thesis.

The author expresses his sincere appreciation to everyone contributed to the successful completion of this work, particularly Prof. S. D. Gedney;. who provided detailed explanations concerning UPML; Dr. Sun. Guilin and Mr. Sadegh Farzaneh Koodiani, who offered valuable suggestions.

Special thanks to my wife Juan Shi for her unwavering patience, support, and understanding.

List of Figures

Chapter One: Introduction

This chapter presents the objectives of this research and the structure of this thesis. It also provides some background information about the finite difference time domain (FDTD) method.

1.1 Motivation

The development of microstrip circuit techniques made the geometry and material properties increasingly complex. Designing these circuits requires more sophisticated and dedicated CAD tools. Many dielectric materials used in waveguides, microwave integrated circuits (MICs), and monolithic MICs (MMICs) are anisotropic. The anisotropic effects should be taken into account in the numerical models to allow for the accurate prediction of their characterizing parameters. From another point of views, the anisotropic nature of these materials cannot be seen as having only a disadvantageous or anomalous impact on their overall characteristics and performances. Rather, it should be understood as another parameter, or another degree of freedom in their relevant electromagnetic (EM) fields' problems, allowing for the controlling and tuning of their characteristics.

Due to its intrinsic advantage, FDTD method can easily describe object

geometry and can integrate anisotropic and dispersive properties into main algorithms. As a dedicated CAD tool, FDTD method is one of the most convenient methods for solving this kind of problems. Some inherent advantages make it a powerful EM simulation tool. It supports dispersive, anisotropic mediums; one simulation can model broadband frequency response, etc. The above advantages make FDTD method a convenient technique of simulating EM wave problems on complex mediums. The absorbing boundary condition (ABC) is one of critical issues that enable the application of the FDTD methods in EM waves interacting with unbounded regions. The perfectly matched layer (PML) method is a highly effective ABC.

Some difficulties arise when FDTD method is used to solve problems composed by complex mediums. For example, for anisotropic cases, we need to develop sets of updating parts and corresponding ABC parts. For a dispersive case, we need to develop completely new sets of equations. This is not a problem for one single application. But when we apply FDTD method to different problems with different medium properties, this is not efficient, sometimes time consuming. We need a simpler solution that requires a minimum of changes for the core updating equations and for the ABC.

1.2 Objectives

In response to this need, FDTD algorithms based on a four-step updating process **(D, E, B, and H)** are presented. The anisotropic medium properties arise from the

relationship of developing **D** from **E** and **H** from **B**. And the EM wave marching steps are made possible by developing **D** from **H** and **B** from **E**. Our original purpose of this work was to develop algorithms for arbitrary anisotropic properties; however, in doing so, we found that this approach can be easily extended to modeling dispersive properties, thus rendering it applicable to more general cases. This thesis therefore details the applications of this method on anisotropic, dispersive and anisotropic & dispersive mediums.

The objectives of this thesis are:

- Investigate 3D Finite Difference Time Domain algorithms applicable to arbitrary anisotropic properties.
- Study the appropriate approach of the Perfectly Matched Layer (PML) applicable to arbitrary anisotropic.
- Realize the 'seamless' transition of PML and the main FDTD part.
- Verify results by applying our methods to several applications: a microstrip patch antenna with an anisotropic medium, weakly magnetic ferrite absorbers with punctured holes, and waveguides loaded with heterogeneous anisotropic magnetic materials.

1.3 FDTD background information and thesis structure

The behaviour of EM wave in anisotropic and dispersive mediums is very

complex, thus rendering the application of an analytical method difficult. Numerical methods are preferred in such situation. The Finite-Difference Time-Domain (FDTD) method is chosen for numerical analysis instead of other numerical methods, Due to its simplicity and versatility, an increasing number of scientists and engineers are interested in this method, prompting a drastic increase in papers published covering various application areas of this topic **[1].**

The FDTD method is a direct extension of Maxwell's equations. In this method, Maxwell's equations in differential form are converted into discrete forms using the central-difference method. From the solution of these discrete equations, we can compute EM fields' values such as field distributions, propagation coefficients, reflection coefficients, etc. Compared with other computational methods in EM, FDTD is an explicit approach; there is no need to convert coupled electric and magnetic field equations into uncoupled electric or magnetic fields' equations, which provides great mathematical simplicity in many problems. This approach performs the calculations for both electric and magnetic fields.

Simulation results based on this method provide the values of the electric and magnetic fields in time steps, which are time samples of electric and magnetic fields. Computed values in the time domain are enough for some cases; however, some research projects require the frequency response, which can be extracted using the Fourier Transform techniques. Generally, in the FDTD method just one simulation can yield a wide range of frequency responses. This makes it a convenient choice in EM simulations,

as other numerical techniques usually require different simulation runs for different frequencies.

Chapter Two reviews some commonly used numerical techniques for EM simulations, including their applications and classifications. These techniques are the Method of Moment (MoM), the Finite Element Method (FEM), the Transmission Line Matrix (TLM), and the Optical Methods are given.

Chapter Three provides the theoretical background of FDTD method, including finite difference schemes, Yee's grid, the 3D FDTD formulation for the lossy medium, the stability condition, the realization approach of different sources, a method for plane wave generation, the total field/scattered field method, and frequency domain analysis of FDTD data. Also there are introduction about the concept of Perfectly Matched Layer (PML), Uniaxial-PML (UPML) and simplified PML. This simplified PML has been modified to work for anisotropic medium. Realizing method of the PML is presented.

Chapter Four are formulated FDTD algorithms for anisotropic, anisotropic & dispersive mediums. The formulation is developed based on the relationship of electric field versus electric flux and magnetic field versus magnetic flux. These relationships are modified to fit Yee's grids. Special treatments of PEC boundary are presented.

Chapter Five uses previously investigated methods to study the following applications. These applications are: a microstrip patch antenna with an anisotropic medium, a weakly magnetic ferrite absorber with punctured holes, and a waveguide loaded with heterogeneous anisotropic magnetic material. Results are given for each

application.

Chapter Six presents the conclusion and the future work that arise from this thesis. It is the author's intention to show that this FDTD algorithm is an efficient method for mediums with anisotropic and dispersive properties.

Appendix has useful information and formulations related to this thesis.

Charter Two: Literature Review

2.1 Impact of computational electromagnetics

Electromagnetic (EM) field computation is becoming increasingly important in science and technology. Modern electronic and wireless systems are becoming more compact and the components are more complex and closer together. Furthermore, designers need systems that are less susceptible to increasingly complex electromagnetic environments. Because of these, modeling of EM waves has become very complex and can no longer be handled by analytical approaches.

Nevertheless, advances in modern computer technology make it possible to provide more computational power and memory that can be used to simulate complex EM system and processes. Compared with experimental and analytical techniques, numerical techniques are fast, inexpensive, and allow more flexibility in parameter variations. Beginning in the 1960s and becoming popularised in the 1980s, many numerical techniques for EM problems have been developed to solve practical, complex EM problems for which closed-form analytical solutions are either intractable or do not exist **[2]**.

EM simulation methods can be used in many engineering applications, including antennas, Radar Cross Section (RCS), propagation analysis, biomedical engineering,

Electromagnetic Compatibility (EMC)/Electromagnetic Interference (EMI). And more applications can be in figure 2-1.

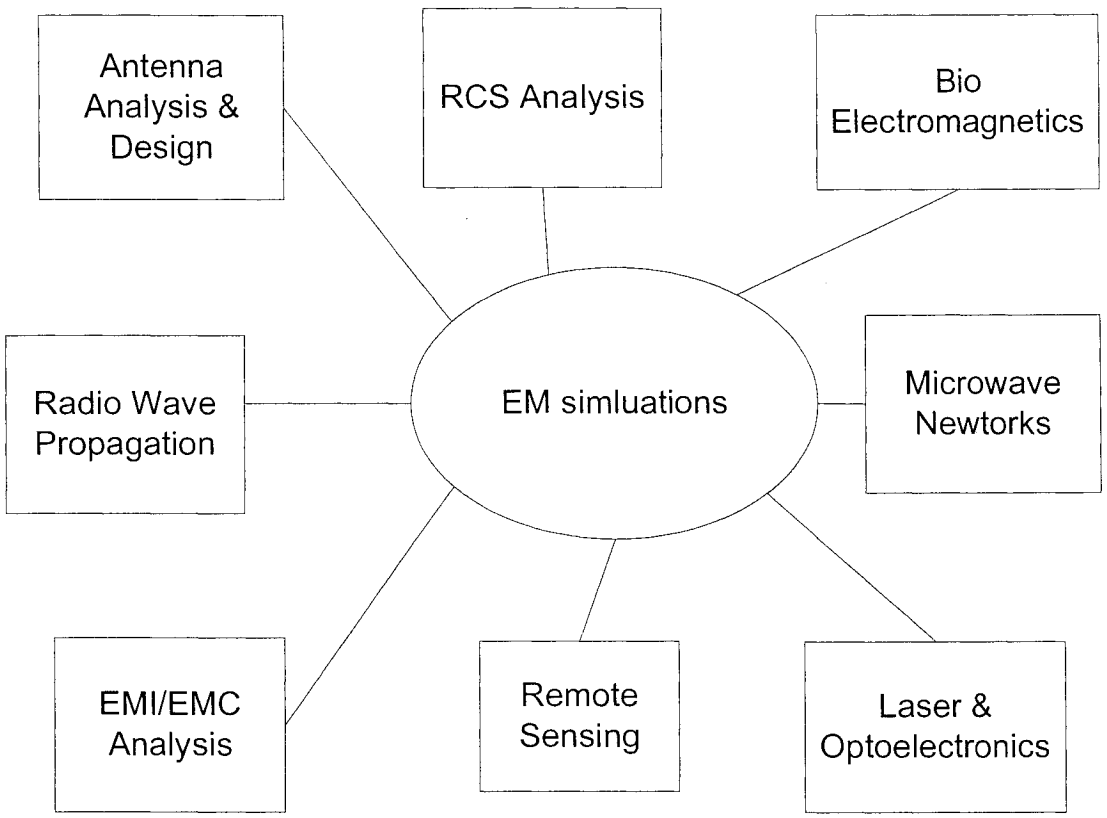

Figure 2-1: Applications of EM Simulation Methods

2.2 The Classification of EM Simulation Methods

Simulation methods for EM analysis can be categorized into four groups: differential equations methods, integral equations methods, optical methods, and miscellaneous. Differential equations methods, such as FEM and FDTD methods require the discretization of the entire problem region. Integral equations methods such as MoM only require discretization over the structure surface. Each of these methods was

developed from the Maxwell's equations in time domains or time-harmonic forms. Optical methods are methods developed from optic theory to analyze the interaction of EM waves with electrically large objects. Miscellaneous methods are methods such as the differential method for determination of eigenvalues, variational related methods, and Monte Carlo Methods **[2].**

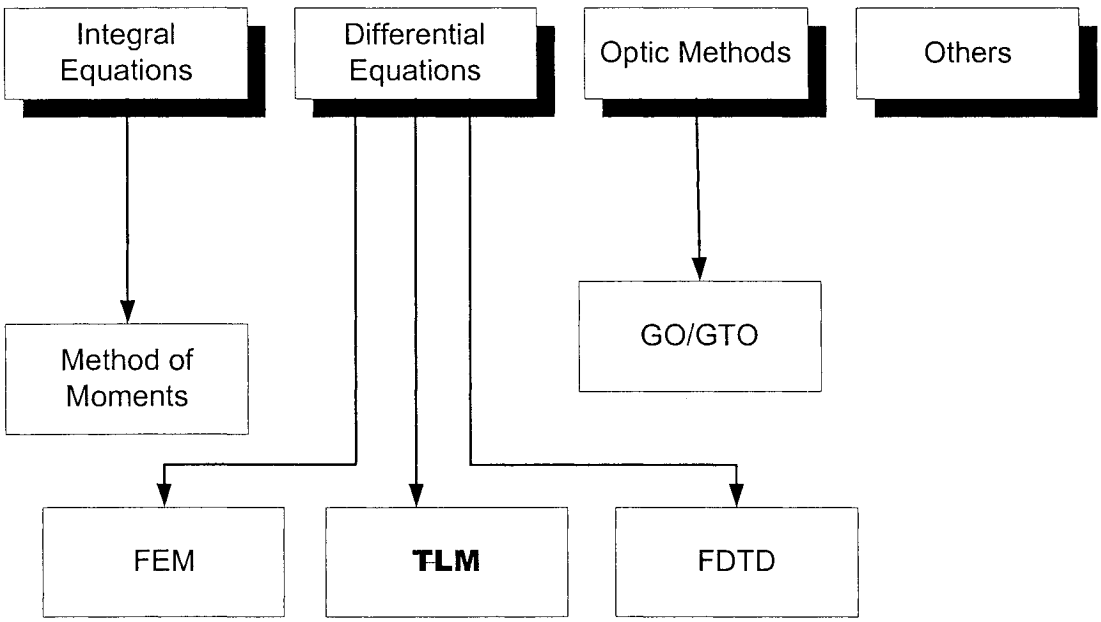

Figure 2-2: Simulation methods in EM

2.3 Integral Equation Methods

Integral Equation Methods rely upon integral forms. Method of Moments (MoM) is one of the most widely used computational methods developed from Integral Equation Methods. Typically, the moment method solves integral equations by reducing them to a system of linear equations, from which we can obtain the input impedance, radiation

patterns, and so on. The equations solved by the MoM technique are generally in the forms of the Electrical Field Integral Equation (EFIE) or the Magnetic Field Integral Equation (MFIE), both of which can be derived from Maxwell's equations. Starting from Maxwell's integral forms determines the main application areas of MoM technique. For example, EFIE may be particularly well-suited for modeling thin wire structure. Although MoM can also be applied in the time domain, the majority applications of this approach are in the frequency domain. MoM can model anisotropic medium with some limits.

The primary formulation of MoM is an integral equation obtained through the use of Green's functions **[3]**. MoM reduces integral equations to a system of linear equations by applying the method of weighted residuals. Harrington popularised the term Method of Moments in the world of electrical engineering. His works demonstrated the power and flexibility of this numerical technique for solving EM problems.

The weighted residuals methods begin by establishing a set of trial solutions with one or more variable parameters. The residuals are the measurements of difference between the real solution and the trial solution. The variable parameters are determined in a manner that guarantees the best fit of the trial function based on minimizing residuals.

MoM generally begins with a form of EFIE or MFIE, both of which can be derived from Maxwell's equations by considering the problem of a field scattered by a perfect conductor (or a lossless dielectric).

MoM can successfully analyze many important 3D radiation and scattering problems. General purpose MoM codes are very efficient in modeling wire antennas or

wires attached to large conducting surfaces.

NEC is a non-commercial package **[4]**, an MoM technique-based package used for the currents induced on metallic structures by sources or by an incident field. Antenna or RCS modeling is possible if the structure is modeled as a collection of thin wires. This package is especially handy in modeling wire antennas with lengths up to several wavelengths.

2.4 Differential Equation Methods

Wave equations with differential form are comparatively easy to analyse. Many numerical methods have been developed to treat these kinds of problems. FDTD and FEM are methods developed from differential equations, and TLM can be treated as a kind of differential equation.

2.4.1 Finite Element Method

FEM is a very general method and can be used in many areas. The general steps of the FEM method area as follows:

1. Discretizing the solution region into a finite number of elements
2. Developing governing equations for a typical element
3. Connecting all elements in the solution region

4. Solving obtained equations

The governing issue is the derivation of governing equations for the elements. This step is quite similar to the requirement of deriving Green's function in MoM techniques. The difficulty encountered in FEM is the process of mesh generation. Many techniques have been developed for this purpose **[5]**.

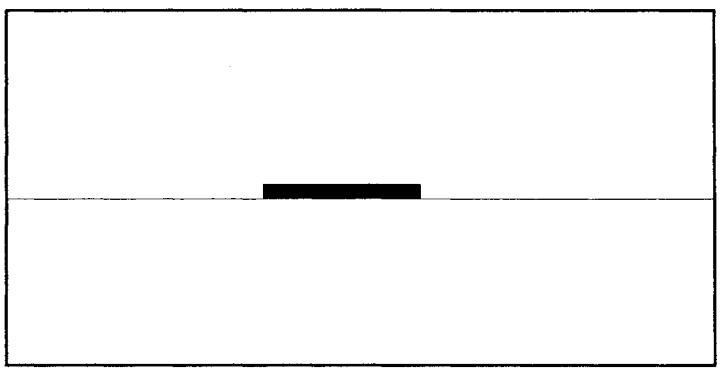

Figure 2-3: Structure Geometry of the computation region

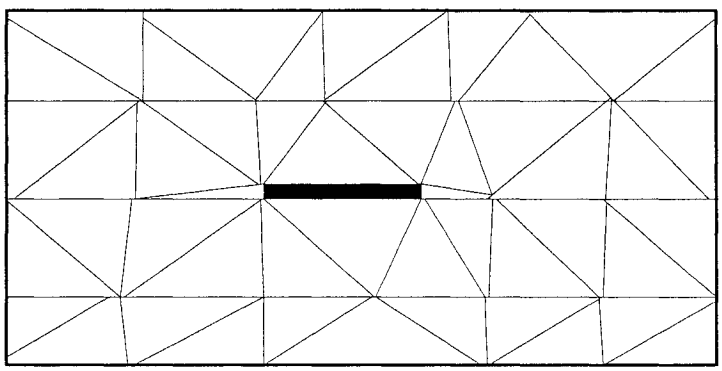

Figure 2-4 FEM Mesh for the Structure

Most FEMs are developed from variational methods, which work by minimizing or maximizing the expression that is, in theory, stationary with respect to the true value.

For the EM problems, FEMs solve the unknown field quantities by minimizing the energy in the an energy function. The energy function is an expression that describes all the energy associated with the configuration being analyzed. For 3D cases, this function can be represented as:

$$F = \int_v \left(\frac{u|H|^2}{2} + \frac{\varepsilon|E|^2}{2} - \frac{J \cdot E}{2jw}\right) dv \qquad \textbf{(2-1)}$$

The first two terms in the integral represent energy stored in the magnetic and electric fields. The third term is the energy dissipated or supplied by the conducting currents. Expressing $\boldsymbol{H}$ in terms of $\boldsymbol{E}$ and setting the derivative of this function with respect to $\boldsymbol{E}$ equals to zero yields an equation of the form $f(J \cdot E) = 0$. A k^{th} order approximation of the function f is then applied at each of the N modes and boundary conditions are enforced. This results in the following system of equations:

$$[J] = [Y][E] \qquad \textbf{(2-2)}$$

The value of J on the left side of the equations is treated as the source term; it represents the known excitations. The elements in Y are functions of the problem geometry and boundary constraints. Since each element interacts only with elements in its own neighbourhood, the Y matrix is generally sparse. E represents the unknown electric fields at each node. These values are obtained by solving the above equation system.

In order to obtain a unique solution, it is necessary to constrain the field values at the boundary nodes. For example, all tangential electric fields located at the microstrip conductor are set to zero. The advantages of FEM in EM problems depend on the fact

that the electrical and geometric properties of each element can be independently defined. This allows a large number of small elements into regions of complex geometry and a smaller number of larger elements into relatively open regions. In this way, it can model EM problems that have complicated geometries and many arbitrarily shaped regions in a relatively efficient manner. FEM has the ability to model anisotropic medium. But for dispersive medium, this method requires different treatment for different frequency.

2.4.2 Transmission Line Matrix

The TLM method is a time-domain method for solving field problems using a circuit equivalent concept. It is developed through the discretisation of EM fields by a network of lumped elements, using the equivalent relation of electric field, magnetic field in Maxwell's equations, and voltage and current in transmission line equations. The steps of TLM techniques are as follows:

1. Replacing a field problem with the equivalent circuit problem
2. Using iterative methods to solve the equivalent network

This method is a time-domain method, so it can model anisotropic or dispersive medium. This method calculates both electric and magnetic fields and is relatively straightforward to implement.

2.4.3 Finite-Difference Time-Domain

The FDTD method is a direct solution of the Maxwell's equations in the time domain. The geometry of the solution region is divided into small cells. The time and spatial-partial derivatives are handled with the finite difference method. Electric field and magnetic field components are calculated at different locations of each cell. Besides the different positions in the meshes, the electric and magnetic fields have half-time step differences. The main advantage of the FDTD method is that it provides a direct solution to the Maxwell's curl equation in the time domain. It can easily take into account material properties. Electric field and magnetic field calculations are carried on alternatively. A detailed introduction of the FDTD theory is presented in the next chapter.

2.5 Optical methods

At high frequencies, the behaviour of EM wave propagation can be approximated as optical rays; thus, we can use optical theories to analyze EM problems. The main methods used are: Geometrical Theory of Diffraction (GTD), Physical Optics (PO), or Geometrical Optics (GO) **[6].**

In GO, ray concept and the law of energy conservation are the base for the foundation. GO assumes light propagating in an infinitesimal tube. Ray intensity obeys the conservation of energy flux in a ray tube. In a homogenous medium, rays intend to travel the extreme path (usually minim), the direction that is natural to their wave fronts.

Figure 2-5 explains this. In classical GO, only direct, reflected, and refracted rays are considered. This cannot provide an accurate prediction in the zero area predicted by GO, as there are discontinuities between the dark region and the illuminated region. In GTD theory, after considering the diffraction from the edges of the conducting surface, accurate results are archived in predicting values in shadow regions.

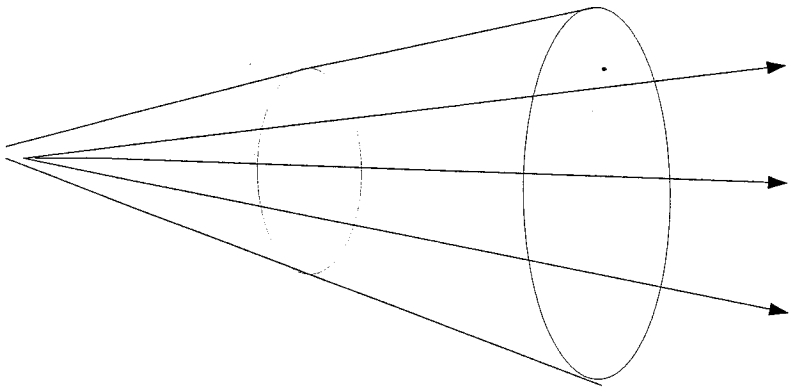

Tube of rays for a spherical radiated wave

Figure 2-5: Ray Tub in GO Concept

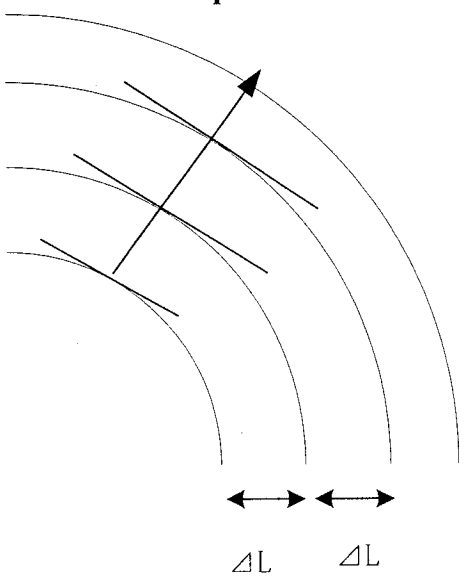

Figure 2-6: Traveling Path of Rays in Homogenous Medium

The reflection of rays obeys Snell's Law, but rather than a single ray, it is an

infinitesimal small tub. Diffraction is a special phenomenon that occurs in the perfect conducting edge. When a ray reaches the conducting edge, a group of diffracted rays is generated. Detailed information and formulation about GO and GTD is available **[6].**

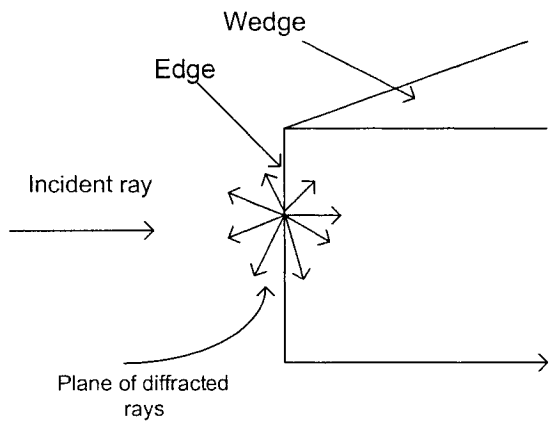

Figure 2-7: Diffraction happened when ray reached the edge

2.6 Time Domain and Frequency Domain

Time harmonic Maxwell's equations are not suitable for non-linear systems, as time-harmonic formulations are expressions of steady states for sinusoidal signals. This is also the reason that harmonic forms are not suitable for transient states. The Method of Moment and FEM usually employ time-harmonic formulations. As a result, these methods are confined to linear systems in general. The FDTD and TLM are developed in time-domain. The electric and magnetic field components in the FDTD and TLM methods are transient fields, which are functions of time and space. This makes

non-linear and dielectric propriety easy to incorporate with in both methods.

In general, only one frequency is considered for frequency domain methods, whereas time domain methods can yield either a wide-band frequency response or a single-frequency response. In this way, we can obtain a group frequency response using the time domain method in just one simulation. Also, this is the reason that non-linear, anisotropic proprieties can be modeled into algorithms in time domain methods **[7].**

We usually describe a system in the frequency domain, in terms of its frequency response. System modeling in the frequency domain is comparatively easier than modeling in the time domain. To obtain the frequency response, we must use a Fourier transform in the time domain methods. If seek a time domain response, we must employ an Inverse Fourier transform to obtain the time domain response in the frequency domain method.

Chapter Three: FDTD Formulation Review

3.1 Introduction

The FDTD method offers many advantages including **[7]:**

1. It is a direct solution technique for Maxwell's equations.
2. It is a fully explicit method with no intrinsic upper boundary to the computation domain.
3. It is accurate and robust.
4. It treats nonlinear behaviours naturally and it offers a simple way of visualization.

In 1966, Yee was the first to present the idea of FDTD **[8]**. After 1980s, the acceptance of FDTD method accelerated researches on this topic, particularly Mur **[9]** and Berenger's PML **[10]**, which greatly increased the capabilities of this method. This method has become one of the mostly widely used techniques in EM simulation. There are some books dedicated to this method **[7]**, **[11]**, **[12]**, **[13]**.

The original Yee algorithm is used for isotropic, linear materials. Researchers began to explore the possibility of extending FDTD method to the anisotropic medium in the early 1980s. The major research concerning the application of the FDTD method to anisotropic materials is listed below:

- In 1986, Choi and Hoefer **[14]** were the first to apply the FDTD method to solving anisotropic substrates.
- In 1993, Schneider and Hudson **[15]** described the application of the FDTD method to materials with full permittivity and conductivity tensors.
- In 1993, Hunsberger et al. **[16]** used a recursive convolution FDTD scheme to analyze magnetized plasmas (which are both dispersive and anisotropic).
- In 1999, Zhao published a 3D approach **[17]** based on the D, E, and H fields to handle general anisotropic dielectric media.
- In 2004, Akyurtlu and Werner published their research on the application of the FDTD method to a uniaxial bianisotropic medium **[18]**.
- In 2004, Mosallaei and Sarabandi analyzed magneto-dielectrics using the FDTD method **[19]**.

Much research has been devoted to applying the FDTD method to the analysis of magnetized ferrites that have frequency-dispersive permeability tensors with off-diagonal terms.

- In the early work on this subject, Reineix et al. **[20]** and Pereda et al. **[21]** employed a discretized form of auxiliary differential equations that describes the relationship between the magnetic field and the magnetization current in time domain.
- Schuster and Luebbers **[22]** analysed magnetized ferrites using a recursive convolution technique that allows for arbitrary orientation of the biasing field.

- Using the Z transform method, Hruskovec and Chen developed another method for magnetized ferrites **[23].**

Recognizing that traditional ABCs cannot be applied to general anisotropic materials, Zhao et al. **[17]** extended Berenger's PML to permit the matching of anisotropic materials. In 2002, Moss and Teixeira analysed numerical dispersion for anisotropic mediums **[24].**

3.2 Finite difference Schemes

This part provides a brief overview of the FDTD method for the solution of Maxwell's equations. The purpose is to introduce some mathematical background related to the FDTD method.

EM problems can be described in terms of differential, integral equations or combination of both. If the solution region is complex or boundary conditions are time-dependent or inhomogeneous or anisotropic, classical analytical approaches may fail. For this reason, numerical solutions are applied in EM problems. The finite difference methods are more easily understood, more universally applicable than others with respect to solving differential equations.

For a given a function $f(x)$, we can approximate its derivation at x_0 with three forms.

The forward difference form:

$$f'(x_0) \cong \frac{1}{\Delta x}\left(f(x_0 + \Delta x) - f(x_0)\right) \qquad \textbf{(3-1.a)}$$

The backward difference form:

$$f'(x_0) \cong \frac{1}{\Delta x}\left(f(x_0) - f(x_0 - \Delta x)\right) \qquad \textbf{(3-1. b)}$$

The central difference form:

$$f'(x_0) \cong \frac{1}{2\Delta x}\left(f(x_0 + \Delta x) - f(x_0 - \Delta x)\right) \qquad \textbf{(3-1.c)}$$

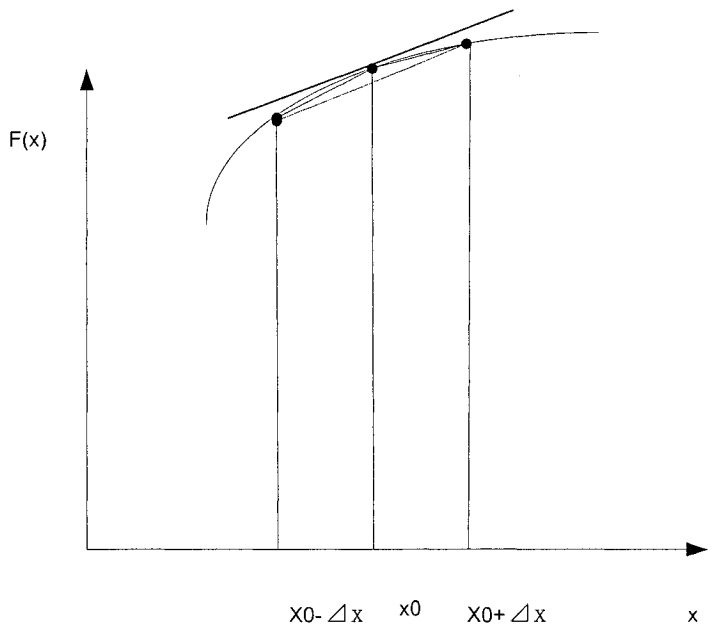

Figure 3-1: Finite difference approximate derivation

We obtain approximation errors by employing Taylor's expansion analysis **[5]**. The errors for forward difference and backward difference form are proportional to the order of Δx, while the errors of central difference form are proportional to the order of $(\Delta x)^2$. This type of errors is called truncation error.

Following the same way, we can also estimate the second order derivation at x_0 as:

$$
\begin{aligned}
f''(x_0) &\cong \frac{1}{\Delta x}\left(f'(x_0 + \Delta x/2) - f'(x_0 - \Delta x/2)\right) \\
&\cong \frac{1}{\Delta x}\left[\frac{f(x_x + \Delta x) - f(x_0)}{\Delta x} - \frac{f(x_x) - f(x_0 - \Delta x)}{\Delta x}\right] \\
&= \frac{f(x_0 + \Delta x) - 2f(x_0) + f(x_x - \Delta x)}{(\Delta x)^2}
\end{aligned}
\tag{3-2}
$$

3.3 Fundamentals of FDTD

The FDTD method is a numerical method that solves the Maxwell curl equations in the time domain and was firstly presented by Yee **[8]**. His algorithm is based on a central-difference solution of Maxwell's equations with spatially staggered electrical and magnetic fields, which are solved alternately at each time step in a leapfrog algorithm. There are six field components in one unit cell. The **E** and **H** fields are interlaced because of the time interval offset by $\Delta t/2$. Every field component can be evaluated since the function is given in a discrete form:

$$
f(x,y,z,t) = f(i\Delta x, j\Delta y, k\Delta z, n\Delta t) = f^n\,|_{i,j,k} \tag{3-3}
$$

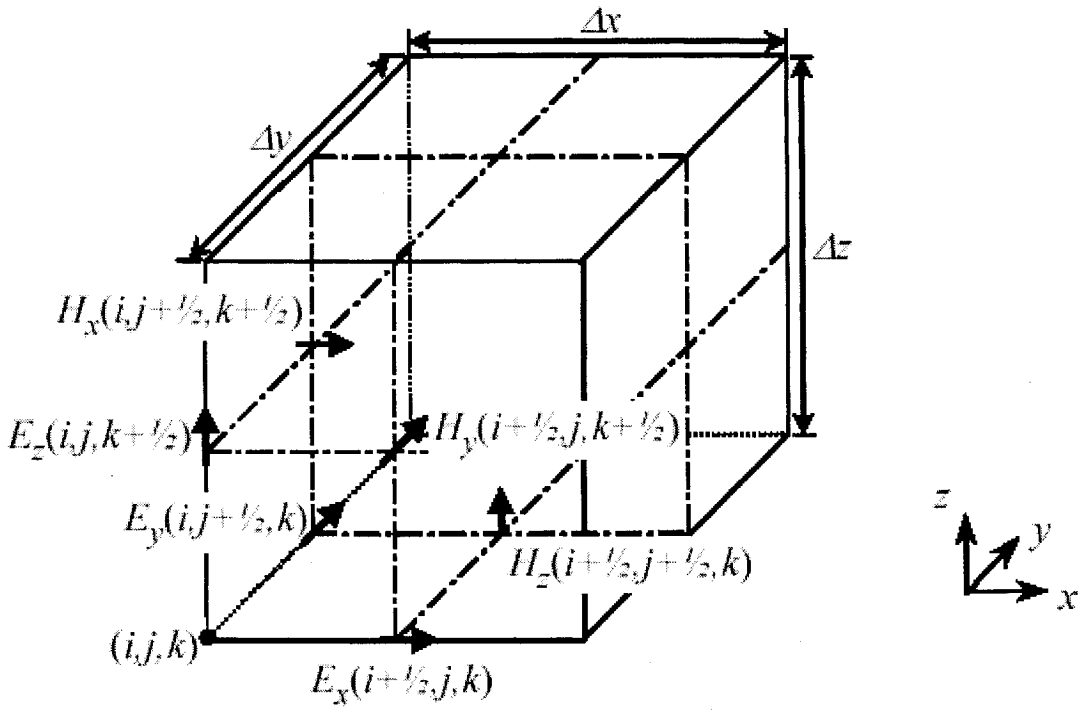

Figure 3-2: Yee's grid in 3D Cartesian coordinates

Δx, Δy, and Δz, are spatial increments in the different axis and Δt is the time step. Using the above notation and the concept of Yee's grid, we can solve Maxwell's equations for the field values in a computational domain. Figure 3-3 shows the sequence of field calculation.

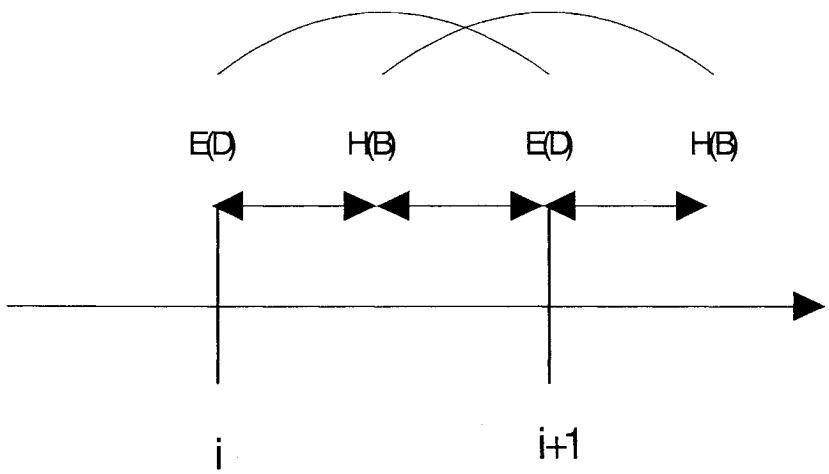

Figure 3-3: Calculation Sequence in FDTD

The starting formulation is from the differential form of Faraday and Ampere's law or Maxwell's curl equations.

$$\frac{\partial \vec{B}}{\partial t} = -\nabla \times \vec{E} - \vec{M}; \tag{3-4.a}$$

$$\frac{\partial \vec{D}}{\partial t} = \nabla \times \vec{H} - \vec{J}; \tag{3-4.b}$$

We can write out the vector components of the curl equations in Cartesian coordinates. For the sake of clarity, we start from a simple situation: materials are assumed to be isotropic, non-dispersive, electric, and magnetic properties; or isotropic, non-dispersive electric losses that attenuate the E and H field and have no electric or magnetic source. The the above equation can then be expressed as a set of six coupled scalar equations in Cartesian coordinates:

$$\frac{\partial H_x}{\partial t} = \frac{1}{\mu}\left[\frac{\partial E_y}{\partial z} - \frac{\partial E_z}{\partial y}\right] \tag{3-5.a}$$

$$\frac{\partial H_y}{\partial t} = \frac{1}{\mu}\left[\frac{\partial E_z}{\partial x} - \frac{\partial E_x}{\partial z}\right] \tag{3-5.b}$$

$$\frac{\partial H_z}{\partial t} = \frac{1}{\mu}\left[\frac{\partial E_x}{\partial y} - \frac{\partial E_y}{\partial x}\right] \tag{3-5.c}$$

$$\frac{\partial E_x}{\partial t} = \frac{1}{\varepsilon}\left[\frac{\partial H_z}{\partial y} - \frac{\partial H_y}{\partial z} - \sigma E_x\right] \tag{3-5.d}$$

$$\frac{\partial E_y}{\partial t} = \frac{1}{\varepsilon}\left[\frac{\partial H_x}{\partial z} - \frac{\partial H_z}{\partial x} - \sigma E_y\right] \tag{3-5.e}$$

$$\frac{\partial E_z}{\partial t} = \frac{1}{\varepsilon}\left[\frac{\partial H_y}{\partial x} - \frac{\partial H_x}{\partial y} - \sigma E_z\right] \qquad \textbf{(3-5.f)}$$

This is an example of the corresponding difference equation **[11]:**

$$\frac{H_x\big|^{n+1/2}_{i,j+1/2.k+1/2} - H_x\big|^{n-1/2}_{i,j+1/2}}{\Delta t}$$

$$= -\frac{1}{\mu}\left(\frac{E_y\big|^{n}_{i,j+1/2,k+1} - E_y\big|^{n}_{i,j+1/2,k}}{\Delta z} - \frac{E_z\big|^{n}_{i,j+1,k+1/2} - E_z\big|^{n}_{i,j,k+1/2}}{\Delta y}\right) \qquad \textbf{(3-6.a)}$$

$$\frac{E_x\big|^{n+1}_{i+1/2,j,k} - E_x\big|^{n}_{i+1/2,j,k}}{\Delta t}$$

$$= -\frac{1}{\varepsilon}\Bigg(\frac{H_y\big|^{n+1/2}_{i+1/2,j,k+3/2} - H_y\big|^{n+1/2}_{i+1/2,j,k+1/2}}{\Delta z}$$

$$- \frac{H_z\big|^{n+1/2}_{i+1/2,j+3/2,k} - H_z\big|^{n+1/2}_{i+1/2,j+1/2,k}}{\Delta y} \qquad \textbf{(3-6.b)}$$

$$+ \sigma \cdot E^{n+1/2}{}_x(i+1/2, j, k)\ \Bigg);$$

Here we just solve for the expression of E_x. Similar process can be applied to the other components.

Since,

$$E^{n+1/2}{}_x\big|_{i+1/2,j,k} = \frac{E^{n+1}{}_x\big|_{i+1/2,j,k} - E^{n}{}_x\big|_{i+1/2,j,k}}{\Delta t} \qquad \textbf{(3-7)}$$

we can substitute the above equation into **(3-6.b)** to obtain an explicit time-stepping relation for E_x:

$$E_x\big|^{n+1}_{i+1/2,j,k} = \left(\frac{1 - \frac{\sigma.\Delta t}{2\varepsilon}}{1 + \frac{\sigma\ .\Delta t}{2\varepsilon}}\right) E_x\big|^{n}_{i+1/2,j,k}$$

$$+\left(\frac{\frac{\Delta t}{\varepsilon}}{1+\frac{\sigma \Delta t}{2\varepsilon}}\right)\left(\frac{H_z\Big|_{i+1/2,j+1,k+1/2}^{n+1/2}-H_z\Big|_{i+1/2,j,k+1/2}^{n+1/2}}{\Delta y}-\frac{H_y\Big|_{i+1/2,j,k+3/2}^{n+1/2}-H_y\Big|_{i+1/2,j,k+1/2}^{n+1/2}}{\Delta z}\right) \quad \textbf{(3-8)}$$

Through the same procedure, updating equations of $\mathbf{E_y}$, $\mathbf{E_z}$, $\mathbf{H_x}$, $\mathbf{H_y}$, and **Hz** can be derived. By updating these equations, we can calculate the field distributions in the modeling area. Through field values, we can calculate eigenvalue, cutoff frequency, reflection coefficient, and antenna patterns. Here is the complete list of updating equations:

The magnetic field updating equation sets are given by:

$$H_x\Big|_{i,j+1/2,k+1/2}^{n+1/2}=H_x\Big|_{i,j+1/2,k+1/2}^{n-1/2}+\left(\frac{\Delta t}{\mu}\right)\left(\frac{E_y\Big|_{i,j+1/2,k+1}^{n}-E_y\Big|_{i,j+1/2,k}^{n}}{\Delta z}-\frac{E_z\Big|_{i,j+1,k+1/2}^{n}-E_z\Big|_{i,j,k+1/2}^{n}}{\Delta y}\right) \quad \textbf{(3-9.a)}$$

$$H_y\Big|_{i+1/2,j,k+1/2}^{n+1/2}=H_y\Big|_{i+1/2,j,k+1/2}^{n-1/2}+\left(\frac{\Delta t}{\mu}\right)\left(\frac{E_z\Big|_{i,j+1/2,k}^{n}-E_z\Big|_{i+1/2,j,k}^{n}}{\Delta x}-\frac{E_x\Big|_{i+1/2,j,k+1}^{n}-E_z\Big|_{i+1/2,j,k}^{n}}{\Delta z}\right) \quad \textbf{(3-9.b)}$$

$$H_z\Big|_{i+1/2,j+1/2,k}^{n+1/2}=H_z\Big|_{i+1/2,j+1/2,k}^{n-1/2}+\left(\frac{\Delta t}{\mu}\right)\left(\frac{E_x\Big|_{i+1/2,j+1,k}^{n}-E_x\Big|_{i+1/2,j,k}^{n}}{\Delta y}-\frac{E_y\Big|_{i+1,j+1/2,k}^{n}-E_y\Big|_{i,j+1/2,k}^{n}}{\Delta x}\right) \quad \textbf{(3-9.c)}$$

The electric field updating equation sets are given by:

$$E_x\Big|_{i+1/2,j,k}^{n+1}=\left(\frac{1-\frac{\sigma.\Delta t}{2\varepsilon}}{1+\frac{\sigma.\Delta t}{2\varepsilon}}\right)E_x\Big|_{i+1/2,j,k}^{n}$$

$$+\left(\frac{\frac{\Delta t}{\varepsilon}}{1+\frac{\sigma\,\Delta t}{2\varepsilon}}\right)\left(\begin{array}{c}\frac{H_z\,|^{n+1/2}_{i+1/2,j+1,k+1/2}-H_z\,|^{n+1/2}_{i+1/2,j,k+1/2}}{\Delta y}\\ -\frac{H_y\,|^{n+1/2}_{i+1/2,j,k+3/2}-H_y\,|^{n+1/2}_{i+1/2,j,k+1/2}}{\Delta z}\end{array}\right) \quad \textbf{(3-10.a)}$$

$$E_y\,|^{n+1}_{i,j+1/2,k}=\left(\frac{1-\frac{\sigma.\Delta t}{2\varepsilon}}{1+\frac{\sigma\,\Delta t}{2\varepsilon}}\right)E_y\,|^{n}_{i,j+1/2,k}$$

$$+\left(\frac{\frac{\Delta t}{\varepsilon}}{1+\frac{\sigma.\Delta t}{2\varepsilon}}\right)\left(\begin{array}{c}\frac{H_x\,|^{n+1/2}_{i,j+1/2,k+3/2}-H_x\,|^{n+1/2}_{i,j+1/2,k+1/2}}{\Delta z}\\ -\frac{H_z\,|^{n+1/2}_{i+3/2,j+1/2,k}-H_z\,|^{n+1/2}_{i+1/2,j+1/2,k}}{\Delta x}\end{array}\right) \quad \textbf{(3-10.b)}$$

$$E_z\,|^{n+1}_{i,j,k+1/2}=\left(\frac{1-\frac{\sigma.\Delta t}{2\varepsilon}}{1+\frac{\sigma\,\Delta t}{2\varepsilon}}\right)E_z\,|^{n}_{i,j,k+1/2}$$

$$+\left(\frac{\frac{\Delta t}{\varepsilon}}{1+\frac{\sigma.\Delta t}{2\varepsilon}}\right)\left(\begin{array}{c}\frac{H_y\,|^{n+1/2}_{i+1,j+1/2,k+1/2}-H_y\,|^{n+1/2}_{i,j+1/2,k+1/2}}{\Delta x}\\ -\frac{H_x\,|^{n+1/2}_{i,j+3/2,k+1/2}-H_x\,|^{n+1/2}_{i,j+1/2,k+1/2}}{\Delta y}\end{array}\right) \quad \textbf{(3-10.c)}$$

From the above expressions, we can see that the new value of any electromagnetic field vector component at any point depends only upon its previous value, the previous value of the adjacent points of the other field vector components.

3.4 Perfect Matched Layer

3.4.1 Introduction

For open space problems, the size of volume simulated by FDTD is limited by computer memory. There are two methods to deal with such limitation. The first method is analytical formulation that works on simulating the extension lattice to infinity. The second method is Absorbing Boundary Condition (ABC) method, which assumes that waves are completely absorbed on the boundary by artificial materials leaving no reflection back to computational space. The ABC method is widely used and can be applied to most situations. In ABC method, EM waves are absorbed in the outer boundary of the computation lattice, which is an analogue to the walls of an anechoic chamber. PML firstly presented and developed by J.P. Berenger **[10]**, is one of the most flexible and efficient ABC methods. J.P. Berenger's method is basically the truncation of the computational domain by a layer that absorbs impinging plane waves with no reflection, irrespective of their frequency and angle of incidence. Using PML method, the plane waves of arbitrary incident angle, polarization, and frequency are matched at the boundary. This method is quite a powerful tool in FDTD techniques, but has one main disadvantage: Maxwell's equations must be modified. This will result in a new set of equations with 12-vector field components satisfying coupled second-order partial differential equations in 3D problems. This will result additional memory requirements and problems of modifying electric and magnetic field values at the interface of PML and the computation domain.

In fact, a PML is a dispersive medium with intrinsic wave impedance equals to the wave impedance of a vacuum and the phase velocity in this medium is equal to vacuum velocity. This medium also has electrical and magnetic attenuation parts so that the wave magnitude is attenuated exponentially.

Following the work of J.P. Berenger, Uniaxial PML (UPML), a more general form of PML, is proposed. In the outbound of the computation domain, an imaginary uniaxial anisotropic medium has both magnetic and electric permittivity tensors. The losses of the tensor in the medium make it a perfectly matched absorbing medium. Gedney first presented this method in 1995 and published it in 1996 **[25].** It is an unsplit method and obeys the formulation of Maxwell's equations. Extensive research concerning UPML has been performed. In fact, the above two methods are similar, as UPML can develop the same wave equation using Berenger's method **[26]**. Although the PML concept was originally introduced as a mesh truncation method for FDTD simulation, its introduction of anisotropic material medium generates new research interests in this field. The challenge now is to physically realize PML.

Some difficulties exist for UPML: its programming is difficult; for inhomogeneous mediums, PML' conductivity varies with the medium, requiring more memory and rendering the program increasingly complex; for dispersive or anisotropic mediums, it is difficult to realize a "seamless" transition from the main problem space to the PML.

In 1996 D. M. Sullivan presented a simplified PML **[27].** The modifications

include the introduction of factious conductivity, and the introduction of some parameters to replace varying conductivity in the PML. This method is easy to program, easy to realize a "seamless" transition for dispersive or anisotropic mediums and PML parameters will not change if the medium is inhomogeneous.

Nevertheless, the simplified PML does have some disadvantages. Because of the introduced parameters, there is no way to predict the reflection from the boundary of PML. While the original PML or UPML have this ability. Also because we cannot control the reflection, optimal PML parameters may not be controlled.

An improvement about the simplified PML is presented and used in this research. This method is easily matched to anisotropic or dispersive mediums and has predictable reflections from the boundary, which is similar to Zhao's MIPML that uses split-field expressions, but this method realized in non-split expressions. Details about this method and formulation development are discussed in appendix.

3.4.2 Approach of Realizing PML in 3D

Although this is a simplified PML method, it is still difficult to realize in 3D; debugging the errors is particularly so. To make it easy, recall that any EM wave can be treated as a TM wave plus a TE wave **[6]**; then we can realize a TM mode-PML program first, and then go to TE mode. After both are functioning correctly, we can easily combine them to realise a complete PML code.

Under 2D conditions, directional conductivity $\sigma x(x)$ exist only in the lower and upper regions of PML along the x-axis and directional conductivity $\sigma y(y)$ exists only in the lower and upper regions of PML along the y-axis.

Figure 3-4 can be an aid in our understanding of the concept of PML. In the corner region, we can see that both conductivities are existed in the corner region.

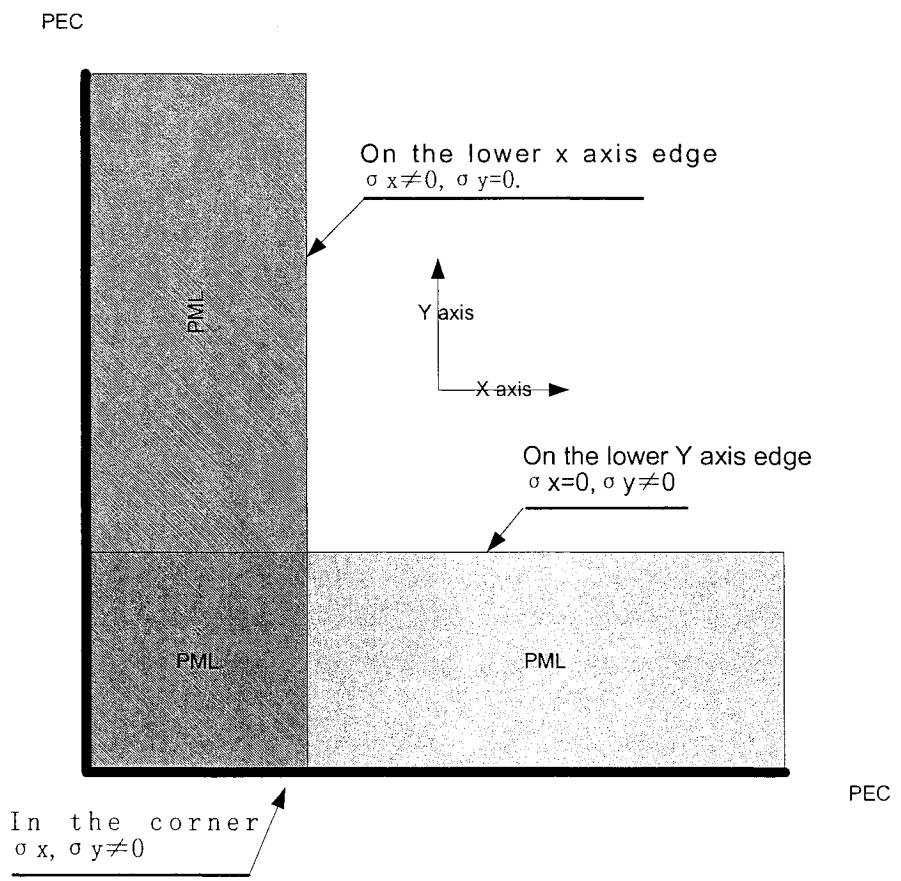

Figure 3-4: PML in the corner region

Maxwell's equations may be written as the following forms, for **TM** mode:

$$j\omega(1+\frac{\sigma(x)}{j\omega\varepsilon_0})(1+\frac{\sigma(y)}{j\omega\varepsilon_0})D_z = C_0(\frac{\partial Hy}{\partial x}-\frac{\partial Hx}{\partial y}); \qquad \textbf{(3-11)}$$

$$j\omega(1+\frac{\sigma(x)}{j\omega\varepsilon_0})^{-1}(1+\frac{\sigma(y)}{j\omega\varepsilon_0})B_x = -C_0(-\frac{\partial Ez}{\partial y}); \quad \textbf{(3-12)}$$

$$j\omega(1+\frac{\sigma(x)}{j\omega\varepsilon_0})(1+\frac{\sigma(y)}{j\omega\varepsilon_0})^{-1}B_y = -C_0(-\frac{\partial Ez}{\partial x}); \quad \textbf{(3-13)}$$

The solutions are given by the following equations:

$$\begin{aligned} D_z\big|_{i,j}^{n+1} &= gi3(i)\cdot gj3(j)\cdot D_z\big|_{i,j}^{n} \\ &+ gi2(i)\cdot gj2(j)\cdot c_0\cdot\Delta t \\ &\times\left[\frac{H_y\big|_{i+1/2,j}^{n+1/2} - H_y\big|_{i-1/2,j}^{n+1/2}}{\Delta x} - \frac{H_x\big|_{i,j+1/2}^{n+1/2} - H_x\big|_{i,j-1/2}^{n+1/2}}{\Delta y}\right]; \end{aligned} \quad \textbf{(3-14)}$$

In equation 3-14, the definitions of *gi2(i), gi3(i), gj2(j),*and *gj3(j)* can be found in appendix from equation A-68 to equation A-76. C_0 is the speed of light in vacuum.

$$\begin{aligned} B_x\big|_{i,j+1/2}^{n+1/2} &= fj3(j+1/2)\cdot B_x\big|_{i,j+1/2}^{n-1/2} \\ &+ fj2(j+1/2)\times c_0\Delta t \\ &\times\left[-\left(\frac{E_z\big|_{i,j+1}^{n} - E_z\big|_{i,j}^{n}}{\Delta y}\right) + fi1(i)\times\sum_{t=1}^{n} -\left(\frac{E_z\big|_{i,j+1}^{n} - E_z\big|_{i,j}^{n}}{\Delta y}\right)\right] \end{aligned} \quad \textbf{(3-15)}$$

$$\begin{aligned} B_y\big|_{i+1/2,j}^{n+1/2} &= fi3(i+1/2)\cdot B_y\big|_{i+1/2,j}^{n-1/2} \\ &+ fi2(i+1/2)\times c_0\Delta t \\ &\times\left[-\left(\frac{E_z\big|_{i+1,j}^{n} - E_z\big|_{i,j}^{n}}{\Delta x}\right) + fj1(j)\times\sum_{t=1}^{n} -\left(\frac{E_z\big|_{i+1/2,j}^{n} - E_z\big|_{i,j}^{n}}{\Delta x}\right)\right] \end{aligned} \quad \textbf{(3-16)}$$

In equation 3-15 and equation 3-16, the definitions of *fi1(i),fi2(i), fi3(i), fj1(j),fj2(j),*and *fj3(j)* can be found in appendix from equation A-77 to equation A-85. C_0 is the speed of light in vacuum.

For **TE** mode, Maxwell's equations can be written as the following forms:

$$j\omega(1+\frac{\sigma(x)}{j\omega\varepsilon_0})(1+\frac{\sigma(y)}{j\omega\varepsilon_0})B_z = -C_0(\frac{\partial Ex}{\partial y}-\frac{\partial Ey}{\partial x}); \quad \textbf{(3-17)}$$

$$j\omega(1+\frac{\sigma(x)}{j\omega\varepsilon_0})^{-1}(1+\frac{\sigma(y)}{j\omega\varepsilon_0})D_x = C_0(\frac{\partial Hz}{\partial y}); \quad \textbf{(3-18)}$$

$$j\omega(1+\frac{\sigma(x)}{j\omega\varepsilon_0})(1+\frac{\sigma(y)}{j\omega\varepsilon_0})^{-1}D_y = C_0(-\frac{\partial Hz}{\partial x}); \quad \textbf{(3-19)}$$

The solutions are given by the following equations:

$$\begin{aligned} B_z\big|^{n+1/2}_{i+1/2,j+1/2} &= fi3(i+1/2)\cdot fj3(j+1/2)\cdot B_z\big|^{n-1/2}_{i+1/2,j+1/2} \\ &+ fi2(i+1/2)\cdot fj2(j+1/2)\cdot c_0\cdot\Delta t \\ &\times\left[\left(\frac{E_y\big|^n_{i+1,j+1/2}-E_y\big|^n_{i,j+1/2}}{\Delta x}\right)-\left(\frac{E_x\big|^n_{i+1/2,j+1}+E_x\big|^n_{i+1/2,j}}{\Delta y}\right)\right]; \end{aligned} \quad \textbf{(3-20)}$$

In equation 3-20, the definitions of *fi2(i), fi3(i), fj2(j)* and *fj3(j)* can be found in appendix from equation a-77 to equation a-85. C_0 is the speed of light in vacuum.

$$\begin{aligned} D_x\big|^{n+1}_{i+1/2,j} &= gj3(j)\cdot D_x\big|^n_{i+1/2,j} \\ &+gj2(j)\cdot c_0\cdot\Delta t \\ &\times\left[\left(\frac{H_z\big|^{n+1/2}_{i+1/2,j+1/2}-H_z\big|^{n+1/2}_{i+1/2,j-1/2}}{\Delta y}\right)+gi1(i+1/2)\times\sum_{t=1}^{n}\left(\frac{H_z\big|^{n+1/2}_{i+1/2,j+1/2}-H_z\big|^{n+1/2}_{i+1/2,j-1/2}}{\Delta y}\right)\right] \end{aligned} \quad \textbf{(3-21)}$$

$$\begin{aligned} D_y\big|^{n+1}_{i,j+1/2} &= gi3(i)\cdot D_y\big|^n_{i,j+1/2} \\ &+gi2(i)\cdot c_0\Delta t \\ &\left[-\left(\frac{H_z\big|^{n+1/2}_{i+1/2,j+1/2}-H_z\big|^{n+1/2}_{i-1/2,j+1/2}}{\Delta x}\right)+gj1(j+1/2)\times\sum_{t=1}^{n}-\left(\frac{H_z\big|^{n+1/2}_{i+1/2,j+1/2}-H_z\big|^{n+1/2}_{i-1/2,j+1/2}}{\Delta x}\right)\right] \end{aligned} \quad \textbf{(3-22)}$$

In equation 3-21 and equation 3-22, the definitions of *gi1(i),gi2(i), gi3(i), gj1(j),gj2(j)and gj3(j)* can be found at appendix from equation a-68 to equation a-76. C_0 is the speed of light in vacuum.

This is the simulation result for TE mode.

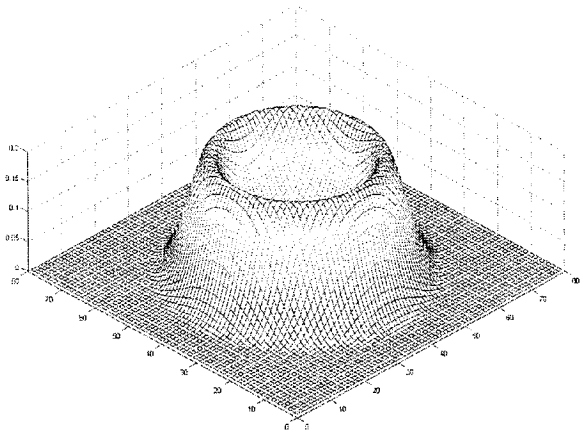

Figure 3-5 : TE Wave propagation from center to the boundary.
Length in x-axis is 80Δx. Length in y-axis is 80Δy. Δx=Δy=0.0037m, Time steps=80. Source located in the center.

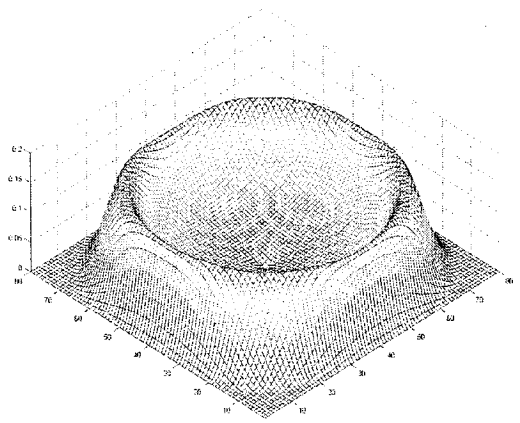

Figure 3-6: TE wave arrived at the PML boundary; some field components had been absorbed.
Length in x-axis is 80Δx. Length in y-axis is 80Δy. Δx=Δy=0.0037m, Time steps=100. Source located in the center.

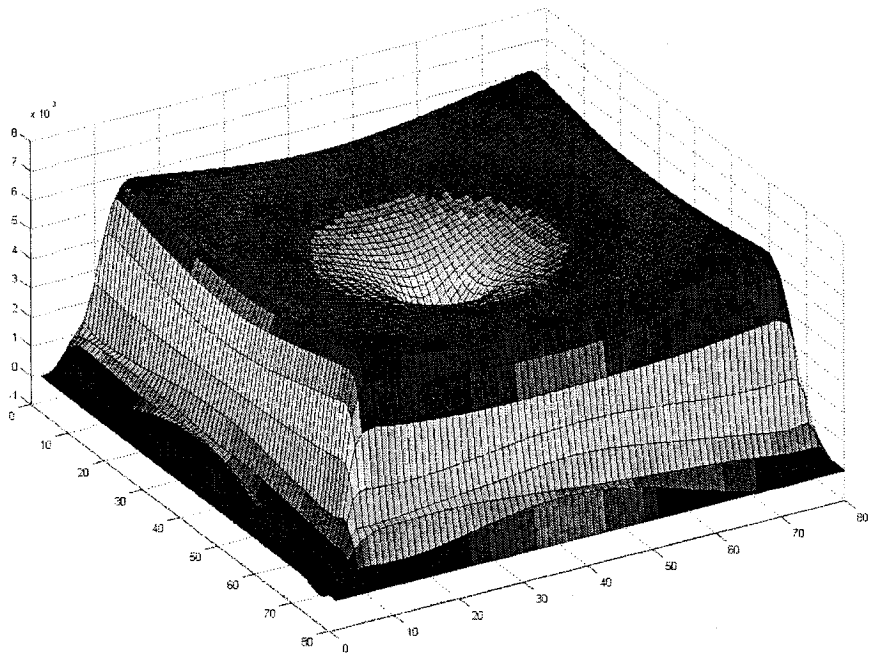

Figure 3-7: Stable statues of the electric field.
Length in x-axis is 80Δx. Length in y-axis is 80Δy. Δx=Δy=0.0037m, Time steps=1000. Source located in the center.

3.5 The choice of spatial grid and time step

For a given FDTD model in applications, there are some rules that restrict our choice of the proper grid parameters **[15]**. The spatial increment must be small enough so that the shortest wavelength must correspond to at least five unit cells. FDTD meshes should represent well enough geometrical details. The smallest geometrical dimensions should be at least two to three unit cells.

To satisfy the stability requirements of the center difference algorithm, there is a relation between the time step and the space discretization. If the spatial discretization is above 10 cells per wavelength, the numerical dispersion will be quite high **[11].** In some particularly sensitive cases, the requirement is at least 20 cells per wavelength in order to obtain good accuracy. The time-step size depends on the spatial cell size and the current stability condition. For a 3D case,

$$\Delta t \leq \frac{1}{c\sqrt{\frac{1}{\Delta x^2}+\frac{1}{\Delta y^2}+\frac{1}{\Delta z^2}}}, \qquad \textbf{(3-23)}$$

c is the speed of light in vacuum.

Since a shorter time step does not improve accuracy, we usually choose Δt close to the stability limit. If $\Delta x=\Delta y=\Delta z$, the maximum time step can be $\Delta t = \frac{\Delta}{c\sqrt{3}}$, or, for simplicity in programming, we can chose

$$\Delta t = \frac{\Delta}{2c} \qquad \textbf{(3-24)}$$

3.6 The choice of source

The excitations in FDTD simulation deserve a special attention. The updating makes sense only if there is no zero initial condition or energy source.

There are many source models available; the simplest one is the so-called hard source. At a source location, certain field components will not follow updating equations

and are pre-defined in the time domain. At other locations, field components are updated normally. The condition of the hard source causes any field components that arrive at the hard source location reflected back perfectly. This is an example of a hard source:

$$E_z(x,t) = f(x,t) \tag{3-25}$$

We defined the E_z component as being equal to $f(x,t_0)$ when $t = t_0$. $f(x,t_0)$ is the source function.

A hard source maybe represents an obstacle for application in some problems. To make the source transparent, an additional source term can be added at the source position which is called soft source. This is an example of soft source.

$$E_z(x,t) = E_z(x,t) + f(x,t) \tag{3-26}$$

To simulate a Hertz dipole is simply to excite a single electric field component at one location. If we excite a magnetic dipole, a source function is applied to the single magnetic field.

A plane wave source is a frequently used source. The simplest way of approximating a plane wave is to choose a field component along a line and apply the source function. This is accurate in 2D. It is also easy and convenient to realize in 3D, but is not an accurate method. The initial condition wave source is an accurate method to generate a plane wave, but it enlarges the memory requirement and is difficult to realize in dispersive mediums that limit its application. One accurate and widely used method of the plane wave generation method is the Total Field/Scattering Field method **[11]**. This method is discussed in the next section.

Any shaped sources can be used to represent the input source including sinusoidal or Gaussian pulse. A Gaussian pulse has the advantage of providing frequency from DC to the desired cut-off frequency, while the sinusoidal source can provide single-frequency input, which is useful in certain cases.

A Gaussian pulse in continuous form can be expressed as:

$$f(t) = \exp(-\frac{(t-t_0)^2}{\tau^2}) \tag{3-27}$$

t_0 : the value of time delay for the source

τ : the value of time spread of the Gaussian pulse; it can be used to control the bandwidth of Gaussian pulse.

If we rewrite this function in discrete form, it becomes:

$$f(n\cdot\Delta t) = \exp(-\frac{(n\cdot\Delta t - m\cdot\Delta t)^2}{(s\cdot\Delta t)^2}) = \exp(-\frac{(n-m)^2}{s^2}) \tag{3-28}$$

n is the computation time steps

m is time steps of time delay for the Gaussian pulse

s is the time steps of width for the Gaussian pulse

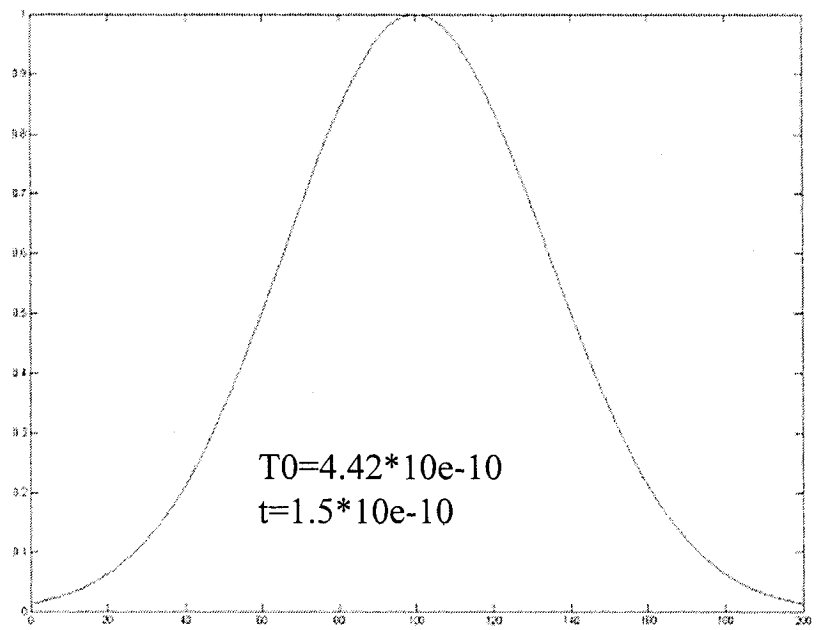

Gaussian Source

Figure 3-8: Gaussian Pulse (Discrete time sample values)

Figure 3-8 shows an example of a Gaussian pulse. `T0` is the time-spread width; `t` is the time delay. The bandwidth of a Gaussian pulse is determined by the time-spread width.

The frequency domain response of a Gaussian pulse is:

$$F(f) = \tau\sqrt{\pi}\exp\left(-(\pi f)^2\tau^2\right)\cdot\exp(-j2\pi f t_0) \qquad \textbf{(3 -29)}$$

The discrete Fourier transform of a Gaussian pulse is shown in Figure 3-9.

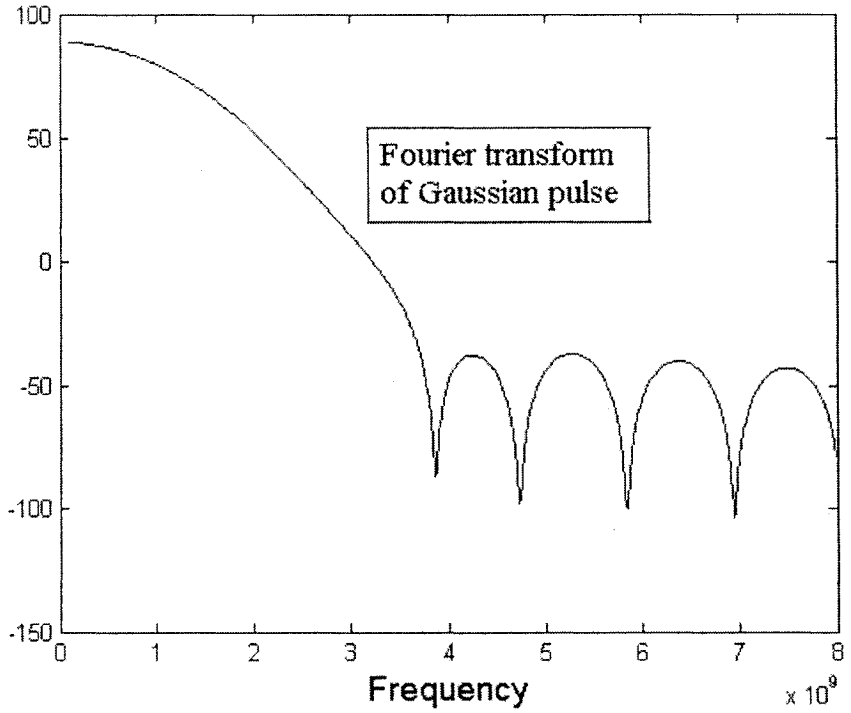

Figure 3-9: Fourier transforms amplitude of the Gaussian pulse

There is one disadvantage for the Gaussian source. There is a DC component in the frequency domain, which is not needed in some applications. To eliminate the DC component, we can use a modulated Gaussian source, which is a Gaussian pulse modulated by a sinusoidal signal that contains zero DC component, see figure 3-9. In the frequency domain, the central position of the spectrum of a Gaussian pulse is moved to the central frequency of f_m.

$$f(t) = \sin(2\pi f_m) \cdot \exp(-\frac{(t-t_0)^2}{\tau^2}) \qquad \textbf{(3-30)}$$

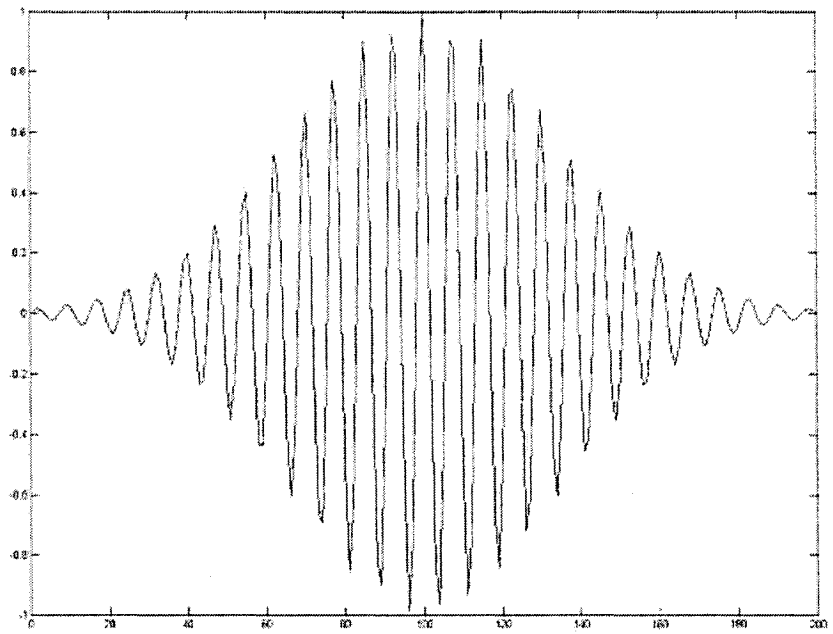

Time Steps

Figure 3-10: Modulated Gaussian Pulse.
Modulate frequency=3×10^{10}, T0=4.41×10^{-10}, t=1.5×10^{-10}

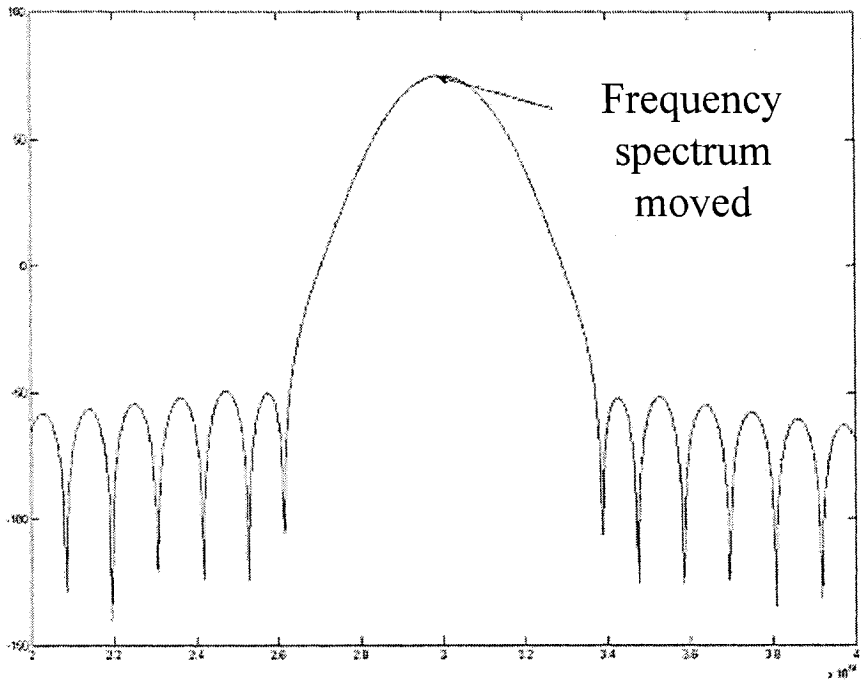

Figure 3-11: Fourier transformation amplitudes of Modulated Gaussian Pulse.

3.7 Total field/ Scattered field method

The Total Field / Scattered Field (TF/SF) method avoids difficulties caused by either the hard source or the initial boundary condition approach. It successfully permits FDTD modeling of arbitrary plane wave propagation **[11]**. The basic concept of TF/SF is described below.

The Total Field /Scattered Field approach is based on the linearity of Maxwell's equation. The electric and magnetic fields can be treated as total fields composed of incident wave plus scattered wave. The incident wave can be treated as a source and the scattered wave can be treated as the reaction to the incident wave and objects.

$$\vec{E}_{total} = \vec{E}_{incident} + \vec{E}_{scattered}; \quad \textbf{(3-31.a)}$$

$$\vec{H}_{total} = \vec{H}_{incident} + \vec{H}_{scattered}; \quad \textbf{(3-31.b)}$$

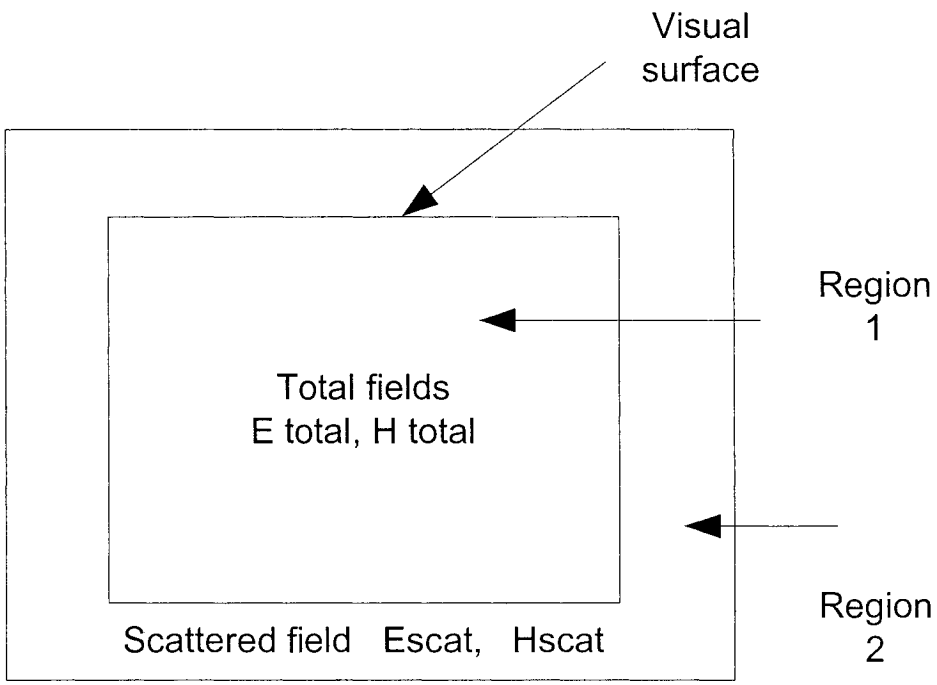

Figure 3-12: Total Field and Scattered field Concept In 2-D

Figure 3-12 illustrates this concept in the application of FDTD. Two regions separate the mesh, region one is composed of the total wave, and region two is composed of the scattered wave. Assuming that there is a visual surface existing in the interface of the two regions, then FDTD can work separately in both regions. The interface need a

special treatments so that we can apply FDTD successfully across the whole region. Assuming only $\mathbf{E_z}$, $\mathbf{H_y}$ exist, here is the interface along the x-axis across the region.

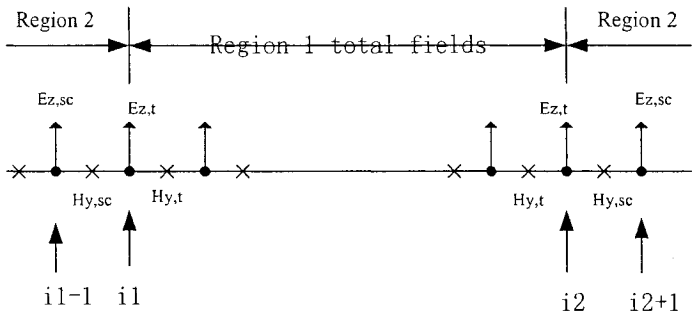

Figure 3-13: Grid Transition Scattered field and Total field

In region one or two, FDTD algorithm will not change because the linearity of Maxwell's equations. The only thing is: how to deal with the interface. In point `i1`, $E_{z,total}\,|_{i1}^{n+1}$ can be expressed as

$$E_{z,total}\,|_{i1}^{n+1} = E_{z,total}\,|_{i1}^{n} + \frac{\Delta t}{\varepsilon_0 \Delta x}\left(H_{y,total}\,|_{i1+1/2}^{n+1/2} - H_{y,total}\,|_{i1-1/2}^{n+1/2}\right) \quad \textbf{(3-32)}$$

Since the total field can be decomposed into a scattered field and an incident field. Therefore, $H_{y,total}\,|_{i1-1/2}^{n+1/2}$ can be expressed as

$$H_{y,total}\,|_{i1-1/2}^{n+1/2} = H_{y,incident}\,|_{i1-1/2}^{n+1/2} + H_{y,scattered}\,|_{i1-1/2}^{n+1/2} \quad \textbf{(3-33)}$$

Then we can rewrite the expression of $E_{z,total}\,|_{i1}^{n+1}$ as in the form,

$$E_{z,total}\,|_{i1}^{n+1} = E_{z,total}\,|_{i1}^{n} + \frac{\Delta t}{\varepsilon_0 \Delta x}\left(H_{y,total}\,|_{i1+1/2}^{n+1/2} - H_{y,scattered}\,|_{i1-1/2}^{n+1/2}\right)$$

$$- \frac{\Delta t}{\varepsilon_0 \Delta x} H_{y,incident}\,|_{i1-1/2}^{n+1/2} \quad \textbf{(3-34)}$$

The TF/SF method can be integrated into our other parts, by making the

simplification that $\vec{E}' = \sqrt{\frac{\varepsilon_0}{\mu_0}}\vec{E}$. This simplification leads to

$$E'_{z,total}|_{i1}^{n+1} = E'_{z,total}|_{i1}^{n} + \frac{\Delta t}{\sqrt{\varepsilon_0 \mu_0}\,\Delta x}\left(H_{y,total}|_{i1+1/2}^{n+1/2} - H_{y,scattered}|_{i1-1/2}^{n+1/2}\right)$$

$$- \frac{\Delta t}{\sqrt{\varepsilon_0 \mu_0}\,\Delta x} H_{y,incident}|_{i1-1/2}^{n+1/2} \quad . \qquad \textbf{(3-35)}$$

Knowing the incident wave value, the FDTD algorithm can carry on through the whole space. The other border will be treated the same way. The technique to generate an incident plane wave is simple. First, a 1D wave that can be treated as an incident wave should be produced. Assuming that this wave propagates through the whole space, we can use the TF/SF method to generate a plane wave in the 2D or the 3D space. The complete set of 3D formulations can be found in **[11]**. Figure 3-14 and figure 3-15 show an example of plane wave generation and disappearing on the boundary of Total field/Scattered field in one slice cut for a 3D space.

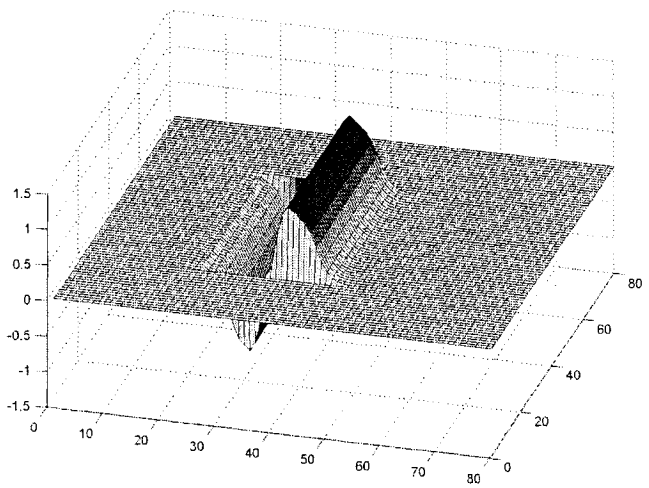

Figure 3-14: Plane wave generating from the left boundary of TF/SF

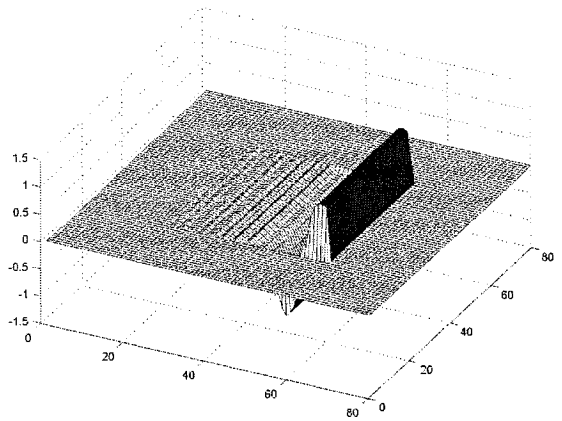

Figure 3-15: Plane wave disappearing on the left boundary

3.8 Fourier transform in FDTD method

When we choose sources that contain multiple frequency components, the outputs of electric fields or magnetic fields contain in multiple frequency components, which are signals in the time domain. In many applications, we need the output in the frequency domain. The Fourier transform is needed to analyse the time domain signal to obtain the frequency domain responses. The general form of the Fourier transform is:

$$E(f_0) = \int E(t) \cdot e^{-j2\pi f_0 t} dt \qquad \textbf{(3-36)}$$

If the above transformation is carried at a discrete time signal, it can be expressed as

$$E(f_0) = \sum_{n=0}^{n} E(n) \cdot e^{-j2\pi f_0 (n \cdot \Delta t)} \qquad \textbf{(3-37)}$$

Or we can write it in the form

$$E(f_0) = \sum_{n=0}^{n} E(n) \cdot \cos(2\pi f_0 \cdot \Delta t \cdot n) - j \sum_{n=0}^{n} E(n) \cdot \sin(2\pi f_0 \cdot \Delta t \cdot n) \qquad \textbf{(3-38)}$$

Δt: the time increment

f_0 : the frequency of the Fourier transform being performed

n : the total number of field value

Detail information concerning Fourier transform can be found in **[28]**.

Charter Four: FDTD for Anisotropic material

4.1 Introduction

Certain natural materials, such as crystals, and man-made materials, such as fibres and ferrites, exhibit anisotropic behaviours. Among these materials, the relationship of **D** components versus **E** components and **B** components versus **H** components is no longer one-to-one. For many materials, the dielectric constant of electric or magnetic or both is anisotropic. "Anisotropic" indicates that the dielectric constant is different along the different crystal directions with respect to the crystal axes. This should be taken into account when they are used in microstrip and dielectric antennas, dielectric feed networks or non-reciprocal structures. Although anisotropic property is sometimes a disadvantage, it also can be a new control method of design. This is the main reason that we are considering anisotropic materials in this study. A full tensor property is the most generalized situation for the anisotropic medium. Numerical methods are especially useful for such analysis. The FDTD method can easily integrate anisotropic properties into its algorithm.

In this chapter, we present the formulation and special treatments of the 3D FDTD method for materials with arbitrary anisotropic permittivity and permeability tensors. Contrary to other methods, this approach is separated into two parts: dielectric

properties parts and wave marching parts. Dielectric anisotropic properties are realized through electric properties----relationships of electric flux versus electric field and magnetic properties---relationships of magnetic flux versus magnetic field. EM wave marching is realized through relationships of magnetic field versus electric flux and electric field versus magnetic flux.

4.2 The FDTD expression for anisotropic materials with full tensor properties.

For the general anisotropic materials, the properties of the medium are expressed in a tensor form. We can rewrite the general form of Maxwell's equations for anisotropic materials as:

$$\frac{\partial \vec{D}}{\partial t} = \nabla \times \vec{H} \qquad \textbf{(4-1.a)}$$

$$\vec{D}(\omega) = [\varepsilon] \bullet \vec{E}(\omega) \Rightarrow \vec{E}(\omega) = [\varepsilon]^{-1} \vec{D} \qquad \textbf{(4-1.b)}$$

$$\frac{\partial \vec{B}}{\partial t} = \nabla \times \vec{E} \qquad \textbf{(4-1.c)}$$

$$\vec{B}(\omega) = [\mu] \bullet \vec{H}(\omega) \Rightarrow \vec{H}(\omega) = [\mu]^{-1} \vec{B} \qquad \textbf{(4-1.d)}$$

Here in equation (4-1), the definition of material properties is:

$$[\varepsilon] = \begin{bmatrix} \varepsilon_{xx} & \varepsilon_{xy} & \varepsilon_{xz} \\ \varepsilon_{yx} & \varepsilon_{yy} & \varepsilon_{yz} \\ \varepsilon_{zx} & \varepsilon_{zy} & \varepsilon_{zz} \end{bmatrix} \Rightarrow [\varepsilon]^{-1} = \frac{1}{\Lambda} \begin{bmatrix} C_{xx} & C_{xy} & C_{xz} \\ C_{yx} & C_{yy} & C_{yz} \\ C_{zx} & C_{zy} & C_{zz} \end{bmatrix} \qquad \textbf{(4-2.a)}$$

$$\Lambda = |\varepsilon| = (\varepsilon_{xx}\varepsilon_{yy}\varepsilon_{zz} + \varepsilon_{xy}\varepsilon_{yz}\varepsilon_{zx} + \varepsilon_{xz}\varepsilon_{yz}\varepsilon_{zy} + \varepsilon_{xz}\varepsilon_{yz}\varepsilon_{zy} - \varepsilon_{xz}\varepsilon_{yy}\varepsilon_{zx} - \varepsilon_{xy}\varepsilon_{yz}\varepsilon_{zz} - \varepsilon_{xx}\varepsilon_{yz}\varepsilon_{zy})\varepsilon_0 \qquad \textbf{(4-2.b)}$$

$$[\mu]=\begin{bmatrix}\mu_{xx} & \mu_{xy} & \mu_{xz}\\ \mu_{yx} & \mu_{yy} & \mu_{yz}\\ \mu_{zx} & \mu_{yz} & \mu_{zz}\end{bmatrix}\Rightarrow[\mu]^{-1}=\frac{1}{\Delta}\begin{bmatrix}d_{xx} & d_{xy} & d_{xz}\\ d_{yx} & d_{yy} & d_{yz}\\ d_{zx} & d_{yz} & d_{zz}\end{bmatrix} \qquad \textbf{(4-2.c)}$$

$$\Delta=|\mu|=(\mu_{xx}\mu_{yy}\mu_{zz}+\mu_{xy}\mu_{yz}\mu_{zx}+\mu_{xz}\mu_{yz}\mu_{zy})\mu_0$$

$$+\mu_{xz}\mu_{yz}\mu_{zy}-\mu_{xz}\mu_{yy}\mu_{zx}-\mu_{xy}\mu_{yz}\mu_{zz}-\mu_{xx}\mu_{yz}\mu_{zy} \qquad \textbf{(4-2.d)}$$

The curl equation forms do not change if we express the medium properties separately. It is only required to regulate the relation of the electric field versus electric flux and the magnetic field versus magnetic flux. The relationships of electric field versus electric flux are:

$$E_x\Big|_{i+1/2,j,k}^{n+1}=\frac{C_{xx}}{\Lambda}D_x^{n+1}\Big|_{i+1/2,j,k}+\frac{C_{xy}}{\Lambda}D_y^{n+1}\Big|_{i+1/2,j,k}+\frac{C_{xz}}{\Lambda}D_z^{n+1}\Big|_{i+1/2,j,k} \qquad \textbf{(4-3.a)}$$

$$E_y\Big|_{i,j+1/2,k}^{n+1}=\frac{C_{yx}}{\Lambda}D_x^{n+1}\Big|_{i,j+1/2,k}+\frac{C_{yy}}{\Lambda}D_y^{n+1}\Big|_{i,j+1/2,k}+\frac{C_{yz}}{\Lambda}D_z^{n+1}\Big|_{i,j+1/2,k} \qquad \textbf{(4-3.b)}$$

$$E_z\Big|_{i,j,k+1/2}^{n+1}=\frac{C_{zx}}{\Lambda}D_x^{n+1}\Big|_{i,j,k+1/2}+\frac{C_{zy}}{\Lambda}D_y^{n+1}\Big|_{i,j,k+1/2}+\frac{C_{zz}}{\Lambda}D_z^{n+1}\Big|_{i,j,k+1/2} \qquad \textbf{(4-3.c)}$$

The position of each component in one unit within the 3D grid Cartesian coordinates is shown in figure 4-1.

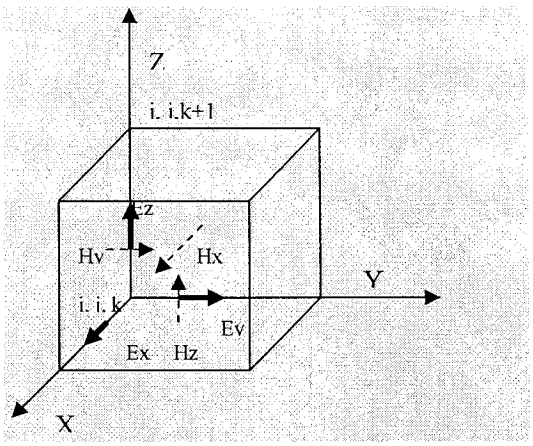

Figure 4-1: E and H grid position in 3-D

It is well known that the electric field or the electric flux has specific positions in Yee's grid; the location should be expressed as follows: $E_z(D_z)\big|_{i,j,k+1/2}$ $E_y(D_y)\big|_{i,j+1/2,k}$ $E_x(D_x)\big|_{i+1/2,j,k}$ and $H_x(B_x)\big|_{i,j+1/2,k+1/2}$ $H_y(B_y)\big|_{i+1/2,j,k+1/2}$ $H_z(B_z)\big|_{i+1/2,j+1/2,k}$. Otherwise, we cannot obtain correct results from our program. From figure 4-1 we notice that $\mathbf{D_y}$ and $\mathbf{D_z}$ in **(4-3.a)** do not fit for the FDTD grid, nor do $\mathbf{D_x}$, $\mathbf{D_z}$; $\mathbf{D_x}$, $\mathbf{D_y}$ in **(4-3.b)**, **(4-3.c)**. One of the methods for solving the above expression is using the finite different method, as discussed in Chapter Three, to obtain their correct expression. Equation **(4-3)** demonstrates the modification of $\mathbf{D_x}$, **Dy**, and $\mathbf{D_z}$.

In equation **(4-3.a)**, **Dy** and $\mathbf{D_z}$ can be expressed as:

$$D_y\big|_{i+\frac{1}{2},j,k} = \frac{1}{4}\left(D_y\big|_{i,j-1/2,k} + D_y\big|_{i,j+1/2,k} + D_y\big|_{i+1,j-1/2,k} + D_y\big|_{i+1,j+1/2,k}\right) \qquad \textbf{(4-4.a)}$$

$$D_z\big|_{i+\frac{1}{2},j,k} = \frac{1}{4}\left(D_z\big|_{i,j,k-1/2} + D_z\big|_{i,j,k+1/2} + D_z\big|_{i+1,j,k-1/2} + D_z\big|_{i+1,j,k+1/2}\right) \qquad \textbf{(4-4.b)}$$

In equation **(4-3.b)**, $\mathbf{D_x}$ and $\mathbf{D_z}$ can be expressed as:

$$D_x|_{i,j+1/2,k}=\frac{1}{4}\left(D_x|_{i-1/2,j,k}+D_x|_{i-1/2,j+1,k}+D_x|_{i+1/2,j+1,k}+D_x|_{i+1/2,j,k}\right) \quad \textbf{(4-5.a)}$$

$$D_z|_{i,j+1/2,k}=\frac{1}{4}\left(D_z|_{i,j+1,k+1/2}+D_z|_{i,j,k+1/2}+D_z|_{i,j+1,k-1/2}+D_z|_{i,j,k-1/2}\right) \quad \textbf{(4-5.b)}$$

In equation **(4-3.c)**, $\mathbf{D_x}$ and **Dy** can be expressed as:

$$D_x|_{i,j,k+1/2}=\frac{1}{4}\left(D_x|_{i+1/2,j,k}+D_x|_{i-1/2,j,k}+D_x|_{i+1/2,j,k+1}+D_x|_{i-1/2,j,k+1}\right) \quad \textbf{(4-6.a)}$$

$$D_y|_{i,j,k+1/2}=\frac{1}{4}\left(D_y|_{i,j+1/2,k}+D_y|_{i,j-1/2,k}+D_y|_{i,j+1/2,k+1}+D_y|_{i,j-1/2,k+1}\right) \quad \textbf{(4-6.b)}$$

The relationship of the magnetic field and magnetic flux is:

$$Hx\Big|_{i,j+1/2,k+1/2}^{n+3/2}=\frac{d_{xx}}{\Delta}Bx\Big|_{i,j+1/2,k+1/2}^{n+3/2}+\frac{d_{xy}}{\Delta}By\Big|_{i,j+1/2,k+1/2}^{n+3/2}+\frac{d_{xz}}{\Delta}Bz\Big|_{i,j+1/2,k+1/2}^{n+3/2} \quad \textbf{(4-7.a)}$$

$$Hy\Big|_{i+1/2,j,k+1/2}^{n+3/2}=\frac{d_{yx}}{\Delta}Bx\Big|_{i+1/2,j,k+1/2}^{n+3/2}+\frac{d_{yy}}{\Delta}By\Big|_{i+1/2,j,k+1/2}^{n+3/2}+\frac{d_{yz}}{\Delta}Bz\Big|_{i+1/2,j,k+1/2}^{n+3/2} \quad \textbf{(4-7.b)}$$

$$Hz\Big|_{i+1/2,j+1/2,k}^{n+3/2}=\frac{d_{zx}}{\Delta}Bx\Big|_{i+1/2,j+1/2,k}^{n+3/2}+\frac{d_{zy}}{\Delta}By\Big|_{i+1/2,j+1/2,k}^{n+3/2}+\frac{d_{zz}}{\Delta}Bz\Big|_{i+1/2,j+1/2,k}^{n+3/2} \quad \textbf{(4-7.c)}$$

Following the same idea, the modification of $\mathbf{B_y}$ and $\mathbf{B_z}$ in **(4-7.a)**

$$B_y|_{i,j+1/2,k+1/2}=\frac{1}{4}\left(B_y|_{i+1/2,j+1,k+1/2}+B_y|_{i+1/2,j,k+1/2}+B_y|_{i-1/2,j+1,k+1/2}+B_y|_{i-1/2,j,k+1/2}\right) \quad \textbf{(4-8.a)}$$

$$B_z|_{i,j+1/2,k+1/2}=\frac{1}{4}\left(B_z|_{i+1/2,j+1/2,k+1}+B_z|_{i+1/2,j+1/2,k}+B_z|_{i-1/2,j+1/2,k+1}+B_z|_{i-1/2,j+1/2,k}\right) \quad \textbf{(4-8.b)}$$

The modification of $\mathbf{B_x}$, $\mathbf{B_z}$ in **(4-7.b)**

$$B_x|_{i+1/2,j,k+1/2}=\frac{1}{4}\left(B_x|_{i+1,j+1/2,k+1/2}+B_x|_{i+1,j-1/2,k+1/2}+B_x|_{i,j+1/2,k+1/2}+B_x|_{i,j-1/2,k+1/2}\right) \quad \textbf{(4-9.a)}$$

$$B_z|_{i+1/2,j,k+1/2}=\frac{1}{4}\left(B_z|_{i+1/2,j+1/2,k+1}+B_z|_{i+1/2,j+1/2,k}+B_z|_{i+1/2,j-1/2,k+1}+B_z|_{i+1/2,j-1/2,k}\right) \quad \textbf{(4-9.b)}$$

The modification of $\mathbf{B_y}$, $\mathbf{B_z}$ in **(4-7.c)**

$$B_x|_{i+1/2,j+1/2,k}=\frac{1}{4}\left(B_x|_{i+1,j+1/2,k+1/2}+B_x|_{i,j+1/2,k+1/2}+B_x|_{i+1,j+1/2,k-1/2}+B_x|_{i,j+1/2,k-1/2}\right) \quad \textbf{(4-10.a)}$$

$$B_y|_{i+1/2,j+1/2,k}=\frac{1}{4}\left(B_y|_{i+1/2,j+1,k+1/2}+B_y|_{i+1/2,j+1,k-1/2}+B_y|_{i+1/2,j,k+1/2}+B_y|_{i+1/2,j,k-1/2}\right) \quad \textbf{(4-10.b)}$$

Now we can see that the updating part of the anisotropic part and the updating

part of PML are separate. There is no need to do logical judgments in the core updating part of the program, which could greatly increase the computation speed and reduce the complexity of the program.

4.3 PEC treatment

On the surface of PEC, the tangential electric field of E should be zero. To realize this, a straightforward method can be employed. This method can also be integrated into the main updating equation, and does not need special treatment. For example, for a PEC located at the k=k0 plane in Cartesian coordinates, the tangential electric field is E_x and E_y; therefore, we set these coefficients equal to zero, as a reference to equation **(4-3.a.b.c)**.

$$C_{xx}(i,j,k)=0; C_{xy}(i,j,k)=0; C_{xz}(i,j,k)=0 \qquad \textbf{(4-11.a)}$$

$$C_{yx}(i,j,k)=0; C_{yy}(i,j,k)=0; C_{yy}(i,j,k)=0 \qquad \textbf{(4-11.b)}$$

Here, we should notice that this part is located in the parameters-setting part; contrary to the method in it does not change the updating part **[17]**.

Special treatment: If the PEC is located on the ground plane, e.g. at the k=0, which is the start position of mesh, then the above equation will not be valid, as some of the points will be outside the mesh. In order to obtain the correct value of **D B**, a backward difference approximation is employed to get the value of $\mathbf{D_x}$, $\mathbf{D_y}$, $\mathbf{D_z}$; $\mathbf{B_x}$, $\mathbf{B_y}$, $\mathbf{B_z}$ fields as follows:

$$D_x\big|_{i+\frac{1}{2},j,0} = \left(2D_x\big|_{i+1/2,j,1} - D_x\big|_{i+1/2,j,2}\right) \quad \textbf{(4-12.a)}$$

$$D_y\big|_{i,j+1/2,0} = \left(2D_y\big|_{i,j+1/2,1} - D_x\big|_{i,j+1/2,2}\right) \quad \textbf{(4-12.b)}$$

$$D_z\big|_{i,j,1/2} = \left(2D_z\big|_{i,j,1+1/2} - D_z\big|_{i,j,2+1/2}\right) \quad \textbf{(4-12.c)}$$

$$B_x\big|_{i,j+1/2,1/2} = \left(2B_x\big|_{i,j+1/2,1+1/2} - B_x\big|_{i,j+1/2,2+1/2}\right) \quad \textbf{(4-13.a)}$$

$$B_y\big|_{i+1/2,j,1/2} = \left(2B_y\big|_{i+1/2,j,1+1/2} - B_y\big|_{i+1/2,j,2+1/2}\right) \quad \textbf{(4-13.c)}$$

$$B_z\big|_{i+1/2,j+1/2,0} = \left(2B_z\big|_{i+1/2,j+1/2,1} - B_z\big|_{i+1/2,j+1/2,2}\right) \quad \textbf{(4-13.c)}$$

4.4 FDTD expression for dispersive permeability

For a weakly magnetized ferrite absorber, the permeability can be expressed as a frequency-dependent function **[30]**. Frequency-dependent permeability can be expressed as:

$$\bar{\mu}_r = 1 + \frac{kf_1}{f_1 + jf} = \mu_r' - j\mu_r'' \quad \textbf{(4-14)}$$

k is the value of static magnetic susceptibility when the frequency is zero. μ_r' is the real part of permeability, and μ_r'' is the imaginary part of permeability.

In order to get the updating expression of permeability, we can use the Fourier Transform method, or a Z transform method to get the time domain expression of ferrite permeability.

Here, we can see clearly that the expression of permeability for weakly magnetized ferrite can be treated as the first order Debye medium **[13].** Using the Z

transform method, we can obtain the Z domain expression like this.

$$H(z) = \frac{B(z) - e^{-\Delta t/t0} \cdot Z^{-1} \cdot S(z)}{1 + \frac{x_1 \cdot \Delta t}{t_0}} \quad \textbf{(4-15-)}$$

$$S(z) = e^{-\Delta t/t0} \cdot Z^{-1} S(z) + \frac{x_1 \Delta t}{t_0} H(z) \quad \textbf{(4-16)}$$

In the updating form, the above equations are expressed as:

$$H^n = \frac{B^n - e^{-\Delta t.2\pi f1} \cdot S^{n-1}}{1 + k \cdot \Delta t \cdot 2\pi f_1} \quad \textbf{(4-17)}$$

$$S^n = e^{-\Delta t \cdot 2\pi f1} \cdot S^{n-1} + k \cdot \Delta t \cdot 2\pi f_1 \cdot H^n \quad \textbf{(4-18)}$$

From the above expression, we can realize the FDTD formulation for dispersive permeability in the relationship of magnetic flux and magnetic field; no other changes will be required.

4.5 FDTD expression for magnetized ferrite

When ferrite is subjected to a strong static magnetic biasing field, it becomes both strongly dispersive and anisotropic. The magnetic field of the EM wave is located in a direction other than the static biasing field; the permeability will depend on the strength of the biasing field, and the ferrites will be strongly anisotropic. If the static biasing field $\mathbf{H}_0$ is **Z** axis directed, the permeability of ferrite can be expressed as a tensor form by: **[6]**, **[13]**

$$\mu^*(\omega) = \mu_0 \tilde{\mu}(\omega) = \mu_0 \begin{bmatrix} 1+\chi_m(\omega) & -jk(\omega) & 0 \\ jk(\omega) & 1+\chi_m(\omega) & 0 \\ 0 & 0 & 1 \end{bmatrix} \tag{4-19}$$

Here

$$\chi_m(\omega) = \frac{(\omega_0 + j\omega\alpha)\omega_m}{(\omega_0 + j\omega\alpha)^2 - \omega^2} \tag{4-20}$$

$$k(\omega) = \frac{-\omega\omega_m}{(\omega_0 + j\omega\alpha)^2 - \omega^2} \tag{4-21}$$

$\omega_0 = \gamma_m H_0$ is the processional frequency

α is the damping constant, γ_m =28GHz/K0 the gyro magnetic ratio

H_0 is the static magnetic biasing field

$\omega_m = \gamma_m 4\pi m_0$ where m_0 is the static magnetization.

Using the time domain convolution method, the **Z** transform method, or magnetic motion equation method, we can have the expressions of magnetic flux and magnetic field in differential forms. Here we adopt the expression developed from the time domain convolution method. The only modification is $B^{n+1} - B^n = -\Delta t \cdot (\nabla \times E)$., which is used to fit for our method.

$$\begin{aligned} H_x^{n+1} = & \frac{1+x^0}{(1+x^0)^2+(k^0)^2} \times H_x^n + \frac{k^0}{(1+x^0)^2+(k^0)^2} \times H_y^n \\ & + \frac{k^0}{(1+x^0)^2+(k^0)^2} \times \left[\sum_{m=0}^{n-1} H_y^{n-m} \cdot \Delta x^m + \sum_{m=0}^{n-1} H_x^{n-m} \cdot \Delta k^m \right] \\ & + \frac{1+x^0}{(1+x^0)^2+(k^0)^2} \times \left[\sum_{m=0}^{n-1} H_x^{n-m} \cdot \Delta x^m - \sum_{m=0}^{n-1} H_y^{n-m} \cdot \Delta k^m \right] \\ & + \frac{1}{\mu_0} \cdot \frac{k^0}{(1+x^0)^2+(k^0)^2} \left(B_y^{n+1} - B_y^n \right) + \frac{1}{\mu_0} \cdot \frac{1+x^0}{(1+x^0)^2+(k^0)^2} \left(B_x^{n+1} - B_x^n \right) \end{aligned} \tag{4-22}$$

$$
\begin{aligned}
H_y^{n+1} &= \frac{1+x^0}{(1+x^0)^2+(k^0)^2}\times H_y^n - \frac{k^0}{(1+x^0)^2+(k^0)^2}\times H_x^n \\
&- \frac{k^0}{(1+x^0)^2+(k^0)^2}\times\left[\sum_{m=0}^{n-1} H_x^{n-m}\cdot\Delta x^m - \sum_{m=0}^{n-1} H_y^{n-m}\cdot\Delta k^m\right] \\
&+ \frac{1+x^0}{(1+x^0)^2+(k^0)^2}\times\left[\sum_{m=0}^{n-1} H_y^{n-m}\cdot\Delta x^m + \sum_{m=0}^{n-1} H_x^{n-m}\cdot\Delta k^m\right] \\
&- \frac{1}{\mu_0}\cdot\frac{k^0}{(1+x^0)^2+(k^0)^2}\left(B_y^{n+1}-B_y^n\right) + \frac{1}{\mu_0}\cdot\frac{1+x^0}{(1+x^0)^2+(k^0)^2}\left(B_x^{n+1}-B_x^n\right)
\end{aligned}
\tag{4-23}
$$

Here, coefficients in the above expression are:

$$
x^0 = re\left(\frac{\omega_m}{\omega_0}\{1-\exp[-\frac{\omega_0}{1+\alpha^2}(\alpha-j)\Delta t]\}\right) \tag{4-24}
$$

$$
k^0 = re\left(\frac{\omega_m}{\omega_0}\cdot\frac{1+j\alpha}{\alpha-j}\{1-\exp[-\frac{\omega_0}{1+\alpha^2}(\alpha-j)\Delta t]\}\right) \tag{4-25}
$$

$$
\Delta x^0 = \left(\frac{\omega_m}{\omega_0}\{1-\exp[-\frac{\omega_0}{1+\alpha^2}(\alpha-j)\Delta t]\}^2\right) \tag{4-26}
$$

$$
\Delta k^0 = \left(\frac{\omega_m}{\omega_0}\frac{1+j\alpha}{\alpha-j}\{1-\exp[-\frac{\omega_0}{1+\alpha^2}(\alpha-j)\Delta t]\}^2\right) \tag{4-27}
$$

Recursive relation for Δx^m and Δk^m are:

$$
\Delta x^{m+1} = \exp\left[-\frac{\omega_0}{1+\alpha^2}(\alpha-j)\cdot\Delta t\right]\cdot\Delta x^m \tag{4-28}
$$

$$
\Delta k^{m+1} = \exp\left[-\frac{\omega_0}{1+\alpha^2}(\alpha-j)\cdot\Delta t\right]\cdot\Delta k^m \tag{4-29}
$$

4.6 FDTD Update Vector processing

Large electromagnetic models increasingly require more computer memory than the past. However, there are two reasons to make auxiliary memory: magnetic disks are usually unsatisfactory, as access times for new data may be milliseconds for a disk versus microseconds for semiconductor central memory; second, data flow rates, such as reading or writing to memory, may be several hundred thousand words per second versus more than 10 million words per second for semiconductor memory. Substantial disk memory resources may have the biggest influence on the execution time of the program to access the data in the hard disk and transfer the data to and from the disk. The input/output capacity is the main constraint for the calculation.

The objects to be modeled in the future are large and complex structures. Wave interaction is observed in the time domain and in the frequency domain. All of these require detailed information regarding structural properties, which generate huge memory requirements. Furthermore, in innovative data display techniques, such as motion picture generation directly from computed output, the output data will be voluminous.

This requires that the iterative methods in large electromagnetic analysis and design should be structured with fully explicit algorithms that are suitable for vector processing. There should be no logical judgement inside the updating loop. This is why "seamless" transition is crucial in the FDTD updating equation.

Now we can see the example of vector processing of updating part. Here is the

example in Matlab for $\mathbf{H}_x$ updating in 2D.

```
for i=1:xmax

    for j=1:ymax

       ihx(i,j)=ihx(i,j)+fi1(i)*(Ez(i,j)-Ez(i,j+1));

       Hx(i,j)=fj3(j)*Hx(i,j)+fj2(j)*0.5*((Ez(i,j)-Ez(i,j+1))+ihx(i,j));

    end

end
```

We can realize the above expression in vector processing like this:

```
ihx(1:xmax,1:ymax)=ihx(1:xmax,1:ymax)...

                +fi1(1:xmax).*(Ez(1:xmax,1:ymax)-Ez(1:xmax,2:ymax));


Hx(1:xmax,1:ymax)=fj3(1:ymax)*Hx(1:xmax,1:ymax)...

                +0.5*fj2(1:ymax).*((Ez(1:xmax,1:ymax)-Ez(1:xmax,2:ymax))...

                +ihx(1:xmax,1:ymax));
```

For an inhomogeneous medium, after normalizing Maxwell's equation, all electric and magnetic properties are carried out in the relationship of $\vec{D}$ and $\vec{E}$, and $\vec{B}$ and $\vec{H}$; even the mediums are dispersive. We do not need to change anything in our PML part or parameters; this greatly reduces the work of the programming.

Our general steps are:

1. We generate the electric flux value from the magnetic field (PML is

integrated in this part)

2. We generate the electric field value from the electric flux. Electric medium properties can be isotropic, anisotropic, or dispersive. Here, we use anisotropic properties.

3. We generate the magnetic flux from the electric field (PML is integrated in this part)

4. We generate the magnetic field value from the magnetic flux

Magnetic medium properties can be isotropic, anisotropic, or dispersive. For our algorithm of FDTD for the anisotropic medium and PML, there is no logical judgement, exterior function calls and implicit arrays calls, so the updating equations can realize vector processing completely.

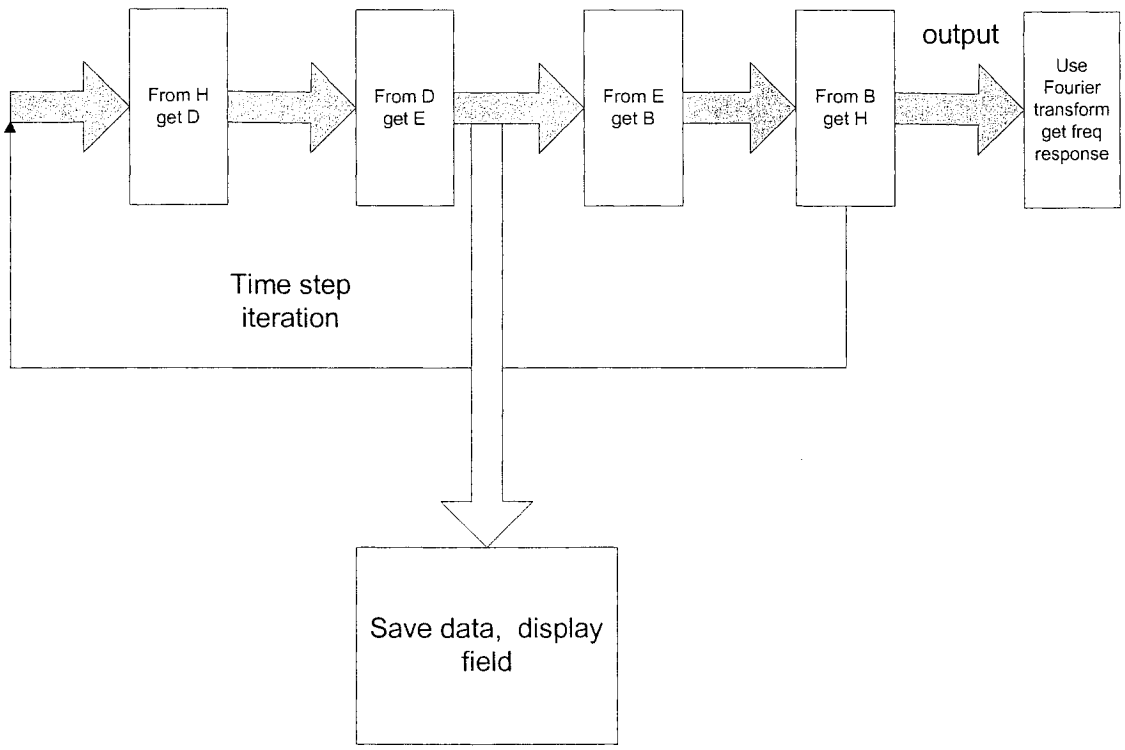

Figure 4-2: The main steps of FDTD calculation

Chapter Five: Numerical Results and Applications

In this chapter we applied the FDTD formulation for anisotropic media presented in chapter four to the analysis of three different applications. These include analysis of microstrip antenna over anisotropic material, ferrite absorber material, and a waveguide loaded with anisotropic ferrite. In these applications, frequency domain responses are obtained from time domain results. In order to get frequency responses in the entire range of frequency, the iteration time should be long enough.

5.1 Patch antenna application

In recent years, FDTD method has been used to analyze microstrip circuit and antenna design. In the past, the research for solving this kind of problem focused on the isotropic substrate properties **[31]**, diagonal tensor permittivity and permeability **[32]**, arbitrary anisotropic permittivity **[29]**, and arbitrary anisotropic permeability **[23].**

In this work, the FDTD algorithm developed for a general anisotropic medium is applied for the analysis of a microstrip patch antenna with arbitrary anisotropic permittivity and permeability.

There are some issues in this simulation. The first issue is accurately calculate the **E** and **H** components according to the Yee's grid. This is why we had to develop the formulation for arbitrary permittivity and permeability mediums in Chapter Four. The

second issue is finding the efficient absorbing boundary condition (ABC) suitable for this situation. Berenger's PML and material-independent PML (MIPML) are split-field methods requiring extra treatment on the interface of PML and simulation space, which doubles the memory requirement, thus rendering these methods unfit for our application. UPML based on **D**, **E**, **B**, and **H** updating looks like a good choice, while in UPML **D** and **B** are not the electric flux and magnetic flux; rather, they are artificial electric and magnetic flux defined by these equations: $D_x = \varepsilon \frac{S_z}{S_x} E_x, B_x = \varepsilon \frac{S_z}{S_x} H_x$ **[11].** This makes them totally different from the actual meaning of electric flux and magnetic flux. Thus, this method is also not a good choice for this application. The developed formulations of PML based on four-step updating **D**, **E**, **B**, and **H** in appendix, which correspond to their physical meaning in electromagnetics. This approach is more flexible and can apply to more general situations.

The microstrip patch antenna with a line feed source is shown in figure 5-1**.** The interested frequency range is from DC to 20 GHz. The microstrip substrate is composed of Duroid with εr=2.2 and a thickness of 1/32 inch (0.794mm). Scattering coefficients were calculated and compared with previous results **[31].**

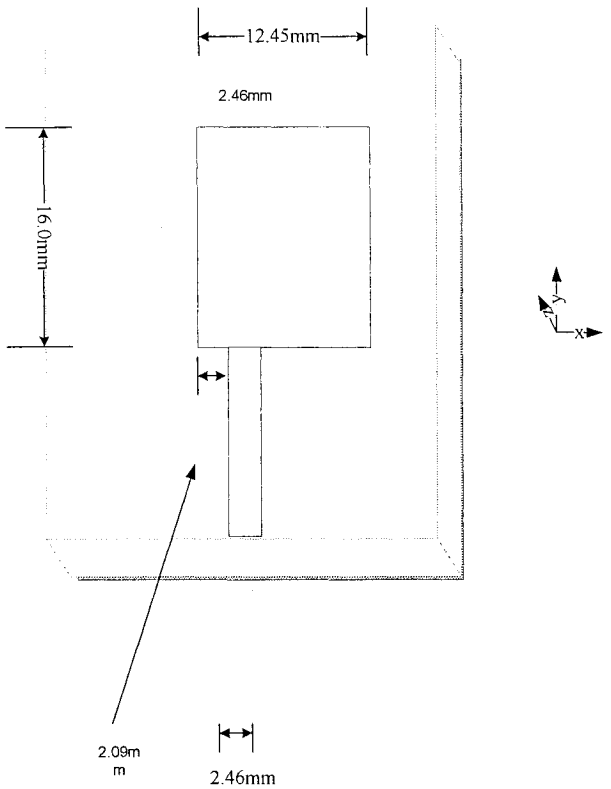

Figure 5-1: Configuration of Microstrip Patch Antenna

Figure 5-1 demonstrates the actual dimensions of the patch antenna. The resonant frequency corresponds to the width of the patch: $\lambda/2$=12.45mm. A good model of geometry, source type, and boundary condition is critical to obtaining accurate results. Since the substrate thickness is quite small compared with the length and the width of the antenna, Δx, Δy, Δz are chosen differently so that the size of the different geometries can be exactly matched. The spatial steps are: Δx=0.389mm, Δy=0.400mm, and Δz=0.265mm. The maximum time step value is carefully chosen to satisfy the stability condition restrictions:

$$\Delta t \leq \frac{1}{c}\sqrt{\frac{1}{\Delta x^2}+\frac{1}{\Delta y^2}+\frac{1}{\Delta z^2}} \qquad \textbf{(5-1)}$$

Here, c is the velocity of light in free space. $\Delta t = \Delta z / 2c$ is chosen in this application. The rectangular patch size is thus $32\Delta x \times 40\Delta y$. The length of feed line is $31\Delta y$. The source position is located at $18\Delta y$ away from the patch. A Gaussian pulse is chosen because its spectrum contains a DC component.

There are several ways of generating a plane wave source for a microstrip. The simplest way is imposing an electric field between the strip conductor and the ground plane along the source position. Alternatively, an imaginary perfect magnetic wall beside the source position will yield a better solution **[31].** Both methods will work, but they will have some distortion due to imperfect plane wave model. For a better plane waveform, the total field/scattering field method is applied to generate a plane wave at the source position.

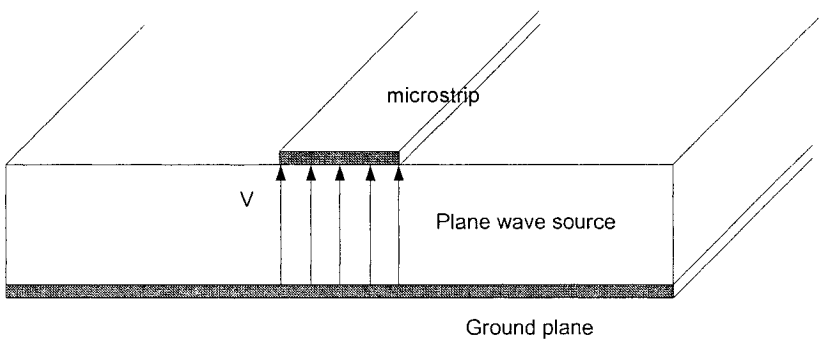

Figure 5-2: Line Source Generation of Microstrip transmission line

The first procedure for this application is to generate the scattering coefficient under the condition of an isotropic medium. And the properties are expressed as below:

$$[\varepsilon r] = 2.2 \times \begin{bmatrix} 1 & 0 & 0 \\ 0 & 1 & 0 \\ 0 & 0 & 1 \end{bmatrix} \quad \textbf{(5-2.a)}$$

$$[ur] = 1 \times \begin{bmatrix} 1 & 0 & 0 \\ 0 & 1 & 0 \\ 0 & 0 & 1 \end{bmatrix} \quad \textbf{(5-2.b)}$$

To verify the validity of this program the generated numerical results will compare with the experimental results

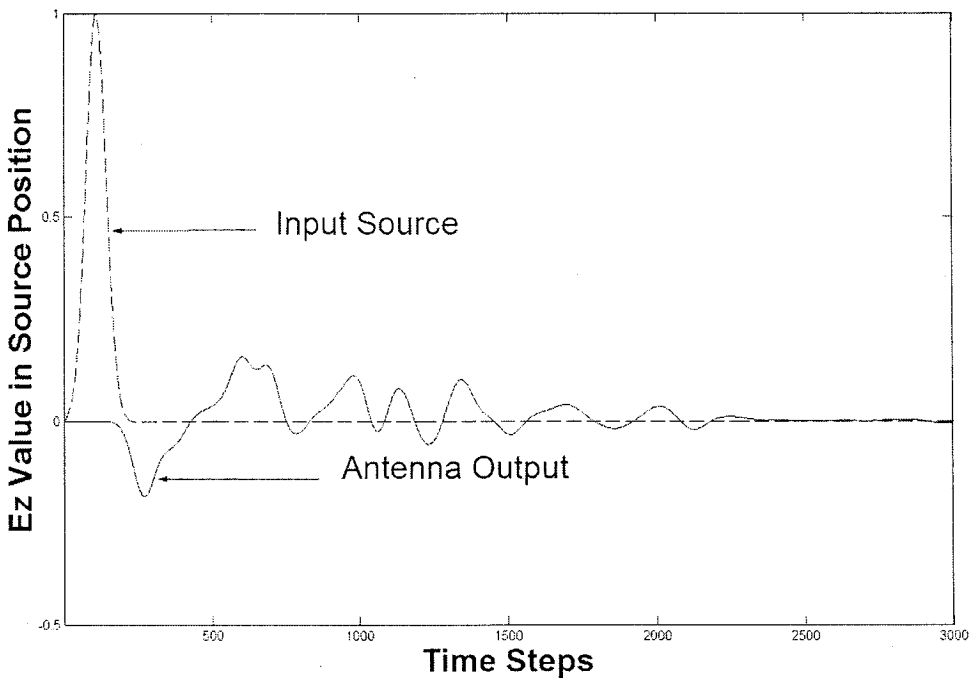

Figure 5-3: Normalized input and output electric fields (E_z) just beneath the metal strip of the microstrip patch antenna. Time step=3000.

The time domain simulation results for the input and reflected signals are shown in figure 5-3. They are the results of the normalized incident and reflected electric fields. The corresponding frequency response is computed over a range from DC to a very high frequency---20GHz and shown in figure 5-4. The scattering parameter S_{11} is defined as

the output divided by the input. Normally, we prefer decibel dimension, which can be expressed as:

$$S_{11} = 20 \times \log_{10} \left| \frac{E_{ref}}{E_{inc}} \right| \qquad \textbf{(5-3)}$$

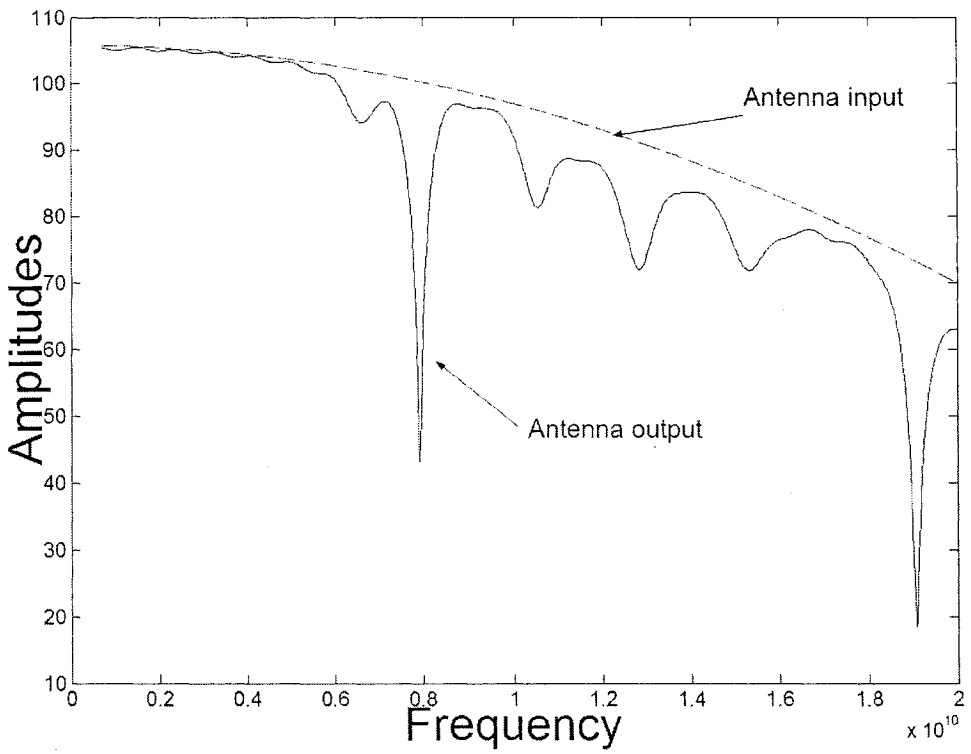

Figure 5-4: Amplitudes of Fourier Transform of Input Signal and Patch Antenna Output.
Time step=3000, Δx=0.389mm, Δy=0.4mm, Δz=0.265mm.

The result for S11 is shown in figure 5-5.

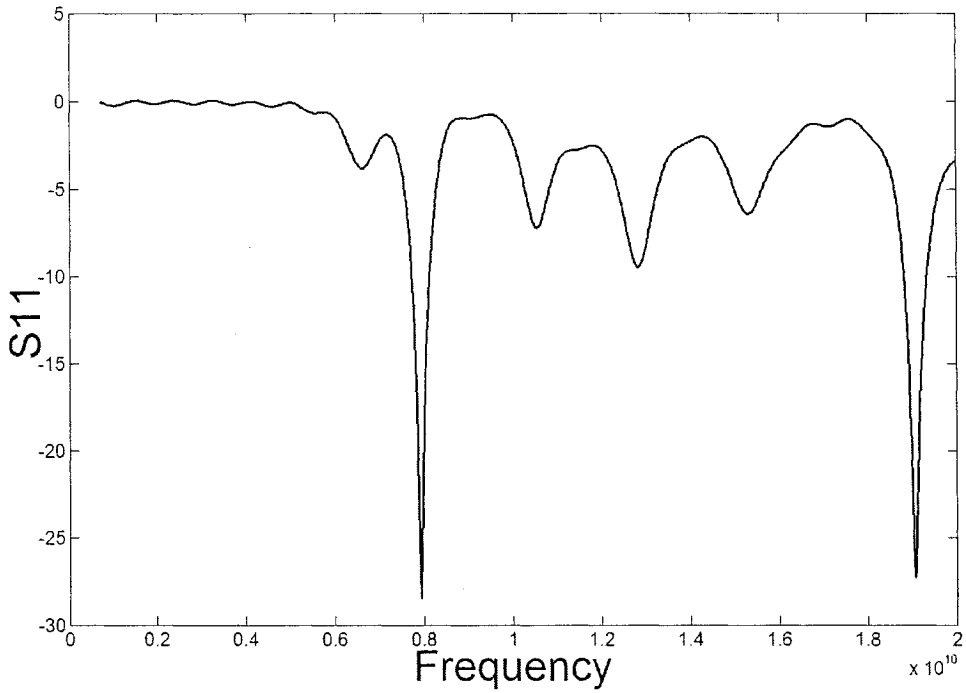

Figure 5-5: S_{11} parameters of microstrip patch antenna (Normalized Value).
Time step=3000, Δx=0.389mm, Δy=0.4mm, Δz=0.265mm.

These results are in good agreement with the measured results reported in **[31]**. From figure 5-5, we can observe designed resonances around 8Ghz and high mode resonances near 18 GHz.

The second application is to generate the scattering coefficient under the condition of anisotropic medium with arbitrary permittivity. Using the same method, we will get a scattering coefficient when the relative permittivity is expressed as **[33]:**

$$(\varepsilon_r) = \begin{pmatrix} \varepsilon_{xx} & \varepsilon_{xy} & \varepsilon_{xz} \\ \varepsilon_{yx} & \varepsilon_{yy} & \varepsilon_{yz} \\ \varepsilon_{zx} & \varepsilon_{zy} & \varepsilon_{zz} \end{pmatrix} \qquad \textbf{(5-4)}$$

$$
\begin{aligned}
&\varepsilon_{xx} = \varepsilon_1 \cos^2\theta + \varepsilon_2 \sin^2\theta; \\
&\varepsilon_{yy} = \varepsilon_1; \\
&\varepsilon_{zz} = \varepsilon_1 \sin^2\theta + \varepsilon_2 \cos^2\theta; \\
&\varepsilon_{xz} = \varepsilon_{zx} = (\varepsilon_1 - \varepsilon_2)\cdot \sin\theta\cos\theta; \\
&\varepsilon_{xy} = \varepsilon_{yx} = \varepsilon_{zy} = 0;
\end{aligned}
\qquad \textbf{(5-5)}
$$

θ is the angle between the optical axis and the x direction.

Assuming that the optical axis for both permittivitis is located in the **XZ**-plane. There are three values of $\theta \in (0, \pi/4, \pi/2)$ and $\varepsilon_1 = 2.31, \varepsilon_2 = 2.19$. This result is shown in Figure 5-6. The input impedance around the first resonant frequency is shown in figure 5-7. Results are pretty matched to previous research results reported in **[17].** These results can serve as a proof supporting the effectiveness of our method.

We can note that:1 Frequency changes if the optical angle changes. 2. The optical angle's changes result in small changes in resonant frequency, when the optical angle changes from 0 to π/2, for the first resonant frequency, and the resonant frequency changes only 1.5%. For the second resonant frequency, the resonant frequency change is about 1.5%. 3. The bandwidth is the same as the bandwidth for the isotropic substrate.

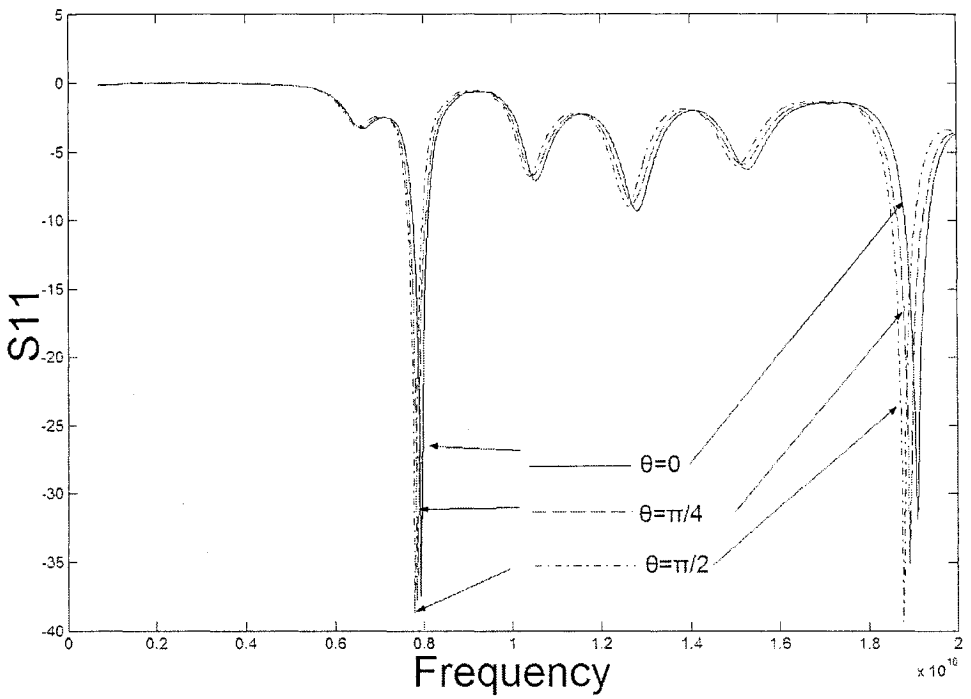

Figure 5-6: The normalized S11(dB value) of the microstrip patch antenna as a function of frequency.

The optical axis lies in the YZ plane. Time step=8000, Δx=0.389mm, Δy=0.4mm, Δz=0.265mm.

From the above discussion, we can see that for substrates with only anisotropic permittivity property, the optical angle's change does not affect to much the antenna resonant frequency and the bandwidth.

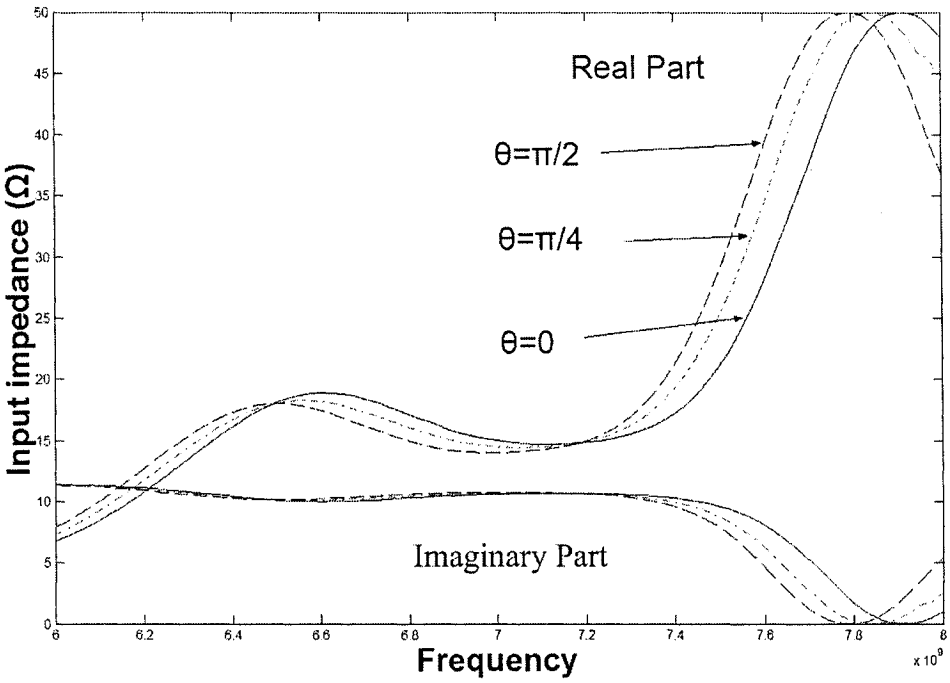

Figure 5-7: The Input Impedance of the Microstrip Antenna with Anisotropic Permittivity. The optical axis lies in the YZ plane.

The third procedure is to generate the scattering coefficient for a substrate with arbitrary permittivity and permeability. We will also check the effects due to optical angle changes. Medium properties can be expressed as:

$$(\varepsilon_r) = \begin{pmatrix} \varepsilon_{xx} & \varepsilon_{xy} & \varepsilon_{xz} \\ \varepsilon_{yx} & \varepsilon_{yy} & \varepsilon_{yz} \\ \varepsilon_{zx} & \varepsilon_{zy} & \varepsilon_{zz} \end{pmatrix} \qquad \textbf{(5-6.a)}$$

$$(\mu_r) = \begin{pmatrix} \mu_{xx} & \mu_{xy} & \mu_{xz} \\ \mu_{yx} & \mu_{yy} & \mu_{yz} \\ \mu_{zx} & \mu_{zy} & \mu_{zz} \end{pmatrix} \qquad \textbf{(5-6.b)}$$

Assuming that the optical axis for both permittivity and permeability is located in the **XZ**-plane, the expression of each component is given by **[33]:**

$$
\begin{aligned}
&\varepsilon_{xx} = \varepsilon_1 \cos^2\theta + \varepsilon_2 \sin^2\theta; \\
&\varepsilon_{yy} = \varepsilon_1; \\
&\varepsilon_{zz} = \varepsilon_1 \sin^2\theta + \varepsilon_2 \cos^2\theta; \\
&\varepsilon_{xz} = \varepsilon_{zx} = (\varepsilon_1 - \varepsilon_2)\cdot \sin\theta\cos\theta; \\
&\varepsilon_{xy} = \varepsilon_{yx} = \varepsilon_{zy} = 0; \\
&\mu_{xx} = \mu_1 \cos^2\theta + \mu_2 \sin^2\theta; \\
&\mu_{yy} = \mu_1; \\
&\mu_{zz} = \mu_1 \sin^2\theta + \mu_2 \cos^2\theta; \\
&\mu_{xz} = \mu_{zx} = (\mu_1 - \mu_2)\cdot \sin\theta\cos\theta; \\
&\mu_{xy} = \mu_{yx} = \mu_{zy} = 0;
\end{aligned}
\qquad \textbf{(5-7)}
$$

Here, θ is the angle between the optical axis and the x direction. In this example, θ=0, π/4, π/2, $\varepsilon_1 = 2.31, \varepsilon_2 = 2.19, \mu_1 = 1.007$, and $\mu_2 = 1.001$. The S_{11} parameter for above case is shown in figure 5-8. Figure 5-9 shows the variation of input impedance around the first resonant frequency for the purposes of better understanding input impedance and bandwidth around the first resonant frequency.

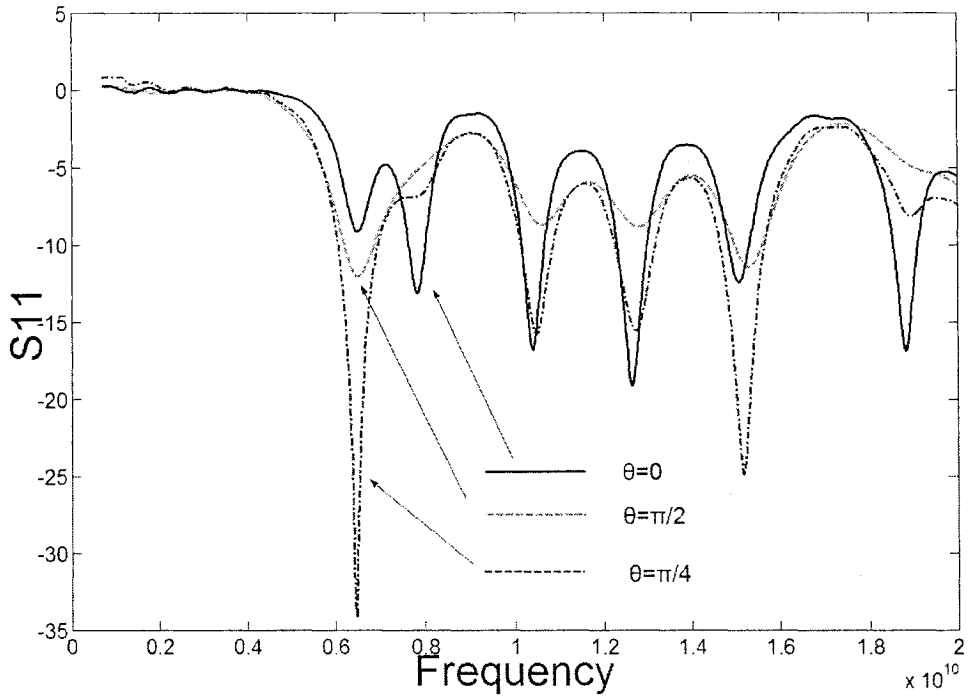

Figure 5-8: Normalized S11(dB) of the Microstrip Patch Antenna as a Function of θ.

The optical axis lies in the YZ plane. Time step=3000, Δx=0.389mm, Δy=0.4mm, Δz=0.265mm.

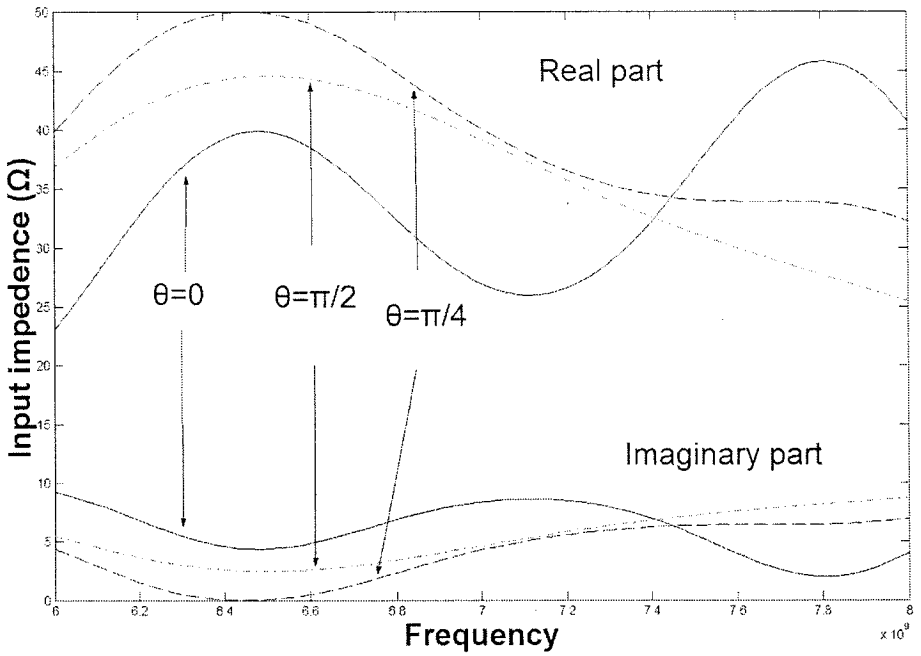

Figure 5-9: The Input Impedance of the Microstrip Antenna with Anisotropic Permittivity and Permeability. The optical axis lies in the YZ plane.

In this case, the variation in resonant frequency and bandwidth become more complicated. Around the first resonant frequency: 1.Resonant frequencies shift to a lower frequency, from 7.8GHz to 6.45GHz, which is about 16.6%, as θ changes from 0 to π/2. 2. The bandwidth is increased, which could be seen more clearly from the input impedance results in figure 5-9. Comparing Figures 5-7 and 5-9, we can see that bandwidth of input impedance is greatly increased.

There are another four resonant frequencies below 20GHz for different optical angles, which are more obvious if $\theta<\pi/2$. This might the enable the patch antenna to have more working bands.

From the above discussion, it is interesting to note that arbitrary permittivity and arbitrary permeability can add another design freedom for antenna design, especially for a dielectric antennas or an array antenna with dielectric elements.

5.2 Ferrite Microwave Absorber

Rapid developments in the wireless communication industry have increased the demand of EM wave absorbers. For example, working at 1.9 GHz a cellular phone needs absorbers to suppress EM wave radiation into human beings. At 2.4 GHz, WLAN need absorbers to reduce extra energy and prevent EM wave interference or multi-reflection from obstacles.

Conventional ferrite materials could provide a simple solution to these demands; however, one obstacle has deterred their applications in the past. The manufacturing procedure is very complex, as there are many conditions that affect ferrite properties, including controlled sintered temperature, pressure, and the ratio of composite materials **[34].** Thus, there might be a slight frequency shift from the design frequency for these products. We can deal with this problem by punching out small holes in the rubber ferrite. This can improve the matching characteristics and adjusting the working frequency band. Also the method avoids the complexities of adjusting conditions in the manufacturing procedure. Matching adjusting is achieved by changing the geometrical size of the holes. The FDTD method is an efficient tool to get an accurate matching frequency for the

ferrite with small holes. Figure 5-10 shows the fundamental formation of the EM wave absorber with small holes punched in rubber ferrite.

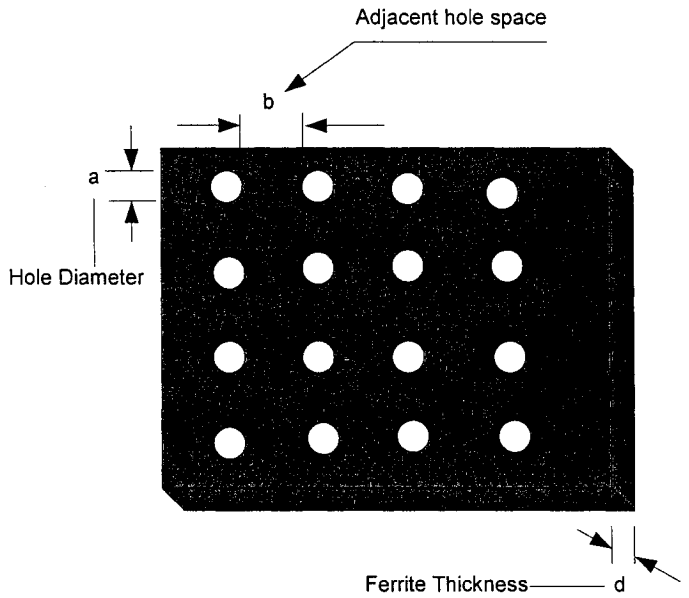

Figure 5-10: Structure of Ferrite Absorber

It is valid that a circular hole can be approximated by a square hole if the size of the hole is smaller than the wavelength **[34]**. This is necessary for reducing memory size and processing time for computer analysis. Circular holes are more easily manufactured than square ones.

For a weakly magnetized ferrite absorber, permeability can be expressed as a frequency-dependent function . Frequency dependent permeability can be expressed as:

$$\bar{\mu}_r = 1 + \frac{kf_1}{f_1 + jf} = \mu_r' - j\mu_r'' \qquad \textbf{(5-8)}$$

k is the value of static magnetic susceptibility when frequency is zero

μ_r' is the real part of permeability

$\mu_r^{''}$ is the imaginary part of permeability

In order to update FDTD expression for the above permeability, we can use the Fourier Transform method, or a Z transform method to obtain the time domain expression of ferrite permeability.

We can express the relative permeability in a form like this:

$$\bar{\mu}_r = 1 + \frac{x}{1 + j2\pi t_0 f} \tag{5-9}$$

Here, we can clearly see that the expression of permeability for weakly magnetized ferrite can be treated as the first order Debye medium **[35]**. By the method of Z transform, we can obtain the Z domain in the form,.

$$H(z) = \frac{B(z) - e^{-\Delta t/t0} \cdot Z^{-1} \cdot S(z)}{1 + \frac{x_1 \cdot \Delta t}{t_0}} \tag{5-10}$$

$$S(z) = e^{-\Delta t/t0} \cdot Z^{-1} S(z) + \frac{x_1 \Delta t}{t_0} H(z) \tag{5-11}$$

In updating form, the above equations are expressed as:

$$H^n = \frac{B^n - e^{-\Delta t.2\pi f1} \cdot S^{n-1}}{1 + k \cdot \Delta t \cdot 2\pi f_1} \tag{5-12}$$

$$S^n = e^{-\Delta t \cdot 2\pi f1} \cdot S^{n-1} + k \cdot \Delta t \cdot 2\pi f_1 \cdot H^n \tag{5-13}$$

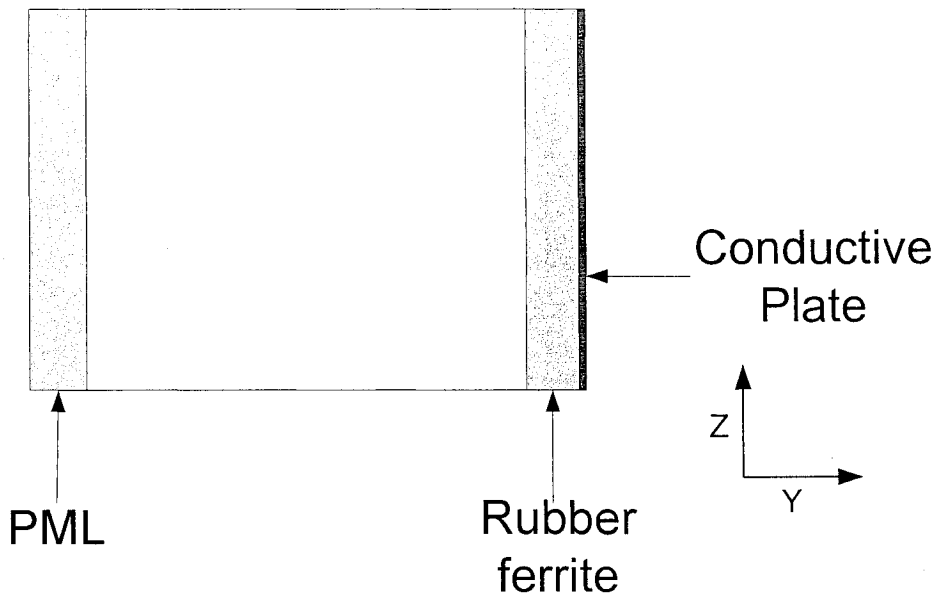

Figure 5-11: Cross Section of Ferrite Absorber Modeling in FDTD simulation domain

In our FDTD simulations, only the normal incident waves are considered. We can analyze the reflection coefficient by models presented in Figure 5-11. On the right side is the rubber ferrite with holes backed by a conductive plane, and on the left side is the PML absorbing layer. In the rubber ferrite, circular holes are replaced by equivalent square holes.

The result in figure 5-12 show the dependence of the reflection coefficient on the relative permittivity and absorbing frequency under the condition that there is no hole in the ferrite absorber. The results are in excellent agreement with the results of reference **[34]**. Figure 5-12 demonstrates that relative permittivity affects ferrite-absorbing frequency. Higher permittivity means lower absorbing frequency. The relative permittivity can be controlled in manufacturing procedures in the range of 10 to 25.

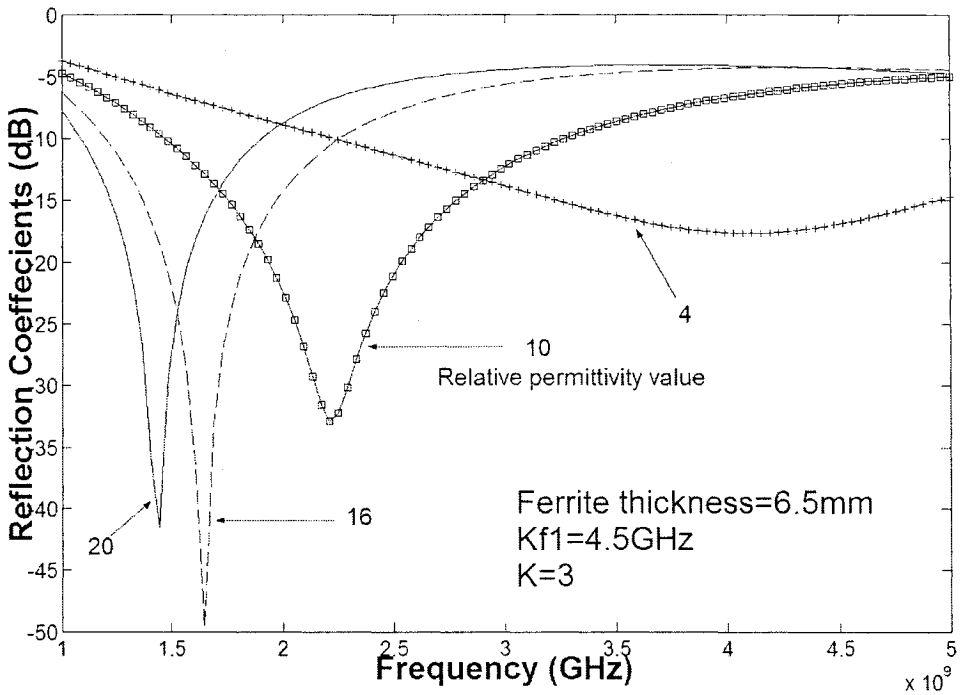

Figure 5-12: The Effects of Changing Relative Permittivity (no hole).

kf1=4.5GHz, k=3, ferrite thickness=6.5mm, ε_r =16. Time step=6000, Δx=0.2mm, Δy=0.1mm, Δz=0.2mm.

Figure 5-13 describes the dependency of absorbing frequency on the hole-size. We can see that the absorbing frequency shifts to a higher value if the hole size increases and other parameters do not change.

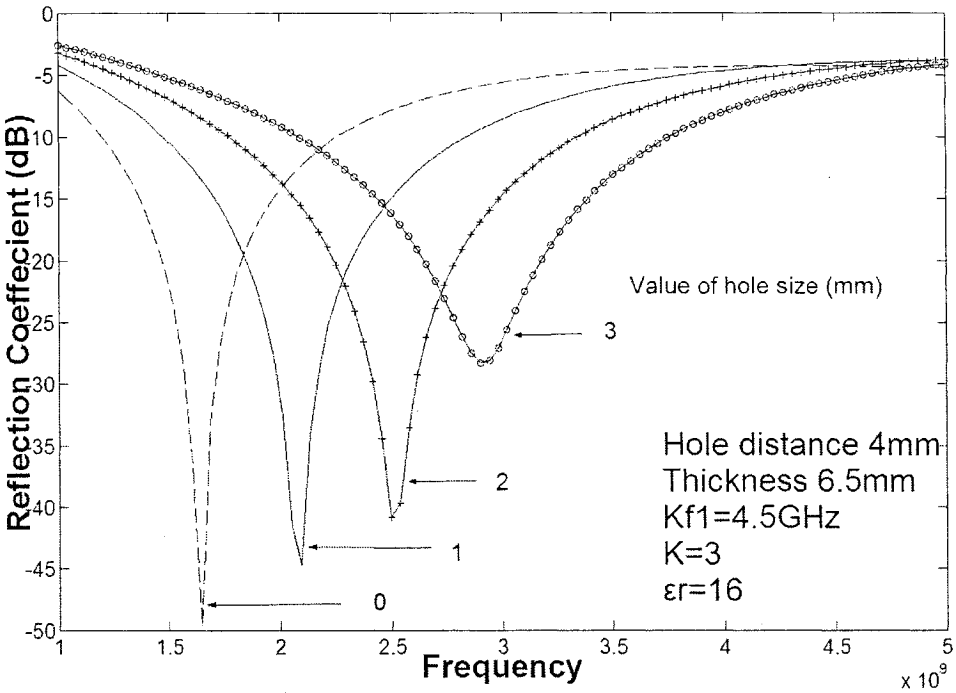

Figure 5-13: The Effects of Changing Hole Size.
Hole distance= 4mm, kf1=4.5GHz, k=3, ferrite thickness=6.5mm, ε_r=16. Time step=6000, Δx=0.2mm, Δy=0.1mm, Δz=0.2mm.

Figure 5-14 shows the results when the hole-distance is regarded as a variable and other parameters do not changes. We can see that the absorbing frequency shifts to a higher frequency when the hole distance decreases.

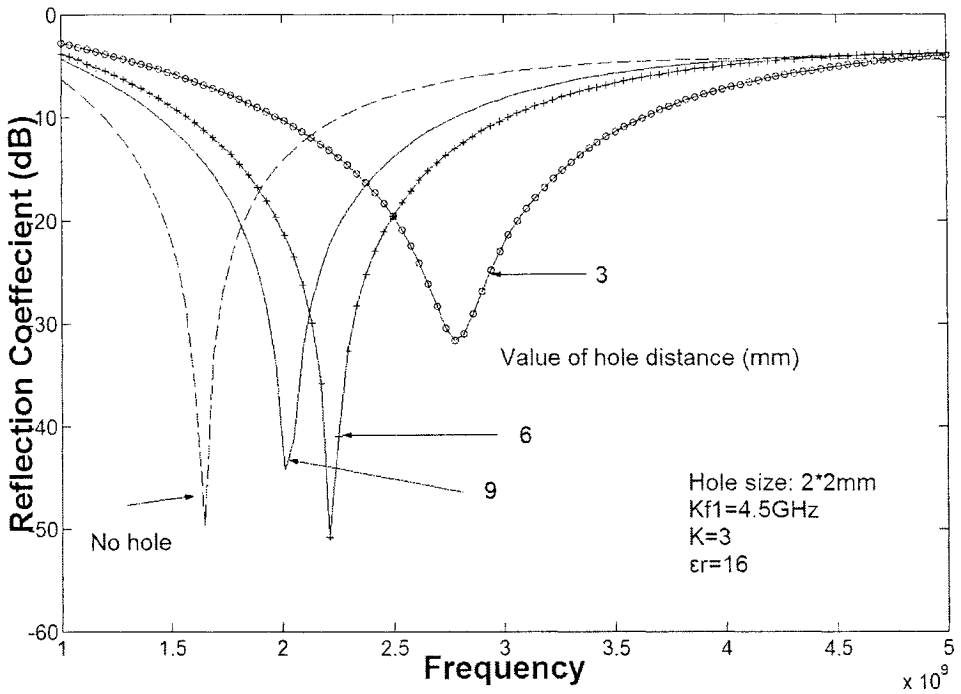

Figure 5-14: Effects of Changing Hole Distance Hole size.
Hole size=2×2mm, kf1=4.5GHz, k=3, ferrite thickness=6.5mm, ε_r =16. Time step=6000, Δx=0.2mm, Δy=0.1mm, Δz=0.2mm.

After these investigations, we may conclude: 1. The absorbing frequency is shifted to a higher frequency region if the size of hole increases; 2. The absorbing frequency is shifted to a higher frequency region if the distance among holes decreases..

In practice, in order to adjust the absorbing frequency, we just change the space distance among the holes. Using FDTD simulations, we can produce and adjust the working frequency for the given ferrite absorber materials.

5.3 Waveguides loaded with Heterogeneous Anisotropic Ferrites

The effects of ferrite materials under a static magnetic biasing field make them widely used in microwave devices. This utilization requires knowledge of a permeability tensor, which makes these kinds of devices difficult to study analytically. Numerical methods such as the FDTD method are an ideal tool for this kind of problems.

After applying static biasing magnetic field, the permeability of ferrites shows strong anisotropic and dispersive characteristics. It is for this reason that the grid modifications discussed in section 4.1 in conjunction with the formulations developed in section 4.4 should be applied. Thus, $\mathbf{B}_y$ and $\mathbf{H}_y$ in equation **4-22** should be modified according to equation **4-8.a**, and $\mathbf{B}_x$ and $\mathbf{H}_x$ in equation **4-23** should be modified according to equation **4-9.a**.

Rectangular waveguide loaded with two layers of magnetized ferrites is depicted in figure 5-15 and figure 5-16. The interested frequency range is from 8 GHz to 12 GHz. This waveguide is a rectangular waveguide with a=22.86mm, and b=10.16 mm. For the first ferrite layer, the biasing field H_0=200 oersted and the static magnetization 4π Ms=2000 gauss are used. For the second layer, the biasing field H0=-200 oersted and the static magnetization 4π Ms=-2000 gauss are used. The ferrite permittivity ε_r=14.5 and thickness for each layer $l_1=l_2$=5.715mm are used. S_{11} and S_{21} parameters are calculated for this structure.

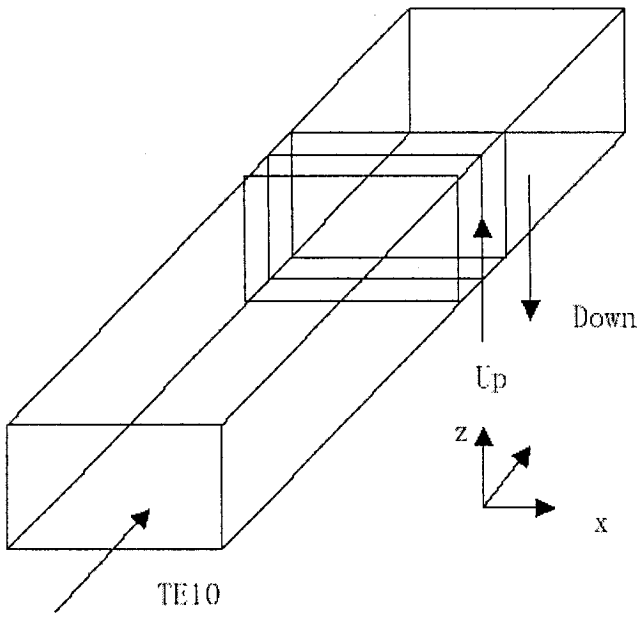

Figure 5-15: Structure of Ferrite Loaded the first layer has up-biasing field, the second layer has down-biasing field, working on TE10 mode [36].

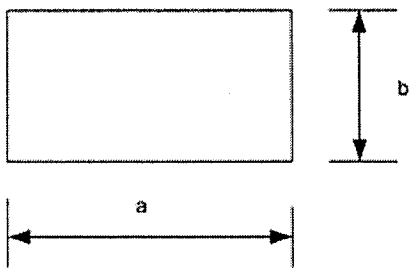

Figure 5-16: Cross-section of Waveguide (XZ Plane). a=22.86mm, b=10.16mm.

Figure 5-17 describes FDTD modeling of this waveguide in YZ plane. The PML ABCs are applied to truncate the computational domain. Excitation at the waveguide is given by the follow expression.

$$E_z(t,x) = 0; t < 0 \qquad \textbf{(5-14)}$$

$$E_z(t,x) = \sin(\frac{\pi x}{a}) \cdot \exp(-\frac{(t-t_0)^2}{\tau^2}), t >= 0 \qquad \textbf{(5-15)}$$

t_0 : the value of the time delay for the source;

τ : the value of the time spread of the Gaussian pulse;

a: the width of the waveguide.

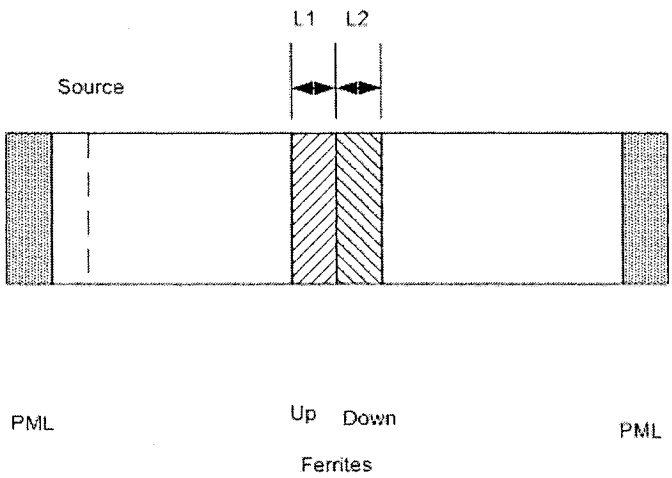

Figure 5-17: FDTD Modeling of This Waveguide L_1=L_2=5.715mm

This source allows only the TE10 mode to propagate in the waveguide. The Gaussian pulse can cover a wide frequency range response in just one simulation. For interfaces of air/ferrite and ferrite/ferrite, a modified explicit updating equation for the electric field can be derived in order to obtrain better accuracy **[36]**. This method requires a new updating equation at the interface. This update equation is not used for the following reasons: 1. After numerical experiments, results from the modifications show little difference with the original method. 2. We want to keep our general forms of updating equation. On the interface, we change the permittivity value into an average value of ferrite and air, which is processed in the initial parts.

Δx, Δy, Δz are chosen differently so that geometry size can be exactly matched. The time step is chosen to satisfy stability condition given by equation **3-11**. The total field/Scattering field method is applied to generate a plane wave at the source position.

Following the previously discussed procedure, we can calculate S_{11} and S_{21} parameters for this waveguide. The magnetic motion equation method **[21]** is also applied to this structure to generate scattering parameters for comparison. For both methods, the numerical results should be the same. The results are shown in figure 5-18 and figure 5-19. The results for S_{11} parameters are almost identical which show the effectiveness of our method. While for S_{21} parameters, results are different. But both methods can predict the main absorbing frequency around 8.5GHz and 11GHz. For 3D FDTD applications, anisotropic and dispersive materials are not simple to model, especially at the interface of different medium, PEC or PMC, which makes the simulation more difficult. The simulation results should be carefully treated.

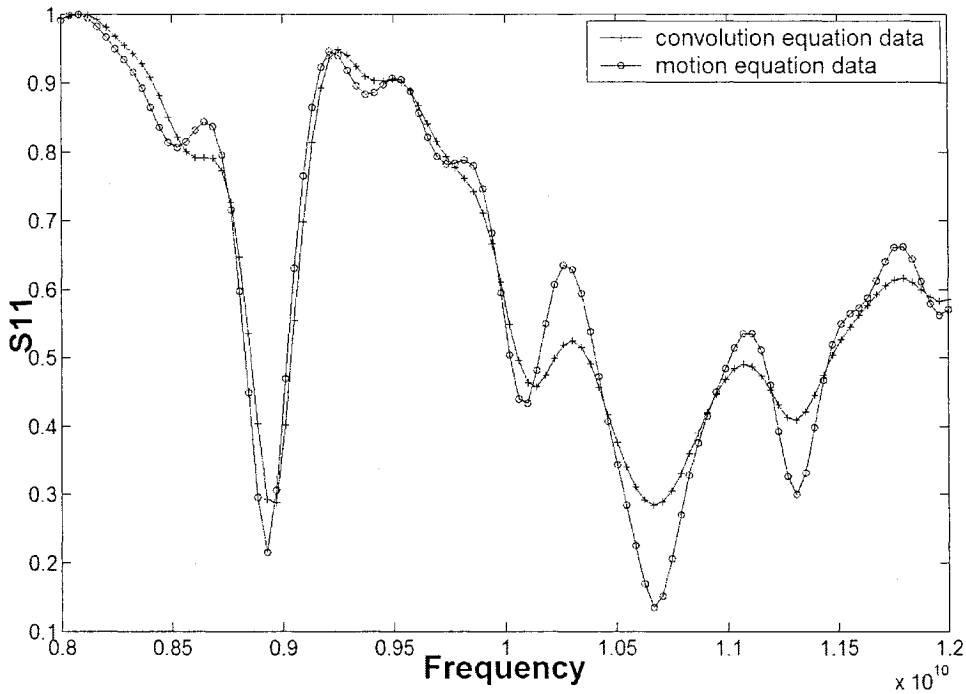

Figure 5-18: S_{11} parameters of waveguide loaded with two ferrite layers.

For up biasing ferrite, H_0=200 oersted, 4 π Ms=2000 gauss, for down biasing ferrite, H_0=-200 oersted, 4 π Ms=-2000 gauss. Time steps=6000, Δx=0.5715mm, Δy=0.5715mm, Δz=0.513mm. Results developed from model method are compared with results from our works [38].

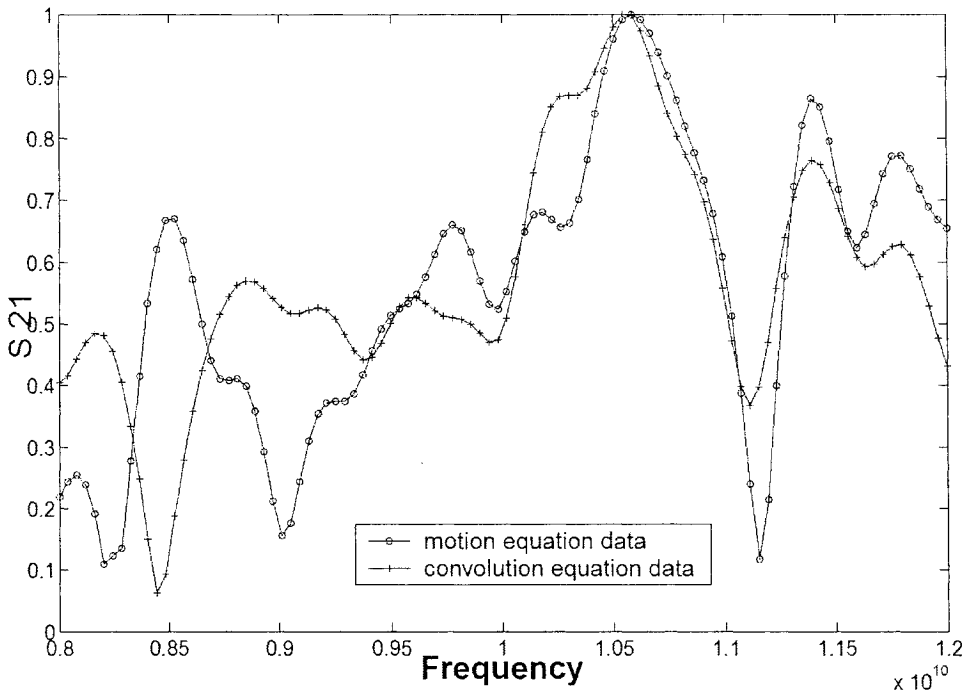

Figure 5-19: S_{21} parameters of waveguide loaded with two ferrite layers.

For up biasing ferrite, H_0=200 oersted, 4 π Ms=2000 gauss, for down biasing ferrite, H_0=-200 oersted, 4 π Ms=-2000 gauss. Time steps=6000, Δx=0.5715mm, Δy=0.5715mm, Δz=0.513mm.

In order to explore the effects of anisotropic characteristics upon system parameters, we can change the biasing field value. Changing the biasing field equals to changing permeability values in tensor expression. By this way we can change system parameters. Figure 5-20 and figure-21 show that: S_{11} and S_{21} change if biasing field change. And absorbing frequency shifts as biasing field value shift. This results support the facts that anisotropic can be another design freedom.

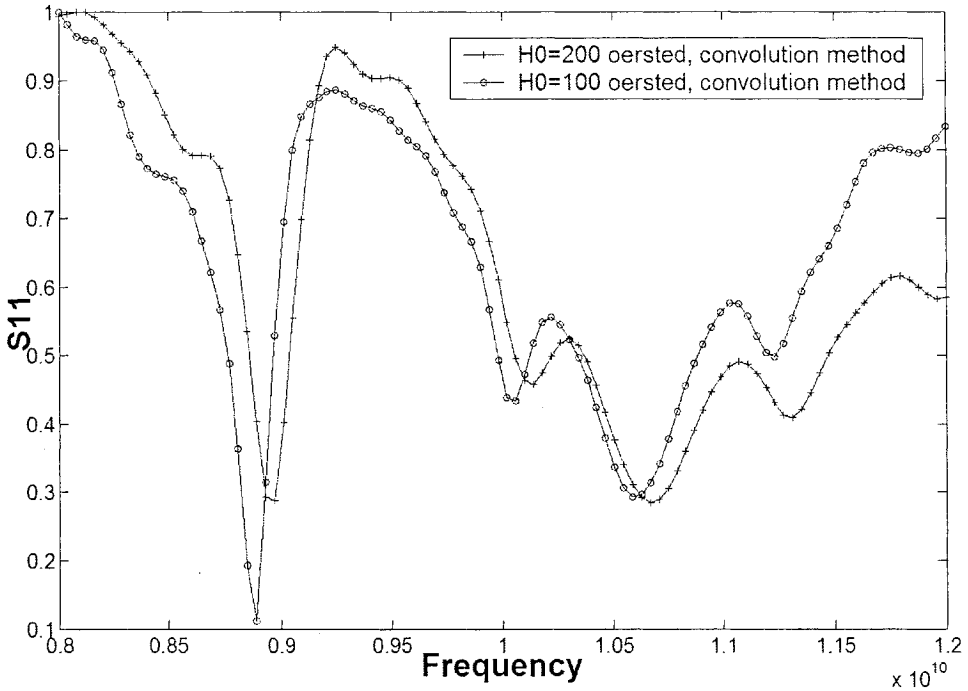

Figure 5-20: S_{11} parameters of waveguide loaded with two ferrite layers.

For up biasing ferrite, H_0=200 oersted and H_0=100 oersted, $4\pi Ms$=2000 gauss, for down biasing ferrite, H_0=-200 oersted, H==-100 oersted, $4\pi Ms$=-2000 gauss. Time steps=6000, Δx=0.5715mm, Δy=0.5715mm, Δz=0.513mm.

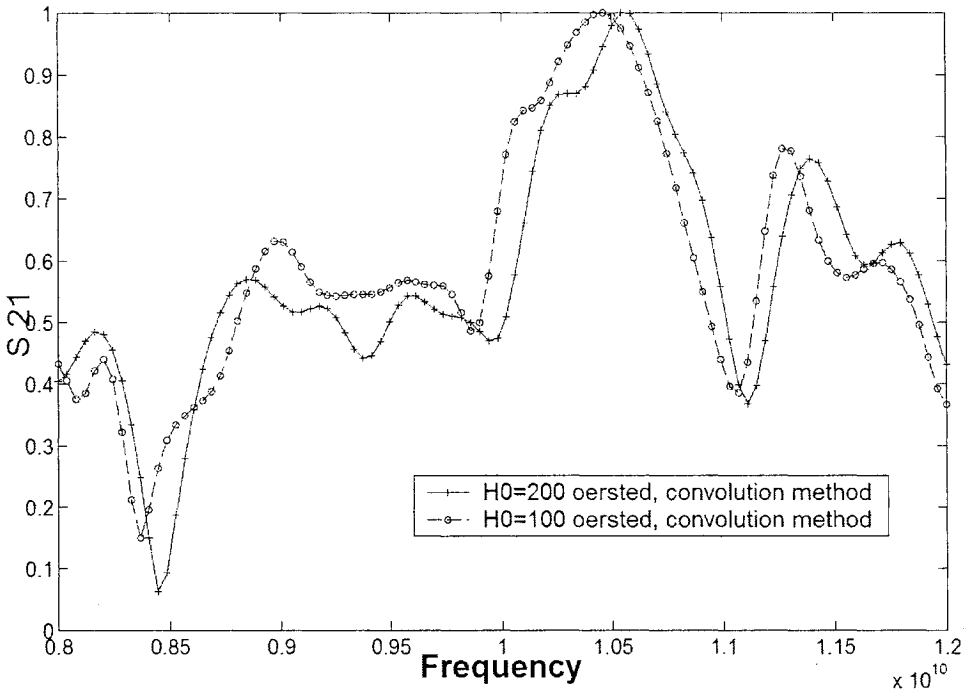

Figure 5-21: S_{21} parameters of waveguide loaded with two ferrite layers.
For up biasing ferrite, H_0=200 oersted and H_0=100 oersted; 4 π Ms=2000 gauss, for down biasing ferrite, H_0=-200 oersted and H_0=-100 oersted; 4 π Ms=-2000 gauss. Time steps=6000, Δx=0.5715mm, Δy=0.5715mm, Δz=0.513mm.

Charter Six: Conclusion and Future Work

6.1 Summary

Advances in modern electronic and RF technology made microstrip circuits and antenna design more and more complex. Compared with experimental and analytical techniques, numerical simulation techniques are better choice, which are cheaper and more convenient. Although anisotropic property is regarded as disadvantageous in many cases, it can also be treated as a design freedom allowing for controlling the overall system performance. Starting from this point view, a FDTD algorithm is developed to investigate the possibility. This FDTD approach can be separated into two parts: the dielectric properties' parts and the wave marching parts. The dielectric properties are expressed separately from the wave marching parts, allowing the expression of full anisotropic in 3D Cartesian coordinates. At the same time, a simplified PML was modified and developed as ABC. In the process of developing the FDTD algorithms for arbitrary anisotropic materials, we found that this approach can be extended to dispersive materials, thus make it applicable to many other situations.

Chapter two is a review on some commonly used techniques in EM problems. Chapter three is the theory introduction on the FDTD method and PML. Chapter four

contains anisotropic formulation development, which is the main contribution of this thesis. Chapter five studied three applications that are a microstrip patch antenna with anisotropic medium, weakly magnetic ferrite absorbers with holes, and waveguides loaded with heterogeneous anisotropic magnetic ferrite. Numerical results support the view point that: anisotropic can be another design freedom.

Taking this point of view, some research has explored the possibility of using anisotropy to change the overall characteristics or performances for EM problems. There is a published work on changing resonant frequency using the controlled biasing static magnetic field **[37].** There is another work on tuning the operating frequency of the microstrip patch antenna through the tensor elements **[17].**

6.2 Conclusions and Contributions

3D FDTD algorithms for full anisotropic materials were analyzed using relationships between electric field, electric flux, magnetic field and magnetic flux. In this FDTD method, both permeability and permittivity can be expressed as tensor form. The objective was to develop a simple way of realizing FDTD method for anisotropic materials. This method can also be applied to anisotropic and dispersive properties with no major modifications for the core updating parts. We examine applications for three cases: full anisotropic permeability and permittivity, dispersive permeability and

dispersive & anisotropic permeability. The corresponding 3D FDTD code was developed.

A modified simplify Perfectly Matched Layer (PML) was used as the Absorbing Boundary Condition (ABC). Good matching of this PML was observed in our applications. This PML can be easily integrated into the main FDTD algorithms for anisotropic and dispersive mediums.

From our numerical results, we can find that anisotropic materials exhibit big influence on microwave devices, which can be served as a design freedom.

At the end of this project, it is essential to point out that: Each of thesis objectives was met and the work outlined in the thesis can be a good start of further works.

The main contributions of this thesis include providing the solution for full anisotropic materials using 3D FDTD method and applying the developed formulation to several electromagnetic engineering problems. The method is a more general solution compared with previous methods and can be easily extended to other medium properties. Based on the numerical results, we found that the electrical performance of materials with full anisotropic properties is improved compared with materials with only isotropic or anisotropic permittivity. This can improve system performance and provide us with more design choices.

6.3 Suggestions for future work

Areas that may be worthy of further investigation including the followings:

The investigation of a generalised FDTD method will allow the solution of magnetic and electric loss with tensor expression.

The implementation of irregular Cartesian mesh auto-generation method can automatically, accurately model the surface of arbitrary objects.

Appendix

Method for Frequency Dependent Media in FDTD

The FDTD is performed at the time domain; therefore, the results are also in the time domain, despite the fact that our interests are in the frequency domain. There are two ways to get the response of the frequency domain in the FDTD method: 1. Using single frequency sources after archiving a stable condition in FDTD, we get the response in the interested frequency. 2. First, getting response in the time domain and then using the discrete Fourier Transform method transforms the time domain signal into frequency domain. Thus, we can have the whole frequency range response in just one time simulation. In the above calculation, dialect constants are assumed to be constant, while for most of the media they vary at different frequencies.

One of the most significant developments in the FDTD method was uncovering a means to simulate frequency-dependent materials. A simple example will illustrate this method. Complex permittivity is described by an equation with one first order pole. Such materials are often called Debye materials and the equation that describes their permittivity is the Debye equation. The relative permittivity is described by

$$\varepsilon_r(\omega) = \varepsilon_r + \frac{\sigma}{j\omega\varepsilon_0} + \frac{\chi}{1 + j\omega t_0} \qquad \textbf{(A-1)}$$

ε_r is the dielectric relative permittivity constant, σ is the dielectric conductivity,

t_0 is the relaxation time.

Three methods extend FDTD to frequency dependent materials. The first is the Fourier Transform method, the second is the auxiliary differential equation method, the third is the Z transform method.

Fourier transform method

In order to simulate the above medium in FDTD, the last term in the above equation in frequency domain is

$\frac{\chi}{1+j\omega t_0}$, and we define the variable:

$$S(\omega) = \frac{\chi}{1+j\omega t_0} E(\omega) \qquad \textbf{(A-2)}$$

The inverse Fourier transform of the above is $(\frac{\chi}{t_0})e^{-(t/t0)}u(t)$, $u(t)$ is rectangular function. $u(t) = \begin{cases} 0, t < 0; \\ 1, t \geq 0; \end{cases}$, while implicit to the algorithm of FDTD is causal, which means for t<0, all fields are set to zero. Then we have the convolution developed from above equation in time domain: $S(t) = \frac{\chi}{t_0}\int_0^t e^{-(t'-t)/t0} E(t') \cdot dt'$. We can approximate this as a summation in the discrete time domain:

$$S^n = \chi.\frac{\Delta t}{t_0}\sum_{i=0}^{n} e^{-\Delta t(n-1)/t0}.E^i = \chi.\frac{\Delta t}{t_0}\left(E^n + \sum_{i=0}^{n-1} e^{-\Delta t(n-i)/t0}.E^i\right) \qquad \textbf{(A-3)}$$

Notice that $S^{n-1} = \chi.\frac{\Delta t}{t_0} e^{\Delta t/t0}\left(\sum_{i=0}^{n-1} e^{-\Delta t(n-i)/t0}.E^i\right)$, so we can get:

$$S^n = \chi.\frac{\Delta t}{t_0}\left(E^n + e^{-\Delta t/t0}S^{n-1}\right) \qquad \textbf{(A-4)}$$

The same procedure can be applied to the whole Debye equation. We can write:

$$\begin{aligned} D^n &= \varepsilon_r E^n + I^n + S^n \\ &= \varepsilon_r.E^n + \left[\frac{\sigma.\Delta t}{\varepsilon_0}\cdot E^n + I^{n-1}\right] + \left[\chi\cdot\frac{\Delta t}{t_0}E^n + e^{-t/t-}\cdot S^{n-1}\right] \end{aligned} \qquad \textbf{(A-5)}$$

Solving E^n, we get

$$\begin{aligned} E^n &= \frac{D^n - I^{n-1} - e^{-\Delta t/t0}S^{n-1}}{\varepsilon_r + \frac{\sigma.\Delta t}{\varepsilon_0} + \chi\cdot\frac{\Delta t}{t_0}} \\ I^n &= I^{n-1} + \frac{\sigma\cdot\Delta t}{\varepsilon_0}\cdot E^n \\ S^n &= e^{-\Delta t/t0}S^{n-1} + \chi\cdot\frac{\Delta t}{t}.E^n \end{aligned} \qquad \textbf{(A-6)}$$

Once again, notice that everything concerning the medium property is contained in the above equation; the other part of FDTD, the calculation of the flux density and magnetic field, will not change.

We can now summarize the general steps for Fourier transform method as follows:

1. Find the Fourier transform expression for the medium property
2. Find the discrete expression of the above transform in the time domain
3. Find the comprehensive updating equation in the FDTD algorithm

Z transforms

We know that in digital signal processing, Z transforms are more general,

versatile, and simple to realize compared with the Fourier transform. For the frequency dependent materials in FDTD, the application of the Z transform should have the advantage compared with the Fourier transform. We begin with a frequency domain equation for the Debye media.

$$D(\omega)=\left(\varepsilon_r+\frac{\sigma}{j\omega\varepsilon_0}+\frac{\chi}{1+j\omega t_0}\right)\cdot E(\omega) \qquad \textbf{(A-7)}$$

By applying the Z transform method, we can avoid convolution integration in the time domain. We have the Z domain expression:

$$D(z)=\varepsilon_r\cdot E(z)+\frac{\sigma\cdot\Delta t/\varepsilon_0}{1-z^{-1}}\cdot E(z)+\frac{\chi.\Delta t/t_0}{1-e^{-\Delta t/t0}z^{-1}}\cdot E(z) \qquad \textbf{(A-8)}$$

In the same way used in the Fourier transform, we can define some auxiliary parameters:

$$\begin{aligned} I(z)&=\frac{\sigma.\Delta t/\varepsilon_0}{1-Z^{-1}}E(z)=Z^{-1}I(z)+\frac{\sigma.\Delta t}{\varepsilon_0}E(z);\\ S(Z)&=\frac{\chi.\Delta t/t_0}{1-e^{-\Delta t/t0}Z^{-1}}\cdot E(z)=e^{-\Delta t/t0}Z^{-1}S(z)+\frac{\chi\cdot\Delta t}{t_0}E(z) \end{aligned} \qquad \textbf{(A-9)}$$

Then $D(z)$ becomes:

$$D(z)=\varepsilon_r\cdot E(z)+z^{-1}I(z)+\frac{\sigma\cdot\Delta t}{\varepsilon_0}E(z)+e^{-\Delta t/t0}Z^{-1}S(z)+\frac{\chi\Delta t}{t_0}E(z) \qquad \textbf{(A-10)}$$

The E(z) expression is:

$$E(z)=\frac{D(z)-z^{-1}I(z)-e^{-\Delta t/t0}z^{-1}S(z)}{\varepsilon_r+\dfrac{\sigma.\Delta t}{\varepsilon_0}+\dfrac{\chi.\Delta t}{t_0}}; \qquad \textbf{(A-11)}$$

So we have the updating equation of:

$$E^n = \frac{D^n - I^{n-1} - e^{-\Delta t/t0} S^{n-1}}{\varepsilon_r + \frac{\sigma.\Delta t}{\varepsilon_0} + \frac{\chi.\Delta t}{t_0}};$$

$$I^n = I^{n-1} + \frac{\sigma.\Delta t}{\varepsilon_0} E^n; \qquad \textbf{(A-12)}$$

$$S^n = e^{-\Delta t/t0} S^{n-1} + \frac{\chi.\Delta t}{t_0} E^n$$

This is the same as the expression obtained from the Fourier transform method; however, we do not need to do integrals and approximations. If the expression of the medium is more complex, the advantage will be more obvious.

Input Impedance for Patch antenna

We can also get the input impedance for the antenna by utilizing the S_{11} from the previous calculation.

$$Z_{in} = Z_0 \frac{1 + S_{11} e^{j2kL}}{1 - S_{11} e^{j2kL}} \qquad \textbf{(A-13)}$$

k: is the wave number of the microstrip, here TM_{010} is the mode we consider

L: is the length from the source position to the edge of the patch antenna

Z_0: is the characteristic impedance of the microstrip line

Properties for Weakly Magnetized Ferrite

For weakly a magnetized ferrite absorber, the permeability can be expressed as a frequency-dependent function. The frequency dependent permeability can be expressed

as:

$$\bar{\mu}_r = 1 + \frac{kf_1}{f_1 + jf} = \mu_r' - j\mu_r'' \qquad \textbf{(A-14)}$$

k is the value of the static magnetic susceptibility when the frequency is zero, μ_r' is the real part of permeability, and μ_r'' is the imaginary part of permeability.

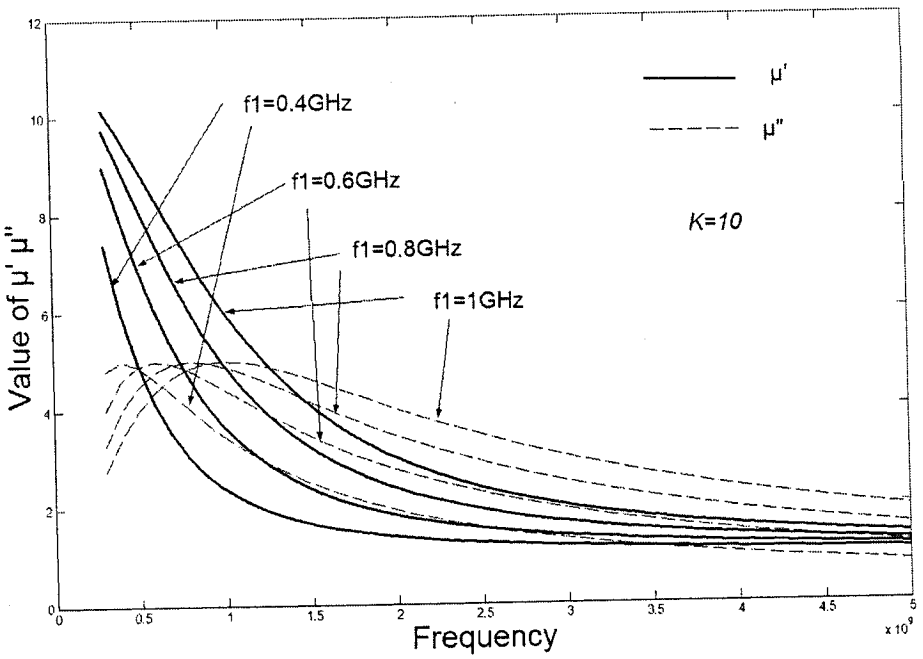

Figure A-1: Permeability of Weakly Magnetized Ferrite

From experimental investigation, we have the following condition that regulates the scope of equation A-14.

$$kf_1 \leq 10GHz \qquad \textbf{(A-15)}$$

From the expression of permeability, we can see that if we increase the value of kf_1, the absolute value of the imaginary part will increase, and the change of kf_1 will mainly change the imaginary part. The change of K mainly affects the real part value of permeability. We knew that when a ferrite slab becomes an ideal absorber, the matching

thickness d_m is approximately given by the following expression:

$$d_m = \frac{\lambda}{2\pi\mu_r''} \tag{A-16}$$

λ is the wave length and μ_r'' is the imaginary part of permeability.

Equation (A-16) is a guideline for designing the thickness of the ferrite absorber for a given frequency. Also, we can see that if we increase μ_r'', the thickness of the absorber will be reduced.

Properties for Magnetized Ferrite

When the ferrite is subjected to a static magnetic biasing field on Z direction and the magnetic fields of the EM wave have no components in the biasing direction, the permeability of the magnetized ferrite can be expressed as a tensor form by:

$$\mu^*(\omega) = \mu_0\tilde{\mu}(\omega) = \mu_0\begin{bmatrix} 1+\chi_m(\omega) & -jk(\omega) & 0 \\ jk(\omega) & 1+\chi_m(\omega) & 0 \\ 0 & 0 & 1 \end{bmatrix} \tag{A-17}$$

Here

$$\chi_m(\omega) = \frac{(\omega_0 + j\omega\alpha)\omega_m}{(\omega_0 + j\omega\alpha)^2 - \omega^2} \tag{A-18}$$

$$k(\omega) = \frac{-\omega\omega_m}{(\omega_0 + j\omega\alpha)^2 - \omega^2} \tag{A-19}$$

$\omega_0 = \gamma_m H_0$ is the processional fr equency

α is the damping constant

γ_m =28GHz/K0 is the gyro magnetic ratio

H_0 is the static magnetic biasing ratio

$\omega_m = \gamma_m 4\pi m_0$ where m_0 is the static magnetization

Permeability under this situation exhibits strong dispersive and anisotropic tendencies, which is quite different from the conventional status.

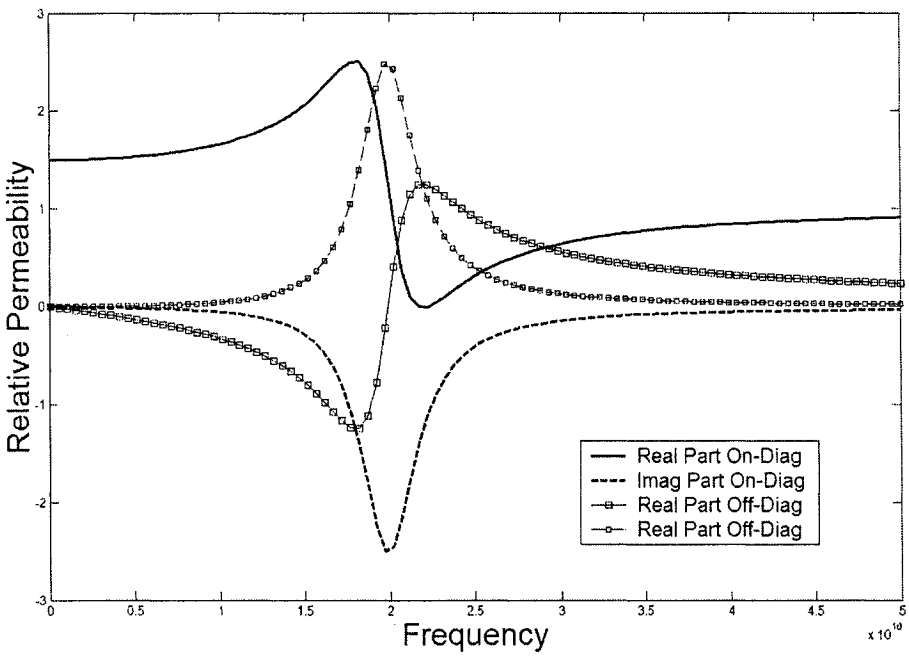

Figure A-2: Real and Imaginary Permeability of the on and off diagonal $\omega_0 = 2\pi \times 20 \times 10^9$, $\omega_m = 2\pi \times 10 \times 10^9$ and $\alpha = 0.10$

Modified Simplified PML Formulation development

We omit the theoretical development of PML is omitted, using the results directly from UPML . We then use simplified PML to develop the formulation in our application . At the same time, we utilize some results in UPML.

Maxwell's curl equations in matched PML in 3D can be written, in the most general form, as:

$$\nabla \times \vec{H} = j\omega \overline{\overline{\varepsilon}} \vec{D}; \qquad \textbf{(A-20.a)}$$

$$\nabla \times \vec{E} = -j\omega \overline{\overline{\mu}} \vec{B} \qquad \textbf{(A-20.b)}$$

and

$$\vec{D} = \varepsilon \cdot \vec{E} \qquad \textbf{(A-21.a)}$$

$$\vec{B} = \mu \cdot \vec{H} \qquad \textbf{(A-21.b)}$$

In Cartesian coordinates, this can be expressed as:

$$\begin{bmatrix} \frac{\partial Hz}{\partial y} - \frac{\partial Hy}{\partial z} \\ \frac{\partial Hx}{\partial z} - \frac{\partial Hz}{\partial x} \\ \frac{\partial Hy}{\partial x} - \frac{\partial Hx}{\partial y} \end{bmatrix} = j\omega \overline{\overline{\varepsilon}} \cdot \begin{bmatrix} Dx \\ Dy \\ Dz \end{bmatrix} \qquad \textbf{(A-22.a)}$$

$$\begin{bmatrix} \frac{\partial Ez}{\partial y} - \frac{\partial Ey}{\partial z} \\ \frac{\partial Ex}{\partial z} - \frac{\partial Ez}{\partial x} \\ \frac{\partial Ey}{\partial x} - \frac{\partial Ex}{\partial y} \end{bmatrix} = -j\omega \overline{\overline{u}} \cdot \begin{bmatrix} Bx \\ By \\ Bz \end{bmatrix} \qquad \textbf{(A -22.b)}$$

$$\overline{\overline{\varepsilon}} = \varepsilon_0 \cdot \begin{bmatrix} \frac{SySz}{Sx} & 0 & 0 \\ 0 & \frac{SxSz}{Sy} & 0 \\ 0 & 0 & \frac{SxSy}{Sz} \end{bmatrix} \qquad \textbf{(A-23)}$$

$$\overline{\overline{\mu}} = \mu_0 \cdot \begin{bmatrix} \frac{SySz}{Sx} & 0 & 0 \\ 0 & \frac{SxSz}{Sy} & 0 \\ 0 & 0 & \frac{SxSy}{Sz} \end{bmatrix} \quad \textbf{(A-24)}$$

And we can define this as:

$$\overline{\overline{S}} = \begin{bmatrix} \frac{SySz}{Sx} & 0 & 0 \\ 0 & \frac{SxSz}{Sy} & 0 \\ 0 & 0 & \frac{SxSy}{Sz} \end{bmatrix} \quad \textbf{(A-25)}$$

We can have several forms of choice for $\mathbf{S_x}$, $\mathbf{S_y}$, and $\mathbf{S_z}$. One of the definitions of $\mathbf{S_x}$, $\mathbf{S_y}$, and $\mathbf{S_z}$ is:

$$Sx = Kx + \frac{\sigma x}{j\omega\varepsilon_0} \quad \textbf{(A-26.a)}$$

$$Sy = Ky + \frac{\sigma y}{j\omega\varepsilon_0} \quad \textbf{(A-26.b)}$$

$$Sz = Kz + \frac{\sigma z}{j\omega\varepsilon_0} \quad \textbf{(A-26.c)}$$

Here we have:

$$Kx = Ky = Kz = k \quad \textbf{(A-27)}$$

Here, $k \in [1,10]$

In our application, we can let k=1, and we use this choice of conductivity:

$$\sigma x(x) = (x/d)^m \sigma x,\max \quad \textbf{(A-28.a)}$$

$$\sigma y(y) = (y/d)^m \sigma y,\max \quad \textbf{(A-28.b)}$$

$$\sigma z(z) = (z/d)^m \sigma z, \max \qquad \textbf{(A-28.c)}$$

x,y,z is the depth in PML; d is the PML thickness alone the layer direction; $m \in [2,4]$; and $\sigma x, \max$ denotes the maximum conductivity at the outmost layer of PML.

If we make the simplification that:

$$\vec{E}' = \sqrt{\frac{\varepsilon_0}{\mu_0}}\vec{E} \qquad \textbf{(A-29)}$$

This system, called Gaussian unites. This gives the E and H fields the same order of magnitude, and makes PML easy to realise. We can then rewrite equation (A-20), (A-21) as:

$$\frac{1}{\sqrt{\varepsilon_0 \mu_0}} \nabla \times \vec{H} = j\omega \overline{\overline{S}} \vec{D} \qquad \textbf{(A-30.a)}$$

$$\frac{1}{\sqrt{\varepsilon_0 \mu_0}} \nabla \times \vec{E}' = -j\omega \overline{\overline{S}} \vec{B} \qquad \textbf{(A-30.b)}$$

$$\vec{D} = \varepsilon_r . \vec{E} \qquad \textbf{(A-31.a)}$$

$$\vec{B} = \mu_r . \vec{H} \qquad \textbf{(A-31.b)}$$

The definition of $\overline{\overline{S}}$ is equation (A-25), and the definition of $\vec{E}'$ is equation (A-29).

Here, we assume that the medium is electric and magnetic. If the material is just magnetic, $\vec{D}$ equals $\vec{E}$; if the material is electric, $\vec{B}$ equals $\vec{H}$. Therefore, the calculation of the properties of materials carries the relation of $\vec{D}$ and $\vec{E}$, $\vec{B}$ and $\vec{H}$, which will avoid the coefficient change for an inhomogeneous medium in UPML, and can give a perfect match to an anisotropic medium.

For the simplicity of programming, we can use this condition, a simplification that

can be omitted if we want a more general expression:

$$\Delta t = \frac{\Delta}{2 \cdot c_0}$$

Δt: the time increment in FDTD

Δ: the smallest spatial increment in FDTD

c_0 the speed in the vacuum

We can have this expression for PML:

$$j\omega\left(1+\frac{\sigma_x(x)}{j\omega\varepsilon_0}\right)\left(1+\frac{\sigma_y(y)}{j\omega\varepsilon_0}\right)\left(1+\frac{\sigma_z(z)}{j\omega\varepsilon_0}\right)^{-1} D_z = c_0\left(\frac{\partial Hy}{\partial x}-\frac{\partial Hx}{\partial y}\right) \qquad \textbf{(A-32.a)}$$

$$j\omega\left(1+\frac{\sigma_x(x)}{j\omega\varepsilon_0}\right)\left(1+\frac{\sigma_y(y)}{j\omega\varepsilon_0}\right)^{-1}\left(1+\frac{\sigma_z(z)}{j\omega\varepsilon_0}\right) D_y = c_0\left(\frac{\partial Hx}{\partial z}-\frac{\partial Hz}{\partial x}\right) \qquad \textbf{(A-32.b)}$$

$$j\omega\left(1+\frac{\sigma_x(x)}{j\omega\varepsilon_0}\right)^{-1}\left(1+\frac{\sigma_y(y)}{j\omega\varepsilon_0}\right)\left(1+\frac{\sigma_z(z)}{j\omega\varepsilon_0}\right) D_x = c_0\left(\frac{\partial Hz}{\partial y}-\frac{\partial Hy}{\partial z}\right) \qquad \textbf{(A-32.c)}$$

$$j\omega\left(1+\frac{\sigma_x(x)}{j\omega\varepsilon_0}\right)^{-1}\left(1+\frac{\sigma_y(y)}{j\omega\varepsilon_0}\right)\left(1+\frac{\sigma_z(z)}{j\omega\varepsilon_0}\right) B_x = c_0\left(\frac{\partial Ey}{\partial z}-\frac{\partial Ez}{\partial y}\right) \qquad \textbf{(A-32.d)}$$

$$j\omega\left(1+\frac{\sigma_x(x)}{j\omega\varepsilon_0}\right)\left(1+\frac{\sigma_y(y)}{j\omega\varepsilon_0}\right)^{-1}\left(1+\frac{\sigma_z(z)}{j\omega\varepsilon_0}\right) B_y = c_0\left(\frac{\partial Ez}{\partial x}-\frac{\partial Ex}{\partial z}\right) \qquad \textbf{(A-32.e)}$$

$$j\omega\left(1+\frac{\sigma_x(x)}{j\omega\varepsilon_0}\right)\left(1+\frac{\sigma_y(y)}{j\omega\varepsilon_0}\right)\left(1+\frac{\sigma_z(z)}{j\omega\varepsilon_0}\right)^{-1} B_z = c_0\left(\frac{\partial Ex}{\partial y}-\frac{\partial Ey}{\partial x}\right) \qquad \textbf{(A-32.f)}$$

This will be solved by the method presented by D. M. Sullivan. We use *Dz* as an example to demonstrate the solution.

We rewrite the first part as:

$$j\omega\left(1+\frac{\sigma_x(x)}{j\omega\varepsilon_0}\right)\left(1+\frac{\sigma_y(y)}{j\omega\varepsilon_0}\right)D_z = c_0\left(1+\frac{\sigma_z(z)}{j\omega\varepsilon_0}\right)\left(\frac{\partial Hy}{\partial x}-\frac{\partial Hx}{\partial y}\right)$$
$$= c_0\cdot\left(\frac{\partial Hy}{\partial x}-\frac{\partial Hx}{\partial y}\right)+c_0\cdot\frac{\sigma_z(z)}{\varepsilon_0}\frac{1}{j\omega}\cdot\left(\frac{\partial Hy}{\partial x}-\frac{\partial Hx}{\partial y}\right); \quad \textbf{(A-33)}$$

In above equation, $\frac{1}{j\omega}\cdot\left(\frac{\partial Hy}{\partial x}-\frac{\partial Hx}{\partial y}\right)$ is an integration that can be realized in time domain.

By using differential method, Fourier transforms, and a time domain convolution in the above equation, Sullivan solves the above equation like this as follows:

$$D_z^{n+1}|_{i,j,k+1/2} = \left(\frac{2\varepsilon_0-\sigma_x(i)\Delta t}{2\varepsilon_0+\sigma_x(i)\Delta t}\right)\left(\frac{2\varepsilon_0-\sigma_y(j)\Delta t}{2\varepsilon_0+\sigma_y(j)\Delta t}\right)D^n{}_z|_{i,j,k+1/2}$$
$$+\left(\frac{2\varepsilon_0}{2\varepsilon_0+\sigma_x(i)\Delta t}\right)\left(\frac{2\varepsilon_0}{2\varepsilon_0+\sigma_y(j)\Delta t}\right)\times c_0\cdot\Delta t$$
$$\times\left(\begin{array}{l}\left(\frac{H_y^{n+1/2}|_{i+1/2,j,k+1/2}-H_y^{n+1/2}|_{i-1/2,j,k+1/2}}{\Delta x}-\frac{H_x^{n+1/2}|_{i,j+1/2,k+1/2}-H_x^{n+1/2}|_{i,j-1/2,k+1/2}}{\Delta y}\right)\\ +\frac{\sigma_z(k+1/2)\Delta t}{2\varepsilon_0}\cdot\sum_{t=1}^{n}\left(\begin{array}{l}\frac{H_y^{n+1/2}|_{i+1/2,j,k+1/2}-H_y^{n+1/2}|_{i-1/2,j,k+1/2}}{\Delta x}\\ -\frac{H_x^{n+1/2}|_{i,j+1/2,k+1/2}-H_x^{n+1/2}|_{i,j-1/2,k+1/2}}{\Delta y}\end{array}\right)\end{array}\right) \quad \textbf{(A-34)}$$

For the simplicity of expression, we can define these notations thus:

$$ch^n|_{i,j,k+1/2} = \left(\begin{array}{l}\frac{H_y^{n+1/2}|_{i+1/2,j,k+1/2}-H_y^{n+1/2}|_{i-1/2,j,k+1/2}}{\Delta x}\\ -\frac{H_x^{n+1/2}|_{i,j+1/2,k+1/2}-H_x^{n+1/2}|_{i,j-1/2,k+1/2}}{\Delta y}\end{array}\right) \quad \textbf{(A-35)}$$

$$Id_z^n|_{i,j,k+1/2} = \sum_{t=1}^{n} \left(\frac{H_y^{n+1/2}|_{i+1/2,j,k+1/2} - H_y^{n+1/2}|_{i-1/2,j,k+1/2}}{\Delta x} - \frac{H_x^{n+1/2}|_{i,j+1/2,k+1/2} - H_x^{n+1/2}|_{i,j-1/2,k+1/2}}{\Delta y} \right) \quad \textbf{(A-36)}$$

$$gi3(i) = \left(\frac{2\varepsilon_0 - \sigma_x(i)\Delta t}{2\varepsilon_0 + \sigma_x(i)\Delta t} \right) \quad \textbf{(A-37)}$$

$$gj3(j) = \left(\frac{2\varepsilon_0 - \sigma_y(j)\Delta t}{2\varepsilon_0 + \sigma_y(j)\Delta t} \right) \quad \textbf{(A-38)}$$

$$gi2(i) = \left(\frac{2\varepsilon_0}{2\varepsilon_0 + \sigma_x(i)\Delta t} \right) \quad \textbf{(A-39)}$$

$$gj2(j) = \left(\frac{2\varepsilon_0}{2\varepsilon_0 + \sigma_y(j)\Delta t} \right) \quad \textbf{(A-40)}$$

$$gk1(k+1/2) = \frac{\sigma_z(k+1/2)\Delta t}{2\varepsilon_0} \quad \textbf{(A-41)}$$

We can then rewrite equation (A-34) as:

$$\begin{aligned} D_z^{n+1}|_{i,j,k+1/2} &= gi3(i).gj3(j).D^n{}_z|_{i,j,k+1/2} \\ &+ gi2(i).gj2(j) \times c_0 \Delta t \times (ch^n|_{i,j,k+1/2} + gk1(k) \cdot Id_z^n|_{i,j,k+1/2}) \end{aligned} \quad \textbf{(A-42)}$$

For the convenience of programming, Simplified PML defined an auxiliary expression, which is to be unconditionally stable.

$$xn(d) = 0.333 \times \left(\frac{d}{l} \right)^m, m = 3; d = i, j, k; \quad \textbf{(A-43)}$$

where i, j, k is the i^{th}, j^{th}, k^{th} slice location in X, Y, Z axis, respectively, and l is the total thickness of the PML slice in the X, Y, Z axes, respectively.

Equation (A-43) is an unconditionally stable result. The introduction of equation (A-43) simplifies the realization of PML. Nevertheless, we cannot control the reflection

from PML backed by PEC. Because so much research based on how to control the reflection and get optimized conductivity in UPML, we utilize some of the existing results. This modification could control or predicate the reflection from simplified PML.

Equation (A-43) is actually the expression:

$$xn(d) = \frac{\sigma(d) \cdot \Delta t}{2 \cdot \varepsilon_0},$$

(A-44)

From the discussion of UPML **[11]**, we have:

$$\sigma(d) = \sigma_{\max} \cdot \left(\frac{d}{l}\right)^m;$$
$$\sigma_{\max} = -\frac{\ln(R(0)) \cdot (m+1)}{2 \cdot \eta_0 \cdot (l \cdot \Delta)} \qquad \textbf{(A-45)}$$

And in our FDTD (2-D or 3-D), we assume that:

$$\Delta t = \frac{\Delta}{2c} \quad . \qquad \textbf{(A-46)}$$

Also, we have this relation: $\eta_0 = \sqrt{\frac{\mu_0}{\varepsilon_0}}$, $c = \frac{1}{\sqrt{\mu_0 \cdot \varepsilon_0}}$, so we can rewrite:

$$xn(d) = -\frac{\ln(R(0)) \cdot (m+1) \cdot \Delta \cdot \sqrt{\mu_0 \varepsilon_0}}{2 \cdot \sqrt{\frac{\mu_0}{\varepsilon_0}} \cdot (l \cdot \Delta) \cdot 2 \cdot \varepsilon_0} \left(\frac{d}{l}\right)^m$$
$$\Rightarrow xn(d) = -\frac{\ln(R(0)) \cdot (m+1)}{4 \cdot l} \left(\frac{d}{l}\right)^m, m \in [2,4] \qquad \textbf{(A-47)}$$

$R(0) \in [10^{-5}, 10^{-12}]$, is the reflection coefficient we wish to achieve.

Here, we can choose the parameters of PML to achieve a controllable reflection, or the optimized choice. For the optimized expression, we have:

$$\sigma_{\max,opt} = \frac{0.8 \cdot (m+1)}{2 \cdot \eta_0 \cdot \Delta} \tag{4-48}$$

$$\Rightarrow xn(d)_{opt} = \frac{0.8 \cdot (m+1)}{4} \left(\frac{d}{l} \right)^m \tag{A-49}$$

We can use above results to get a better performance for simplified PML. As an example, we use optimized choice, and the total PML length is 5, m=3. And we got $xn(d)_{opt} = 0.8 \times \left(\frac{d}{5\Delta} \right)^m$.

PML thickness is 5Δ, the total spatial length=70Δ, and 1000 time steps result. The time spread is 103Δt; the time delay is 25Δt, ε =1, μ =1. The UPML reflection coefficient is an optimized choice obeying formulation (A-48), a simplified method choice obeying formulation (A-43), and an improvement of simplified method obeying formulation (A-49). We can see that results of the modified simplified method indeed approach the UPML results, and that this method is much better than the simplified method.

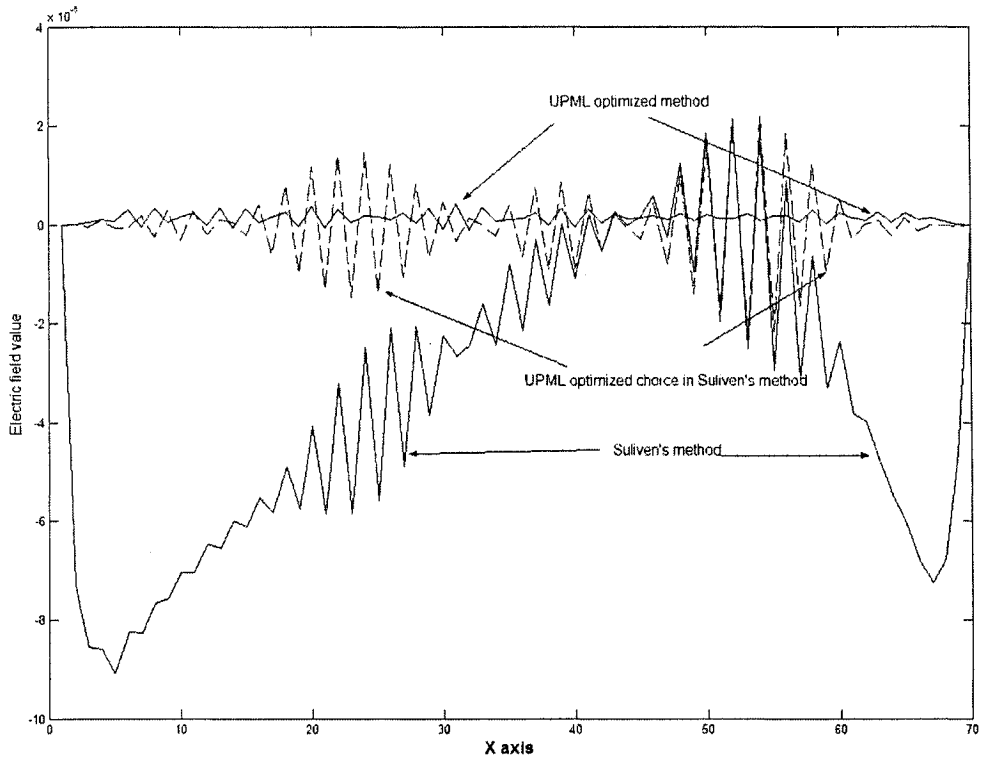

Figure A-3: Comparison of different method results in 1D PML. Thickness is 5⊿, total spatial length=70⊿, time spread=103⊿t, time delay=25⊿t, ε =1, μ =1, 1000 time steps results

The other field component can be developed in the same way. This is the complete list of the solutions.

$$D_x^{n+1}|_{i+1/2,j,k} = gj3(j).gk3(k)\cdot D^n{}_x|_{i+1/2,j,k} + gj2(j).gk2(k)\times c_0\Delta t\times(ch1^{n+1}|_{i+1/2,j,k} + gi1(i+1/2)\cdot Id_x^n|_{i,j,k+1/2}); \quad \textbf{(A-50)}$$

$$ch1^n|_{i+1/2,j,k} = \left(\frac{\dfrac{H_z^{n+1/2}|_{i+1/2,j+1/2,k} - H_z^{n+1/2}|_{i+1/2,j-1/2,k}}{\Delta y} - \frac{H_y^{n+1/2}|_{i+1/2,j,k+1/2} - H_y^{n+1/2}|_{i+1/2,j,k-1/2}}{\Delta z}}{}\right) \quad \textbf{(A-51)}$$

$$Id_x^n|_{i+1/2,j,k} = \sum_{t=1}^{n} \left(\frac{H_z^{n+1/2}|_{i+1/2,j+1/2,k} - H_z^{n+1/2}|_{i+1/2,j-1/2,k}}{\Delta y} - \frac{H_y^{n+1/2}|_{i+1/2,j,k+1/2} - H_y^{n+1/2}|_{i+1/2,j,k-1/2}}{\Delta z} \right) \quad \textbf{(A-52)}$$

$$D_y^{n+1}|_{i,j+1/2,k} = gi3(i).gk3(j).D^n{}_y|_{i,j+1/2,k} + gi2(i).gk2(k) \times c_0 \Delta t \times (ch2^n|_{i,j+1/2,k} + gj1(j+1/2) \cdot Id_y^n|_{i,j+1/2,k}); \quad \textbf{(A-53}$$

)

$$ch2^n|_{i,j+1/2,k} = \left(\frac{H_x^{n+1/2}|_{i,j+1/2,k+1/2} - H_x^{n+1/2}|_{i,j+1/2,k-1/2}}{\Delta z} - \frac{H_z^{n+1/2}|_{i+1/2,j+1/2,k} - H_z^{n+1/2}|_{i-1/2,j+1/2,k}}{\Delta x} \right) \quad \textbf{(A-54)}$$

$$Id_y^n|_{i,j+1/2,k} = \sum_{t=1}^{n} \left(\frac{H_x^{n+1/2}|_{i,j+1/2,k+1/2} - H_x^{n+1/2}|_{i,j+1/2,k-1/2}}{\Delta z} - \frac{H_z^{n+1/2}|_{i+1/2,j+1/2,k} - H_z^{n+1/2}|_{i-1/2,j+1/2,k}}{\Delta x} \right) \quad \textbf{(A-55)}$$

$$D_z^{n+1}|_{i,j,k+1/2} = gi3(i).gj3(j).D^n{}_z|_{i,j,k+1/2} + gi2(i).gj2(j) \times c_0 \Delta t \times (ch3^n|_{i,j,k+1/2} + gk1(k+1/2) \cdot Id_z^n|_{i,j,k+1/2}); \quad \textbf{(A-56)}$$

$$ch3^n|_{i,j,k+1/2} = \left(\frac{H_y^{n+1/2}|_{i+1/2,j,k+1/2} - H_y^{n+1/2}|_{i-1/2,j,k+1/2}}{\Delta x} - \frac{H_x^{n+1/2}|_{i,j+1/2,k+1/2} - H_x^{n+1/2}|_{i,j-1/2,k+1/2}}{\Delta y} \right) \quad \textbf{(A-57)}$$

$$Id_z^n|_{i,j,k+1/2} = \sum_{t=1}^{n} \left(\frac{H_y^{n+1/2}|_{i+1/2,j,k+1/2} - H_y^{n+1/2}|_{i-1/2,j,k+1/2}}{\Delta x} - \frac{H_x^{n+1/2}|_{i,j+1/2,k+1/2} - H_x^{n+1/2}|_{i,j-1/2,k+1/2}}{\Delta y} \right) \quad \textbf{(A-58)}$$

$$B_x^{n+1/2}|_{i,j+1/2,k+1/2} = fj3(j+1/2)\cdot fk3(k+1/2)\cdot B_x^{n-1/2}|_{i,j+1/2,k+1/2} + fj2(j+1/2)\cdot fk2(k+1/2)\times c_0\Delta t \times\left[ce1^n|_{i,j+1/2,k+1/2} + fi1(i)\,Ih_x^n|_{i,j+1/2,k+1/2}\right]; \quad \textbf{(A-59)}$$

$$ce1^n|_{i,j+1/2,k+1/2} = \left(\frac{E_y^n|_{i,j+1/2,k+1} - E_y^n|_{i,j,k+1/2,}}{\Delta z} - \frac{E_z^n|_{i,j+1,k+1/2} - E_z^n|_{i,j,k+1/2}}{\Delta y}\right) \quad \textbf{(A-60)}$$

$$Ih_x^n|_{i,j+1/2,k+1/2} = \sum_{t=1}^{n}\left(\frac{E_y^n|_{i,j+1/2,k+1} - E_y^n|_{i,j,k+1/2}}{\Delta z} - \frac{E_z^n|_{i,j+1,k+1/2} - E_z^n|_{i,j,k+1/2}}{\Delta y}\right) \quad \textbf{(A-61)}$$

$$B_y^{n+1/2}|_{i+1/2,j,k+1/2} = fi3(i+1/2).fk3(k+1/2)\cdot B_y^{n-1/2}|_{i+1/2,j,k+1/2} + fi2(i+1/2)\cdot fk2(k+1/2)\times c_0\Delta t \times\left[ce2^n|_{i+1/2,j,k+1/2} + fj1(j).Ih_y^n|_{i+1/2,j,k+1/2}\right]; \quad \textbf{(A-62)}$$

$$ce2^n|_{i+1/2,j,k+1/2} = \left(\frac{E_z^n|_{i+1,j,k+1/2} - E_z^n|_{i,j,k+1/2}}{\Delta x} - \frac{E_x^n|_{i+1/2,j,k+1} - E_z^n|_{i+1/2,j,k}}{\Delta z}\right) \quad \textbf{(A-63)}$$

$$Ihy^n|_{i+1/2,j,k+1/2} = \sum_{t=1}^{n}\left(\frac{E_z^n|_{i+1,j,k+1/2} - E_z^n|_{i,j,k+1/2}}{\Delta x} - \frac{E_x^n|_{i+1/2,j,k+1} - E_z^n|_{i+1/2,j,k}}{\Delta z}\right) \quad \textbf{(A-64)}$$

$$B_z^{n+1/2}|_{i+1/2,j+1/2,k} = fi3(i+1/2).fj3(j+1/2)\cdot B_z^{n-1/2}|_{i+1/2,j+1/2,k} + fi2(i+1/2)\cdot fj2(j+1/2)\times c_0\Delta t \times\left[ce3^n|_{i+1/2,j+1/2,k} + fk1(k).Ih_z^n|_{i+1/2,j+1/2,k}\right]; \quad \textbf{(A-65)}$$

$$ce3^n|_{i+1/2,j+1/2,k} = \left(\frac{E_x^n|_{i+1/2,j+1,k} - E_x^n|_{i+1/2,j,k}}{\Delta y} - \frac{E_y^n|_{i+1,j+1/2,k} - E_y^n|_{i,j+1/2,k}}{\Delta x}\right) \quad \textbf{(A-66)}$$

$$Ih_z^n|_{i+1/2,j+1/2,k} = \sum_{t=1}^{n} \left(\frac{E_x^n|_{i+1/2,j+1,k} - E_x^n|_{i+1/2,j,k}}{\Delta y} - \frac{E_y^n|_{i+1,j+1/2,k} - E_y^n|_{i,j+1/2,k}}{\Delta x} \right) \quad \textbf{(A-67)}$$

$$gi3(i) = \left(\frac{2\varepsilon_0 - \sigma_x(i)\Delta t}{2\varepsilon_0 + \sigma_x(i)\Delta t} \right) \quad \textbf{(A-68)}$$

$$gj3(j) = \left(\frac{2\varepsilon_0 - \sigma_y(j)\Delta t}{2\varepsilon_0 + \sigma_y(j)\Delta t} \right) \quad \textbf{(A-69)}$$

$$gk3(k) = \left(\frac{2\varepsilon_0 - \sigma_z(k)\Delta t}{2\varepsilon_0 + \sigma_z(k)\Delta t} \right) \quad \textbf{(A-60)}$$

$$gi2(i) = \left(\frac{2\varepsilon_0}{2\varepsilon_0 + \sigma_x(i)\Delta t} \right) \quad \textbf{(A-71)}$$

$$gj2(j) = \left(\frac{2\varepsilon_0}{2\varepsilon_0 + \sigma_y(j)\Delta t} \right) \quad \textbf{(A-72)}$$

$$gk2(k) = \left(\frac{2\varepsilon_0}{2\varepsilon_0 + \sigma_z(k)\Delta t} \right) \quad \textbf{(A-73)}$$

$$gi1(i+1/2) = \frac{\sigma_x(i+1/2)\Delta t}{2\varepsilon_0} \quad \textbf{(A-74)}$$

$$gj1(j+1/2) = \frac{\sigma_y(j+1/2)\Delta t}{2\varepsilon_0} \quad \textbf{(A-75)}$$

$$gk1(k+1/2) = \frac{\sigma_z(k+1/2)\Delta t}{2\varepsilon_0} \quad \textbf{(A-76)}$$

$$fi3(i+1/2) = \left(\frac{2\varepsilon_0 - \sigma_x(i+1/2)\Delta t}{2\varepsilon_0 + \sigma_x(i+1/2)\Delta t} \right) \quad \textbf{(A-77)}$$

$$fj3(j+1/2) = \left(\frac{2\varepsilon_0 - \sigma_y(j+1/2)\Delta t}{2\varepsilon_0 + \sigma_y(j+1/2)\Delta t} \right) \quad \textbf{(A-78)}$$

$$fk3(k+1/2)=\left(\frac{2\varepsilon_0-\sigma_z(k+1/2)\Delta t}{2\varepsilon_0+\sigma_z(k+1/2)\Delta t}\right) \tag{A-79}$$

$$fi2(i+1/2)=\left(\frac{2\varepsilon_0}{2\varepsilon_0+\sigma_x(i+1/2)\Delta t}\right) \tag{A-80}$$

$$fj2(j+1/2)=\left(\frac{2\varepsilon_0}{2\varepsilon_0+\sigma_y(j+1/2)\Delta t}\right) \tag{A-81}$$

$$fk2(k+1/2)=\left(\frac{2\varepsilon_0}{2\varepsilon_0+\sigma_z(k+1/2)\Delta t}\right) \tag{A-82}$$

$$fi1(i)=\frac{\sigma_x(i)\Delta t}{2\varepsilon_0} \tag{A-83}$$

$$fj1(j)=\frac{\sigma_y(j)\Delta t}{2\varepsilon_0} \tag{A-84}$$

$$fk1(k)=\frac{\sigma_z(k)\Delta t}{2\varepsilon_0} \tag{A-85}$$

We should notice that coefficients for **B** and **D** are a little different, which is caused by the different location of **B** and **D** in Yee's grid. Ignoring this condition, significant reflection errors can be observed. For example, for the **Dx** field in the x-axis, the PML slice thickness is $d=(i+\frac{1}{2})\times\Delta x$, whereas for **Dz** field the thickness in the x-axis is different: $d=i\times\Delta x$.

When we apply PML as the ABC in the FDTD program, a "seamless" transition is preferred so that we do not make complex logical judgements in the main updating. It is quite easy to apply this method to an ordinary medium, a dispersive electric and magnetic medium, or an anisotropic medium.

We then understand that outside the PML $xn(d) = 0$; using this value, we can set the expression of the PML parameters as the value in the main updating part. After doing so, we can find that the updating equation for PML becomes the conventional FDTD updating equation.

While in UPML, the conductivity should change if the problem is inhomogeneous which requires more computer memory and programming work. The approach of realizing UPML for dispersive mediums is quite complex; the PML should undergo a major change. Simplified PML circumvents all of the above disadvantages.

Bibliography

[1] Allen Taflove, *Advances in Computational Electrodynamics: The finite Difference Time –Domain Method* Artech House, 1998

[2] A. R. Sebak "*Computational Electromagnetics Lecture Notes*" 2003

[3] R.F. Harrington, *Field Computation by Moment Methods*, Macmillan Co. 1968

[4] G. J. Bruke, A. J. Poggio, "*Numerical Electromagnetic Code- Method of Moments, Part 1: Program Description, Theory*", Technical Document, 116, Naval Electronics System Command (Elex3041), July 1977

[5] Matthew N. O. Sadiku, *Numerical Techniques in Electromagnetics* CRC Press 1992

[6] C. Balanis *Advanced Engineering Electromagnetic Theory* John Wiley & Sons, Inc, 2001 Constantine

[7] Allen Taflove, Susan C. Hagness, *Computational Electrodynamics: The Finite-Dfference Time-Domain Method* Artech House, 2000.

[8] K. S. Yee "*Numerical Solution of Initial Boundary Value Problems Involving Maxwell's Equations in Isotropic Media*" IEEE Trans AP. Vol. AP-14 pp302-307, May 1966

[9] Gerrit Mur "*Absorbing boundary conditions for the Finite-Difference Approximation of the Time Domain Electromagnetic Field Equations*" IEEE Trans Electromagnetic Compatibility, Vol.23, PP.377-382, 1981

[10] J. P. Berenger, "*A perfectly matched layer for the absorption of electromagnetic waves*" Comput Phys., Vol.6, pp97-99 Feb.1996

[11] Allen Taflove, Susan C. Hagness, *Computational Electrodynamics: The Finite-Dfference Time-Domain Method* Artech House, 2000.

[12] Dennis M. Sullivan, *Electromagnetic Simulation Using the FDTD Method* IEEE press series on RF and Microwave Technology, 2000.

[13] Karl S., Kunz, Raymond and J. Luebbers, *The Finite Difference Time Domain Method for Electromagnetics* CRC press, 1993

[14] Choi, D. H. and W. J. R. Hoefer, "*The finite-difference time-domain method and its application to eigenvalue problems*," IEEE Trans. MTT, Vol. 34, pp.1464-1470, 1986

[15] John Schneider and S. Hudson, "*The finite difference time domain method applied to anisotropic material*" IEEE Trans. AP, Vol.41, pp994-999 1993

[16] Hunsberger, F., R. J. Luebbers, "*Finite-difference time-domain analysis of gyrotropic media. I: magnetized plasma,*" IEEE Trans. AP, Vol. 40, pp. 1489-1495 1992

[17] AnPing. Zhao. "*An Efficient FDTD Algorithm for the Analysis of Microstrip Patch Antennas Printed on a General Anisotropic Dielectric Substrate*" IEEE Trans on MTT, Vol.47, no7, pp.1142-1146, July 1999

[18] Akyurtlu, A. and Werner, D.H. "*Modeling of transverse propagation through a uniaxial bianisotropic medium using the finite-difference time-domain technique*" IEEE Trans. AP, Vol.52, pp 3273 – 3279, 2004

[19] Mosallaei, H. and Sarabandi, K., "*Magneto-dielectrics in electromagnetics: concept and applications*" IEEE Trans. AP, Vol.52, pp 1558 – 1567, 2004

[20] A. Reineix and T. Monediere, "*Ferrite Analysis Using the Finite-difference Time-domain (FDTD) Method*" Microwave Opt Tech Lett, Vol.5, pp685-686, Dec.1992

[21] Jose A. Pereda, "*FDTD analysis of Ferrite based on the equation of motion of the magnetization vector*" IEEE Trans MTT Vol.43, No.3, p350-P357 Feb 1995

[22] Schuster, J. W., and R. J. Luebbers, "*Finite difference time domain analysis of arbitrarily biased magnetized ferrites*", Radio Science, Vol.31 pp.923-929, 1996

[23] T. Hruskovec and Zhizhang Chen "*FDTD Modeling of Magnetized Ferrite Using Z Transforms*" Antennas and Propagation Society International Symposium, IEEE Vol. 2, pp1324-1327, July 1999

[24] Moss, C. D., and Tiexiera, F. L., "*Analysis and compensation of numerical dispersion in the FDTD method for layered, anisotropic media*" IEEE Trans. AP, Vol.50, pp1174 – 1184, 2002

[25] S. D. Gedney, "*An anisotropic perfectly matched layer absorbing media for the truncation of FDTD lattices*", IEEE trans. AP, Vol. 44, pp.1630-1639, 1996

[26] S. Gedney, "*Computational Electromagnetic: The finite-difference Time-Domain*" lecture notes, Fall 2003

[27] D. M. Sullivan "*A simplified PML for use with the FDTD method*", IEEE Microwave and Guided Wave Letters, Vol.6 pp97-99, Feb. 1996

[28] Alan V. Oppenheim, *Signal and System* Prentice hall 1997

[29] Tatsuo Itoh and Bijian Houshmand, *Time-domain methods for Microwave structures: Analysis and Design* IEEE Press, 1998

[30] Mitsuhiro Amano and Youji Kotsuka, "*A Method of Effective Use of Ferrite for Microwave Absorber*" IEEE Trans MTT, Vol.51, NO.1, pp238—245 Jan 2003

[31] D. M. Shen, "*Application of the Three-Dimensional Finite-Difference Time-Domain Method to the Analysis of Planar Microstrip Circuits*" IEEE Trans MTT Vol.38, No.7, pp 849-857, July 1990

[32] Yinchao Chen, "*Dispersion Characteristics of Open and Shielded Microstrip Lines Under a Combined Principal Axis Rotation of Electrically and Magnetically Anisotropic Substrates*" IEEE Trans on MTT, Vol.41, No.4 pp673-679, April 1993

[33] S.K. Koul and B. Bhat, "*Generalized analysis of microstrip-like transmission lines and coplanar strops with anisotropic substrate for MIC, electrooptic modulator, and SAW application*" IEEE Trans MTT, Vol-31, No.12, pp1051-1058, Dec.1983.

[34] Y. Kotsuka and H. Yamazaki, "*Fundamental investigation on a weakly magnetized ferrite absorber*" IEEE Trans Electromagnets Compat, Vol.42, pp116-124, May 2000

[35] D. M. Sullivan, "*Frequency-dependent FDTD methods using Z transforms*" IEEE Trans AP vol. AP-40, pp1223-1230 Oct.1992

[36] Karine Berthou-Pichavant, "*Wave propagation in Heterogeneous Anisotropic Magnetic Materials* " IEEE MTT Vol.45 No.5, pp687-690, May 1997

[37] T. Fukusako and M. Tsutsumi, "*Superconducting Microstrip resonater with Yttrium*

Iron Garnet Single Crystals" IEEE Trans MTT Vol. 45, No.11, pp 2013-2017, Nov 1997